

**POLYMER/METAL ADHESION IN HYBRID CARDIOVASCULAR STENT**

A Thesis

by

KARTHIK MOHAN

Submitted to the Office of Graduate Studies of  
Texas A&M University  
in partial fulfillment of the requirements for the degree of

MASTER OF SCIENCE

August 2007

Major Subject: Mechanical Engineering

**POLYMER/METAL ADHESION IN HYBRID CARDIOVASCULAR STENT**

A Thesis

by

KARTHIK MOHAN

Submitted to the Office of Graduate Studies of  
Texas A&M University  
in partial fulfillment of the requirements for the degree of

MASTER OF SCIENCE

Approved by:

Chair of Committee, Nguyen Hung  
Committee Members, James Moore  
Richard Griffin  
Head of Department, Dennis O'Neal

August 2007

Major Subject: Mechanical Engineering

**ABSTRACT**

Polymer/Metal Adhesion in Hybrid Cardiovascular Stent.

(August 2007)

Karthik Mohan, B.E., Anna University

Chair of Advisory Committee: Dr. Nguyen Hung

Angioplasty over the years has proven to be an excellent substitute for open heart surgery where an artery/vien, blocked by atherosclerosis, is expanded using a stent. Metallic and coated metallic stents have been used for angioplasty. Metal stents might induce blood clotting, release cytotoxic heavy metal ions which are potential inducers of allergies, clotting, immune reactions and hyperproliferation of smooth muscle cells and also lead to protein absorption which activates clotting factors. Biodegradable polymers have also been tried as stent materials, but the loss of radial strength over time is a big problem associated with them. The use of a hybrid stent, consisting of biodegradable polymer and biocompatible stainless steel, is proposed. The use of such a system would require excellent adhesion between the stent metal and the biodegradable polymer. This study presents the electrochemically induced micromechanical interlocking to enhance adhesion between 304 stainless steel and high density polyethylene. High density polyethylene was used instead of biodegradable polymer for initial investigation.

Electrochemical etching on the stainless steel wire was accomplished by immersing a stainless steel wire in a sodium carbonate electrolyte while applying a known voltage through the wire. The electrochemical etching of the stainless steel wire resulted in pitting under suitable conditions. The etching time, voltage and electrolyte concentration were varied to achieve different pit sizes and pit distributions on the stainless steel wire. An image analysis was conducted using an image analysis software to find the exact pit size and pit distribution on the stainless steel wire from electrochemical etching. A statistical model based on design of engineering experiments was derived. Etched and the unetched wires were molded with high density polyethylene and a mechanical test was conducted to measure the force required to pull the wire out of

the polymer and verified using calculations based on the pit size and pit distribution of the pits on the surface of the wire.

Electrochemical etching produced burr free surface features. It was observed that the pH level in the electrolyte contributes to the pit size and pit distribution. The results of the statistical model were consistent with the experimental values and it was possible to optimize the electrochemical etching parameters for maximum pit size and pit distribution. It was also observed that while voltage and etching time contribute to pit size and pit distribution, the electrolyte concentration does not have significant effect on the pit size and pit distribution. The calculated pull out force and measured values were off by 22.7%. The lower value of calculated force could result from neglecting some of the smaller pits while performing the image analysis. The average adhesive strength of the etched samples was 276% higher than that of the unetched samples.

## ACKNOWLEDGEMENTS

I would like to thank my advisor Dr. Wayne Hung who has constantly provided me with support in each step of the project. I would like to thank my committee members Dr. R. Griffin and Dr. J. Moore for providing me important ideas which I was able to apply to my project. I would like to thank Prof. L. McDaniel whose input was critical while I was preparing the statistical model. I would like to thank Mr. C. Loggins who helped in manufacturing some of the parts which were critical for the experiment. I would like to thank my parents Mr. T.V. Mohan and Mrs. Usha Mohan for believing in me and providing me with all the support. I would like to thank my best friend Miss Priya Narayanan who has constantly provided me with emotional support. In the end I would like to thank God who made all this possible.

## NOMENCLATURE

1. Thrombogenicity - Thrombogenicity refers to the tendency of a material in contact with the blood to produce a thrombus, or clot (American physiological association, 2007).
2. Atheroma - In pathology, an atheroma is an accumulation and swelling in artery walls that is made up of cells, or cell debris, that contain lipids, calcium and a variable amount of fibrous connective tissue (American physiological association, 2007).
3. Cytotoxicity - Cytotoxicity is the quality of being toxic to cells (Reference, 2007).
4. Hyperproliferation - An abnormally high rate of cell division which results in rapid proliferation of the cells (American physiological association, 2007).
5. Haemocompatibility - Haemocompatibility is the compatibility of a material with blood. It is an important consideration when designing devices that contact blood (American physiological association, 2007).
6. Endothelial cells - Endothelial cells line the entire circulatory system, from the heart to the smallest capillary. These cells reduce friction of the flow of blood (Wikipedia, 2007).
7. Neointimal hyperplasia - A possible complication of stenting, bypass surgery or other treatments for clogged arteries. It involves a thickening of the inner layer of the blood vessel, which could ultimately result in the closing of the newly opened or grafted blood vessel (American physiological association, 2007).
8. Restenosis – Restenosis literally means recurrence of stenosis. There are many mechanisms which lead to restenosis one of them is inflammation which induces tissue proliferation around the implant site (American physiological association, 2007).

## TABLE OF CONTENTS

	Page
ABSTRACT.....	iii
ACKNOWLEDGEMENTS.....	v
NOMENCLATURE .....	vi
TABLE OF CONTENTS .....	vii
LIST OF FIGURES .....	ix
LIST OF TABLES.....	xv
I. INTRODUCTION.....	1
II. OBJECTIVE AND SCOPE .....	5
III. LITERATURE REVIEW .....	6
III.1 Stent materials and adhesion.....	6
III.1.1 Metallic materials.....	6
III.1.2 Biodegradable polymers .....	6
III.1.2.1 Polylactic acid.....	7
III.1.2.2 Poly E-Caprolactone.....	8
III.1.3 Coated stents .....	9
III.1.3.1 Polymeric coating .....	9
III.1.3.2 Semiconductor coating.....	10
III.1.3.3 Elastomeric coating.....	11
III.1.4 Mechanisms of adhesion.....	12
III.1.4.1 Electronic theory.....	12
III.1.4.2 Theory of weak boundary layers.....	12
III.1.4.3 Adsorption theory .....	13
III.1.4.4 Diffusion theory.....	13
III.1.4.5 Chemical bonding theory.....	14
III.1.4.6 Mechanical interlocking.....	14
III.1.5 Metal – Polymer adhesion .....	15
III.1.5.1 Micro sand blasting.....	15
III.1.5.2 Vacuum plasma spray.....	16
III.1.5.3 Pitting.....	17
III.1.5.4 Adhesive forces between metals and polymers .....	18
III.2 Stent manufacture .....	21
III.2.1 Investment casting .....	21
III.2.2 Laser processing.....	22
III.2.3 Biodegradable stents .....	24
III.3 Insert molding.....	25
III.4 Electrochemical etching.....	26
III.4.1 Passivity .....	28

	Page
III.4.2 Effect of pH.....	29
IV. EXPERIMENTS.....	31
IV.1 Surface preparation.....	31
IV.1.1 Mechanical abrasion .....	31
IV.1.2 Chemical etching .....	32
IV.2 Electrochemical etching .....	32
IV.2.1 Setup .....	32
IV.2.2 Etching with sodium carbonate electrolyte.....	36
IV.2.3 Measurement of pH .....	37
IV.2.4 Design of experiment.....	37
IV.3 Molding .....	39
IV.3.1. Molding machine specifications .....	41
IV.3.2 Procedure .....	44
IV.4 Preparation of samples for pull out test .....	45
IV.5 SEM pictures .....	46
IV.6 Statistical study.....	46
IV.6.1 Analysis with image tool .....	47
IV.7 Pull out test.....	48
V. RESULTS AND DISCUSSION .....	52
V.1 Mechanical abrasion .....	52
V.2 Chemical etching .....	54
V.3 Electrochemical etching.....	56
V.3.1 Design of experiment .....	56
V.3.2 Electrochemical etching using sodium carbonate.....	64
V.3.3 Measurement of pH.....	65
V.4 Statistical study .....	66
V.4.1 Calculations.....	67
V.5 Force calculation .....	73
V.5.1 Theoretical values .....	73
V.5.2 Experimental values .....	76
V.6 Discussion .....	78
V.6.1 Surface of stainless steel .....	78
V.6.2 Electrochemical etching .....	80
V.6.3 Molding.....	81
V.6.4 Adhesive strength.....	83
VI. CONCLUSIONS AND RECOMMENDATIONS .....	86
REFERENCES .....	88



	Page
APPENDIX A.....	92
APPENDIX B_.....	100
APPENDIX C.....	106
APPENDIX D.....	112
VITA .....	116



	Page
Figure III.24 - Variation of current density with potential of four stainless steels with different nickel contents in 35% H <sub>2</sub> SO <sub>4</sub> at 40 °C.....	29
Figure III.25 - Variation of corrosion rate in solutions of different pH .....	30
Figure IV.1 - Experimental setup for electrochemical etching.....	33
Figure IV.2 - Details of electrolytic cell to etch a stainless steel wire.....	33
Figure IV.3 - Design for cathode .....	34
Figure IV.4 -Design of the electrolytic cell .....	34
Figure IV.5 - pH measurement .....	37
Figure IV.6 - Drawing for mold 1 .....	40
Figure IV.7 - Drawing for mold 2 .....	40
Figure IV.8 - Cross-section of the assembly .....	41
Figure IV.9 - Injection molding machine .....	42
Figure IV.10 - Mold housing in the machine with the heaters for the mold.....	42
Figure IV.11 - Injection molding machine with all parts (BABYPLAST 6/10, 2000) ....	43
Figure IV.12 - Buehler isomet low speed saw .....	45
Figure IV.13 - Sample picture taken for analysis .....	47
Figure IV.14 - Image analysis with Image Tool (Version 3.00).....	48
Figure IV.15 - Instron universal testing machine M10-24411 .....	49
Figure IV.16 - Pull out test .....	49
Figure IV.17 - Drawing for upper jig .....	50
Figure IV.18 - Drawing for the bottom plate .....	51
Figure IV.19 - Assembly for the pull out test.....	51
Figure V.1 - Surface of 304 stainless steel after unidirectional sanding with 240 grit size sand paper.....	52
Figure V.2 - Surface of 304 stainless steel after cross sanding with 240 grit size paper..	52
Figure V.3 - SEM image of mechanically abraded wire .....	53
Figure V.4 - SEM of mechanically abraded wire .....	53
Figure V.5 - Optical image of stainless steel wire dipped in 35% concentrated hydrochloric acid for 15 minutes .....	54

	Page
Figure V.6 - Optical image of stainless steel wire dipped in 35% concentrated hydrochloric acid for 3 hours.....	54
Figure V.7 - SEM image of stainless steel wire dipped in 35% concentrated hydrochloric acid for 3 hours.....	55
Figure V.8 - SEM image of stainless steel wire dipped in 35% HCl for 3 hours .....	55
Figure V.9 - Stainless steel wire after electrochemical etching in 5% soap solution at a voltage of 6 volts for 10 seconds.....	56
Figure V.10 - Pit depth as a function of time and voltage (equation V.1).....	58
Figure V.11 - Pit density as a function of time and voltage (equation V.3).....	59
Figure V.12 - Desirability as a function of time and voltage.....	59
Figure V.13 - Comparison of pit depth predicted by the model with actual data.....	61
Figure V.14 - Comparison of pit density predicted by the model with actual data .....	62
Figure V.15 - Wire etched at optimum conditions .....	63
Figure V.16 - SEM image of electrochemically etched wire at 6 volts for 20 seconds in an electrolyte having concentration 2.5%.....	63
Figure V.17 - SEM image of electrochemically etched wire at a higher magnification ..	64
Figure V.18 - Stainless steel wire etched in 2.5% sodium carbonate solution at 7 volts for 120 seconds .....	65
Figure V.19 - Magnified view of the pits on the surface of stainless steel etched with 2.5% sodium carbonate solution at 7 volts for 120 seconds .....	65
Figure V.20 - Diameter of pits vs depth of pits .....	66
Figure V.21 - Pit number vs pit diameter (sample number 1, etched at 6 volts for 20 seconds using soap concentration of 2.5% .....	70
Figure V.22 - Pit number vs distance between pits (sample number 1, etched at 6 volts for 20 seconds using soap concentration of 2.5%) .....	70
Figure V.23 - Sample number vs pit diameter .....	72
Figure V.24 - Sample number vs distance between 2 pits.....	72
Figure V.25 - Sample number vs number of pits.....	72
Figure V.26 - Model of the etched wire.....	73
Figure V.27 - Shearing of hemispherical pits .....	74

	Page
Figure V.28 - Displacement vs pullout force for unetched wires .....	77
Figure V.29 - Displacement vs pull out force for etched wires (etched at 6 volts for 20 seconds at soap concentration of 2.5%) .....	77
Figure V.30 - Change in length/original length vs adhesive strength.....	78
Figure V.31 - Average displacement Vs average force .....	78
Figure V.32 - Comparison of different surfaces (a) unetched surface (b) mechanical abrasion (c) chemical etching (d) electrochemical etching .....	79
Figure V.33 - Desirability as a function of time, voltage and concentration.....	81
Figure V.34 - Cross-section of the molded polymer over etched stainless steel wire .....	82
Figure V.35 - Magnified view of cross section of molded polymer over etched stainless steel wire .....	82
Figure V.36 - Comparison of pull off tests (a) comparison of adhesive strengths between an electrochemically etched sample and an unetched sample (b) comparison of interfacial shear strength (IFSS) of glass fibres treated with varying concentrations of $\gamma$ -APS .....	85
Figure A.1 - Standardized effect vs half normal % probability.....	92
Figure A.2 - Internally standardized results vs normal % probability .....	93
Figure A.3 - Actual vs predicted.....	94
Figure A.4 - Lambda vs ln (residuals) .....	95
Figure A.5 - Standardized effect vs half normal % probability.....	96
Figure A.6 - Internally standardized results vs normal % probability .....	97
Figure A.7 - Actual vs predicted.....	98
Figure A.8 - Lambda vs ln (residuals) .....	99
Figure B.1 - Wire etched for 20s at an applied voltage of 3v in soap solution of concentration 2.5% by weight.....	100
Figure B.2 - Wire etched for 10s at an applied voltage of 6v in soap solution of concentration 2.5% by weight.....	100
Figure B.3 - Wire etched for 30s at an applied voltage of 3v in soap solution of concentration 2.5% by weight.....	101

	Page
Figure B.4 - Wire etched for 30s at an applied voltage of 6v in soap solution of concentration 2.5% by weight.....	101
Figure B.5- Wire etched for 10s at an applied voltage of 12v in soap solution of concentration 2.5% by weight.....	102
Figure B.6 - Wire etched for 30s at an applied voltage of 12v in soap solution of concentration 2.5% by weight.....	102
Figure B.7 - Wire etched for 10s at an applied voltage of 3v in soap solution of concentration 5% by weight.....	103
Figure B.8 - Wire etched for 20s at an applied voltage of 6v in soap solution of concentration 5% by weight.....	103
Figure B.9 - Wire etched for 30s at an applied voltage of 12v in soap solution of concentration 5% by weight.....	104
Figure B.10 - Wire etched for 20s for an applied voltage of 12v in soap solution of concentration 5% by weight .....	106
Figure B.11 - Wire etched for 30s at an applied voltage of 6v in soap solution of concentration 5% by weight.....	105
Figure D.1 - Displacement Vs force (unetched sample 1).....	112
Figure D.2 - Displacement Vs force (unetched sample 2).....	112
Figure D.3 - Displacement Vs force (unetched sample 3).....	113
Figure D.4 - Displacement Vs force (unetched Sample 4).....	113
Figure D.5 - Displacement Vs force (etched sample 1).....	114
Figure D.6 - Displacement Vs force (etched sample 2).....	114
Figure D.7 - Displacement Vs force (etched sample 3).....	115

## LIST OF TABLES

	Page
Table IV.1 - Different conditions of electrochemical etching .....	36
Table IV.2 - Input and output data for Design Expert software .....	39
Table V.1 - Deviation of model values of pit depth from actual values.....	60
Table V.2 - Deviation of model values of pit density from actual values .....	61
Table V.3 - pH of sodium carbonate and soap solution.....	66
Table V.4 - Statistical analysis (sample number 1, etched at 6 volts for 20 seconds using soap concentration of 2.5%).....	68
Table V.5 - Comparison with image tool (sample number 1, etched at 6 volts for 20 seconds using soap concentration of 2.5%) .....	69
Table V.6 - Final analysis for etched wire .....	71
Table V.7 – Comparison of average adhesion strength between etched and unetched wire .....	83
Table V.8 - Comparison of theoretical and experimental value of pull out force .....	83
Table C.1 - Statistical Analysis (sample 2).....	106
Table C.2 - Statistical analysis (sample 3).....	107
Table C.3 - Statistical analysis (sample 4).....	108
Table C.4 - Statistical analysis (sample 5).....	109
Table C.5 - Statistical analysis (sample 6).....	110
Table C.6 - Statistical analysis (sample 7).....	111

## I. INTRODUCTION

Angioplasty over the years has proven to be an excellent substitute for open heart surgery where in the blocked artery is expanded with the help of a metallic stent. The manufacture of metallic stents is a very intricate process and great care has to be exercised. But metallic stents still face limitations due thrombogenicity. This has led to the manufacture of coated stents.

The human heart pumps blood to various parts of the body, overtime, a substance called as atheroma starts depositing on the arteries as shown in Figure I.1. This narrows down the cross section of the arteries. When the situation becomes bad it leads to heart attacks which could be fatal.

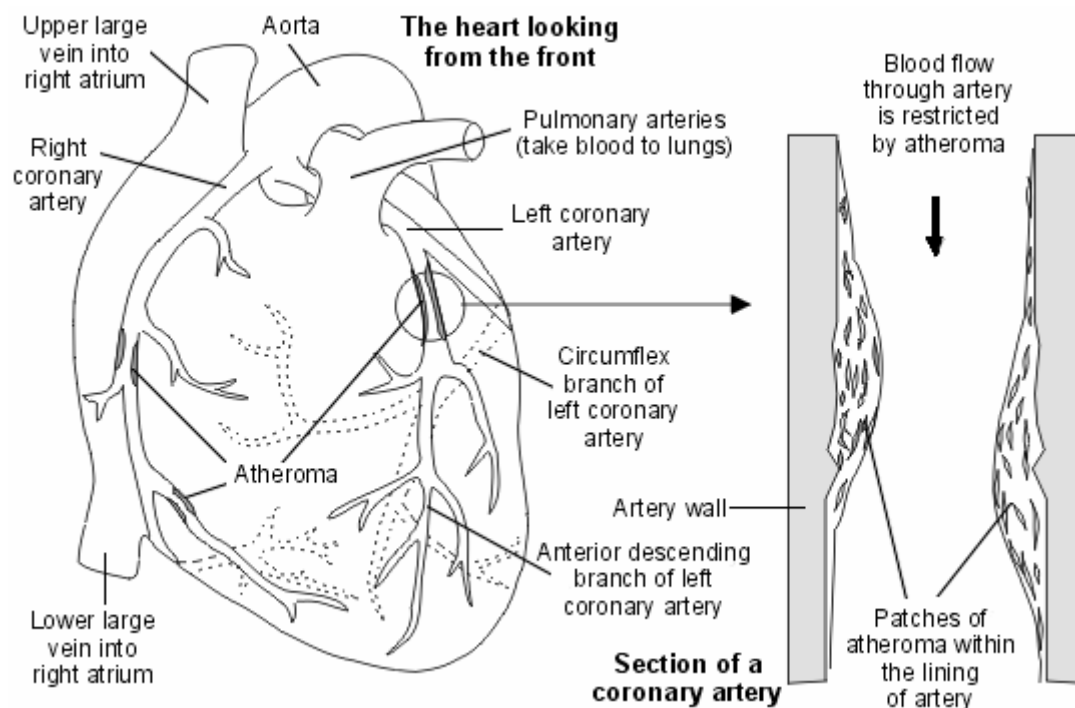


Figure I.1 - Artery with lining of atheroma (Patient-uk, 2005)

---

This thesis follows the format of the International Journal of Machining Science and Technology.



The first successful angioplasty was performed in 1977 and since then it has been used for bringing blood flow to normal in the human body (Ruygrok, 1996).

An angioplasty is a medical procedure that opens up blocked or narrowed blood vessels without surgery. A catheter is placed (a small tube with a balloon on the end) into the blocked or narrowed artery. X-ray and x-ray dye (contrast) are used to help guide the catheter into the correct place in the vessel for the angioplasty. The balloon inflates after it is placed in the narrowed area. Inflating the balloon stretches out the artery, improving blood flow through the area as shown in Figure I.2.

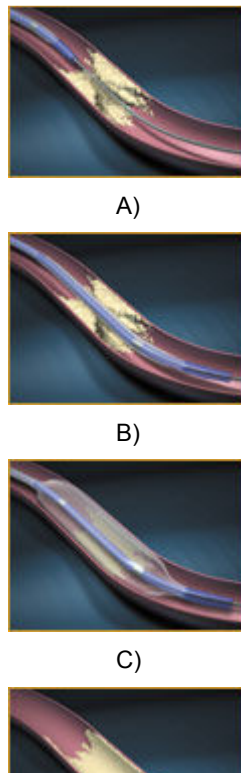


**Figure I.2 - Angioplasty using a balloon. The block is located (B) The balloon is placed in line with the block (C) The balloon is expanded (D) The blood flow is improved (Abbot vascular, 2005)**

The drawbacks of using only a balloon for the angioplasty is, that the there is no force to hold the artery back in its position. This led to the implant of small metallic objects in

the artery known as stents. Stents are small, metal scaffolds similar in size and shape to the spring found in a ballpoint pen.

Before stent implantation, the blocked artery is usually treated and dilated with one or more angioplasty balloons. A stent is tightly mounted on a special angioplasty balloon, this is then guided to the site of the blockage. The angioplasty balloon is inflated to stretch open the stent and implant it into the walls of the blocked artery. The balloon is deflated and removed, and the stent remains permanently in place to hold the artery open as shown in Figure I.3.

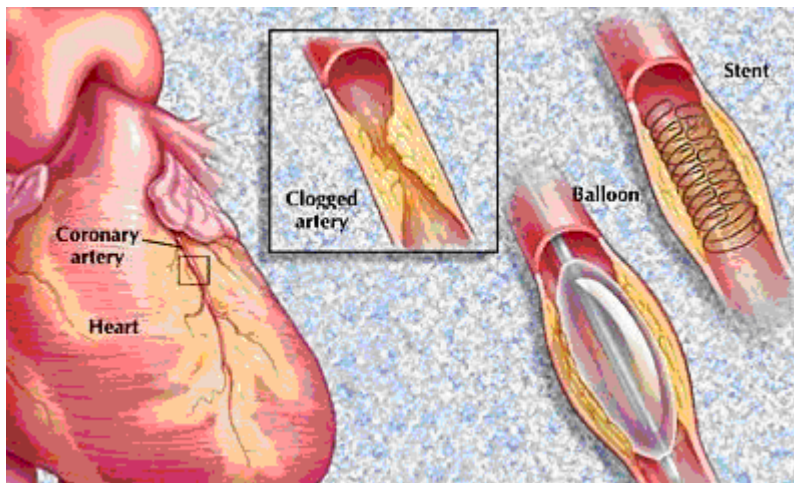


**Figure I.3 - Use and deployment of a metallic stent (Mayo clinic, 2005)**

Metallic stents are very small and hence they require precision manufacturing. Metals such as medical grade stainless steel and shape memory alloy nitinol are commonly used as stent materials.

There are many draw backs of using metallic stents. Stent alloys like stainless steel release cytotoxic heavy metal ions, which are potential inducers of allergies, clotting, immune reactions and hyperproliferation of smooth muscle cells and they also lead to protein absorption which activates clotting factors. Since metallic surfaces are not haemocompatible, metal surfaces inhibit growth and adhesion of endothelial cells (Plasmachem, 2006).

The problems associated with metallic stents led to stents which were coated with substances which could increase haemocompatibility, coated stents have reduced the problems associated with the metallic stents, but post operation problems still persist. This is the reason why, the use of a hybrid stent made of stainless steel and biodegradable polymer has been proposed. Manufacturing this kind of a stent would require good adhesion between metal and polymer while the stent is expanding inside the artery. This project deals with the ways of enhancing adhesion between metal and polymer without using any adhesives but rather by providing micromechanical interlocking between metal and polymer.

## II. OBJECTIVE AND SCOPE

The objective of the project is to study adhesion and shear strength of molded plastics on metal wires.

The scope of the project would be to

Develop appropriate etching technique for stainless steel to enhance interlocking.

1. Create a statistical model for adhesion.
2. Verify the model with experiments using 304 stainless steel and high density polyethylene (HDPE).

### III. LITERATURE REVIEW

#### III.1 Stent materials and adhesion

##### III.1.1 Metallic materials

The most common materials used in manufacture of stents are alloys of nickel and stainless steel, stainless steel is used for its corrosion resistant nature. The 304 and 316L stainless steel are commonly used in biomedical applications including stents. Usually stainless steel has to be treated to get rid of sharp burrs which might lead to neointimal hyperplasia (Bhuyan, 2005).

With the discovery of shape memory alloys, materials like nitinol have taken priority over stainless steel. US Naval Ordnance discovered the shape memory effect for the binary intermetallic compound NiTi in 1963. Nitinol has two interesting properties the one-way effect and hyperpseudoelasticity. Both rely on a diffusionless (lattice shearing) transformation from a high temperature 'austenite' (face-centered cubic) phase to a low temperature martensite (body-centered tetragonal) phase. When the load is removed from a deformed nitinol alloy, it does not change shape. However, when heated, all atoms return to their original lattice positions. This interesting phenomenon is used in stents for expanding them inside arteries. The disadvantages of using metallic stents has been mentioned in the introduction (Turner, 2001).

##### III.1.2 Biodegradable polymers

The hybrid stent is a combination of stainless steel and biodegradable polymer, such as polycaprolactone. This review covers the behavior of biodegradable polymers and discusses a few of the popular ones in detail. Biodegradable polymers are materials which can reduce in mass and size with time while functioning in an organism. The interesting properties of these biodegradable polymers have made them very popular in the field of biomedical engineering (Piskin, 1994).

The Food and Drug Association (FDA) allows the use of four major polymers in the body, namely polylactic acid, polydioxanone, polyglycolic acid and polycaprolactone

(Suji, 2001). Some polymers like polyhydroxybutyrate have also been tried for manufacturing stents. The following sections discuss some of the polymers in detail.

### III.1.2.1 Polylactic acid

Polylactic acid (PLLA) can be directly polymerized by heating, but the polymer obtained is of low molecular weight. Polylactides with higher molecular weight are obtained by ring opening polymerization. Polylactic acid exists in two chiral forms, l and d. The l form is about 40% crystalline and the d form is completely amorphous. Because of superior mechanical properties and lesser degradation rate PLLA is more commonly used in stents. The structure of PLLA is given in Figure III.1. (Hartmann, 1994).

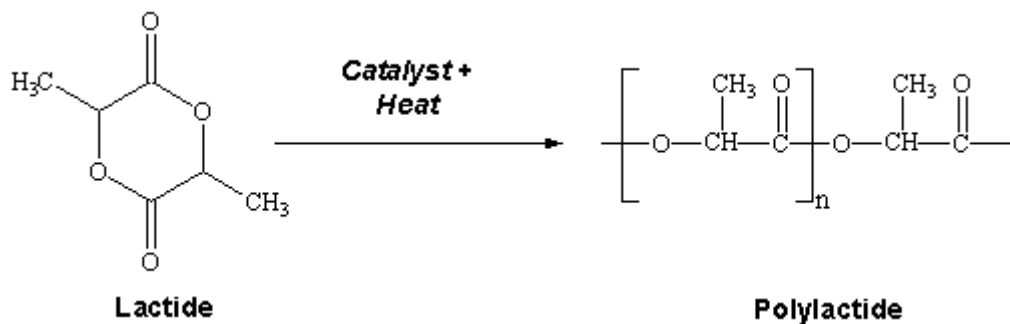


Figure III.1 - Ring opening and structure of PLLA (Hartmann, 1998)

### III.1.2.2 Poly E-Caprolactone

Polycaprolactone was first synthesized by Carothers by ring-opening polymerization of E-caprolactone. It is a hydrophobic semicrystalline polymer (Kharas, 1994). It is in a rubbery state at room temperature. Polycaprolactone has good water, oil and solvent resistance. It has a low melting-point (58-60 °C) and low viscosity. It is easy to process. Polycaprolactone has high permeability which has made it a good candidate for drug delivery systems (Colombo, 2000). The ring opening of e-caprolactone to form polycaprolactone is shown in Figure III.2

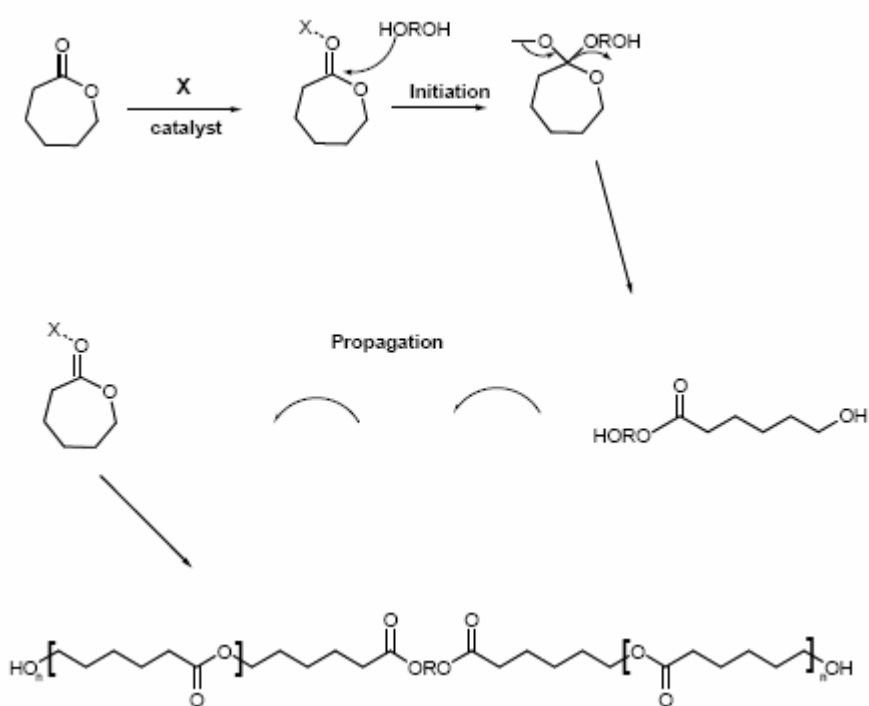
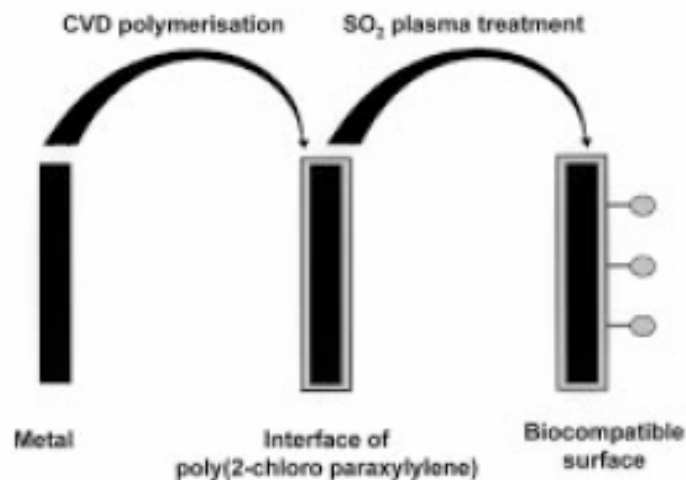


Figure III.2 - Ring opening and structure of polycaprolactone (Solvay, 2004)

### III.1.3 Coated stents

#### III.1.3.1 Polymeric coating

This method deployed the use of polymers to increase the haemocompatibility and decrease the platelet adhesion. Figure III.3 represents how the process was carried out. The basis for this method was chemical vapor deposition. The polymer was passed through a vaporizer and after pyrolysis at a controlled temperature and pressure. The polymer was deposited on the metallic stent in the deposition chamber. Figure III.4 compares a coated stent with a non-coated stent, it was seen that the surface of the coated stent was less rough than the non coated stent. This leads to reduced platelet adhesion in the arteries (Dklee, 1999).



**Figure III.3 - Use of chemical vapor deposition to coat metallic stents with polymers (Dklee, 1999)**



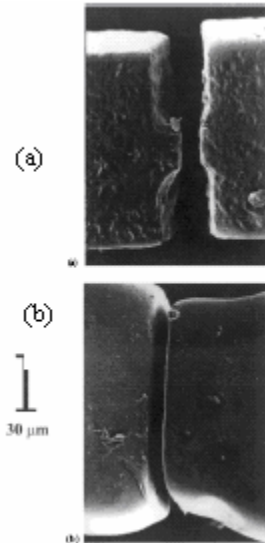


**Figure III.4 - Surface difference between coated and non coated stents (a) Non-coated stent (b) Coated stent (Dklee, 1999)**

### **III.1.3.2 Semiconductor coating**

Lately, semiconductors have also found applications in coating stents. In this method stents were coated with amorphous silicon carbide. The stents coated with amorphous silicon carbide have increased haemocompatibility. Further silicon carbide reduces the chemical reactions and protein degeneration which is a problem in metallic stents (Bolz, 1996).

### III.1.3.3 Elastomeric coating

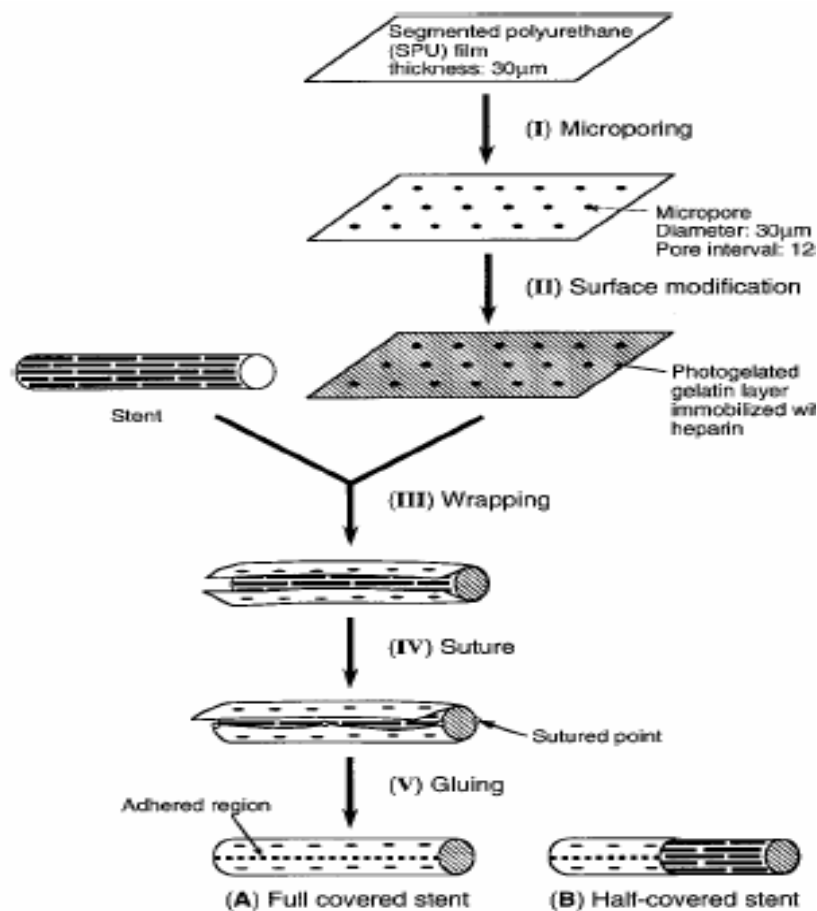


Figure III.5 - Coating stents using elastomeric films (Nakayama, 2002)

Figure III.5 represents how elastomeric films can be used to coat stents. In this process a segmented polyurethane film was first isolated. This was followed by microporing of the film. The surface of the micropored film was modified using photolithography. This film was then wrapped around the surface of the stent and then glued to the surface of the stent using a binder. This process prevents thrombus formation in the acute phase and restenosis in the sub acute to chronic phase after stenting (Nakayama, 2002).

The above mentioned methods have made use of chemical methods for coating stents. This review of methods has shown the advantages of coating stents, but even after significant advancements made in the field of coated stents, problems persist in the long term use of these stents.

### III.1.4 Mechanisms of adhesion

Many theories have been proposed to understand adhesion. The following paragraphs would discuss some of the popular theories of adhesion.

#### III.1.4.1 Electronic theory

The electronic theory of adhesion was proposed primarily by Deryaguin et al in 1948. They suggested that an electron transfer mechanism between the substrate and the adhesive, having different band structures can occur to equalize Fermi levels. This could induce the formation of an electrical double layer at the interface and this resulting electrostatic force contributes significantly to adhesive strength. Figure III.6 shows the charges developed on the surface of the adhesive and the substrate (Pizzi, 2003).

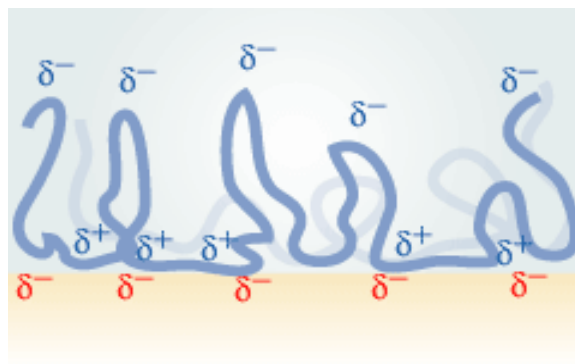


Figure III.6 – Charges developed on the substrate and adhesive (special4chemadhesives, 2007)

#### III.1.4.2 Theory of weak boundary layers

The first approach to this problem is due to Bickerman who stated that the cohesive strength of the weak boundary layer can always be considered as the main factor in determining the level of adhesion, even when the failure appears to be interfacial. According to this assumption, the adhesion energy is always equal to the cohesive energy of the weak interfacial layer. This theory is based primarily on probability considerations

showing that the fracture should never propagate only along the adhesive substrate interface for pure statistical reasons and that cohesive failure within the weaker material near the interface is a more favorable event (Pizzi, 2003).

### III.1.4.3 Adsorption theory

The adsorption model of adhesion is one of the most widely used approaches in adhesion science. This theory is based on the belief that the adhesive will adhere to the substrate because of interatomic and intermolecular forces established **at** the interface. The most common forces result from van der Waals forces as shown in Figure III.7 (Pizzi, 2003).

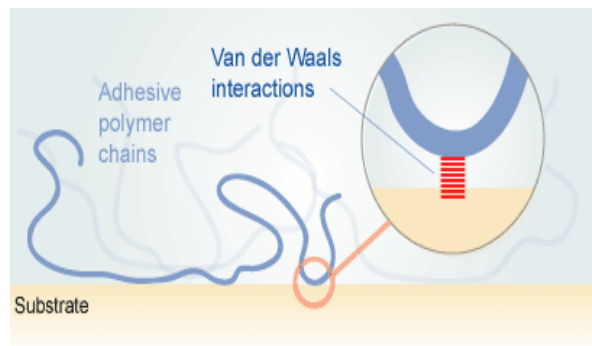


Figure III.7 – Adsorption theory of adhesion (special4chemadhesives, 2007)

### III.1.4.4 Diffusion theory

The diffusion theory of adhesion is based on the assumption that the adhesion strength of polymers to themselves or to each other is due to mutual diffusion of macromolecules across the interphase. Such a mechanism implies that the macromolecular chains are sufficiently mobile and mutually soluble. Figure III.8 shows the inter diffusion process in polymers (Pizzi, 2003).

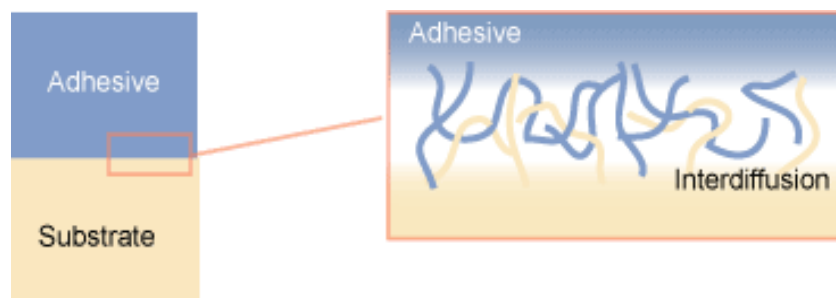


Figure III.8 – Diffusion theory of adhesion (special4chemadhesives, 2007)

#### III.1.4.5 Chemical bonding theory

It is understandable that chemical bonds formed across the adhesive-substrate interface can greatly participate to the level of adhesion between both materials. These bonds are generally considered as primary bonds when compared with physical interactions. The formation of chemical bonds depends on the reactivity of both adhesive and substrate. Figure III.9 shows the chemical bonding between the adhesive and the substrate (Pizzi, 2003).

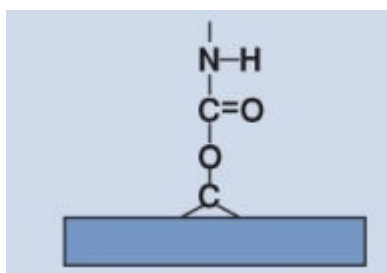
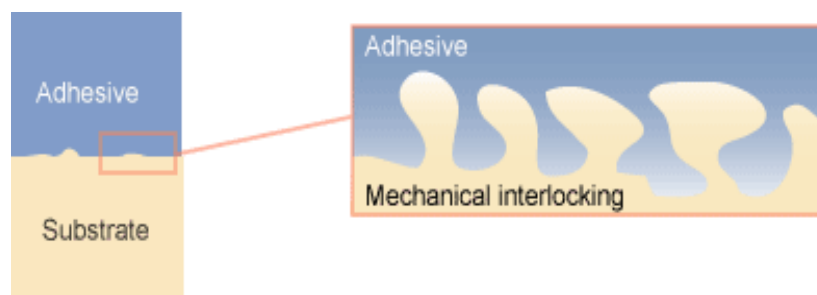


Figure III.9 – Chemical bonding theory of adhesion (DSM, 2007)

#### III.1.4.6 Mechanical interlocking

The mechanical interlocking model was proposed by MacBain and Hopkins in 1925. This model conceives the mechanical keying or interlocking of the adhesive into the cavities, pores and asperities of the solid surface to be the major factor in determining

the adhesive strength. Figure III.10 shows the principle behind mechanical interlocking (Pizzi, 2003).



**Figure III.10 – Mechanical theory of interlocking (special4chemadhesives, 2007)**

### III.1.5 Metal – Polymer adhesion

The hybrid stent would employ the use of biodegradable polymer and stainless steel, the presence of a binder to join them would complicate the manufacturing process. Since adhesion cannot be achieved between metal and polymer using binders or any other chemical process, the only solution is to provide mechanical interlocking which can keep the metal polymer joint from moving. Ways of achieving mechanical interlocking and have been discussed in the following sections.

#### III.1.5.1 Micro sand blasting

Sand blasting is a mechanical way of increasing the surface roughness of a material. Figure III.11 shows an SEM picture of a machined surface of titanium. Figure III.12 shows the SEM of titanium which was sand blasted and acid treated to get rid of the burrs. The difference in the two surfaces can clearly be seen. The surface of the sand blasted and chemically etched titanium was rough and has micro pores (Buser, 1998).

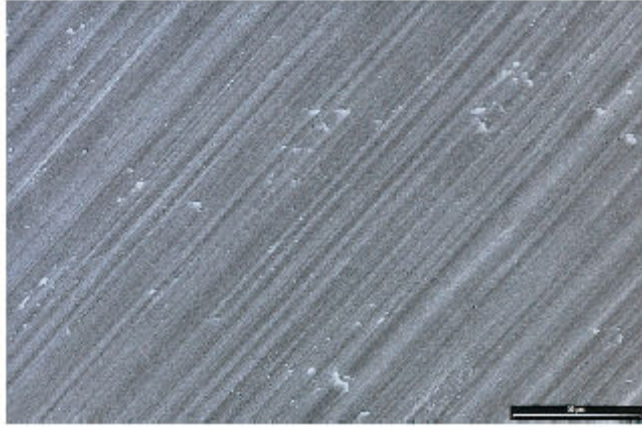


**Figure III.11 - SEM view of a machined surface of titanium (Buser, 1998)**

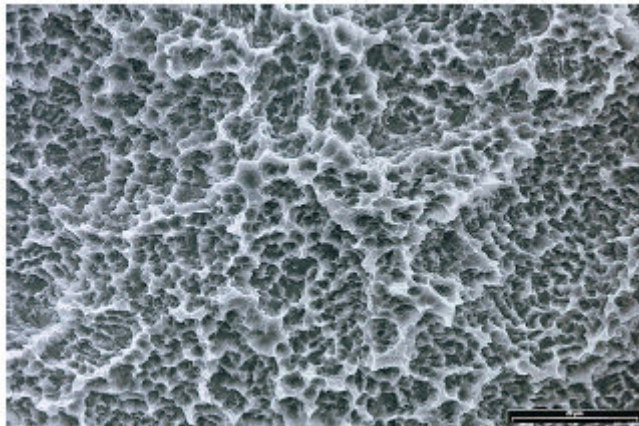


**Figure III.12 - SEM view of a sand blasted and acid treated surface of titanium (Buser, 1998)**

### **III.1.5.2 Vacuum Plasma Spray**

The vacuum plasma spray method employs the use of metallic or ceramic powder which is in the order of 10-50 microns. This ceramic powder is released along with the hot plasma gas at 10000° K. This results in the formation of a substrate with micro pores. This can be used to achieve metal polymer adhesion (Buser, 1998). The effect of plasma spraying can be seen in Figure III.13.

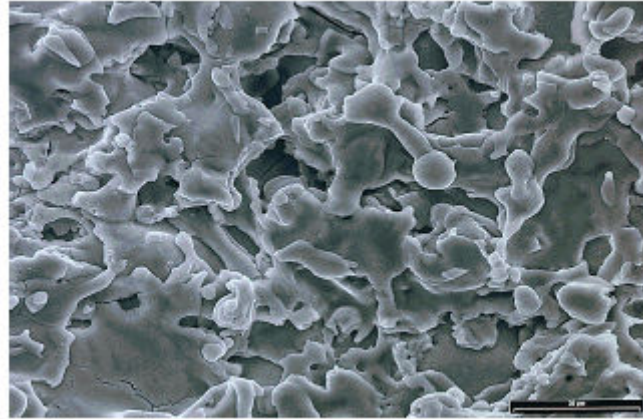


**Figure III.13 - SEM view of a Vacuum Plasma Spray treated surface of titanium (Buser, 1998)**

### **III.1.5.3 Pitting**

Pitting or pitting corrosion is a localized form of corrosion, it leads to the creation of small craters in metals and this phenomenon is mainly due to the lack of oxygen in localized parts of the metal. These parts with lack of oxygen become the equivalent of an anode in an electrochemical cell and the parts with excess of oxygen become the cathode. This leads to the completion of localized galvanic corrosion. This phenomenon is commonly noticed in alloys like stainless steel, nickel alloys and aluminum alloys.

It is observed that pitting is prominent in stainless steel at the chromium depleted zones. There have been several attempts to model the effect of pitting, but pitting is a complex phenomenon and requires insitu observation in order to establish a definite relation between the complex parameters. Figure III.14 shows an atomic force microscopic measurement of a pit (Zhang, 2004).



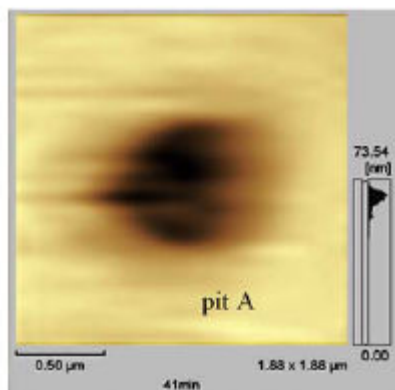


**Figure III.14 - AFM image of solution-treated SUS304 stainless steel during corrosion in 3.5 wt% sodium chloride solution at 298K,  $I = 10\text{A/m}^2$  (Zhang, 2004)**

#### **III.1.5.4 Adhesive forces between metals and polymers**

There are a number of theories established to understand metal polymer adhesion, and in this case since there is no adhesive binder being used, the adhesion mainly arises due to interlocking between the two surfaces.

Previous work in this field has been covered (Lee et al, 2003). The surface modification was done on a Cu based alloy leadframe (commercial name: EFTEC-64t), sodium hydroxide and sodium phosphate based hot alkaline solutions were used to form a black oxide layer on the alloy. Figure III.15 shows the SEM micrograph of the oxidized lead frame surface after an oxidation time of 1 minute. The oxidized samples were molded with epoxy molding compound (EMC) into a sandwiched double cantilever beam structure. The rough surface of the alloy facilitated better interlocking between metal and polymer.

The adhesion strength was based on the fracture toughness of the oxides. For the samples which had not been oxidized the fracture toughness was nearly zero. There was an increase in fracture toughness with oxidation time. The samples were tested mechanically and the failure path of the material was developed. The path was formed based on the detachment of the  $\text{Cu}_2\text{O}$  needles from the leadframe. Further, an adhesion model was formed and an analysis was done to show how the material fails (Lee et al, 2003).

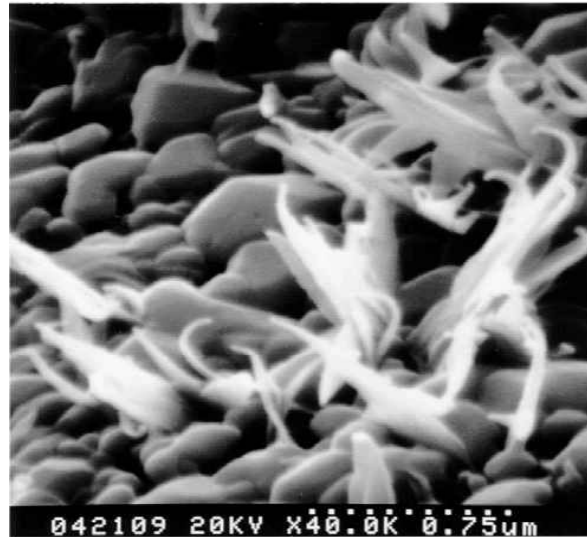


**Figure III.15 - SEM micrograph of oxidized leadframe surface (Lee et al, 2003)**

There are more theories which explain friction and adhesion theoretically. According to these theories the resistive forces on rough surfaces develop due to true contact area between asperities. This was proven using analytical results which showed that with the increase in the surface roughness there was an increase in coefficient of friction, which agreed well with experimental results (Karpenko, 2001).

Kragelsky made an attempt to relate friction to elastic deformation and shear strength of adhesion, the author assumed that the asperities are a collection of unequal elastically deformable rods and used a statistical analysis to predict the linear height distribution of the rods whose ends were assumed to be fixed (Kragelsky, 1965).

Greenwood and William modeled the contact of rough surfaces assuming that the surfaces are composed of hemispherically tipped asperities. The asperities were given a Gaussian distribution across the plane. The equivalent rough surface was estimated by summing up the heights, which helped in getting an effective elastic modulus (Greenwood, 1966).

Adhesion models require to be backed by experimental data. A simple experimental setup used is demonstrated in Figure III.16. In this experiment the

interfacial strength between composites was determined by molding an epoxy microbead on a glass fiber. The experiment was done with different samples of glass; some of them were not treated and some of them were treated with different concentrations of 3-aminopropyltriethoxysilane. The interfacial bond strength of the composite was measured using a pullout test. The results of the test are given in Figure III.17 (Qian, 1994). From the graph it can be seen that there is a sharp drop in the force after the sample was pulled out for some time, this point represents the maximum adhesive strength of the epoxy bead on the glass rod.

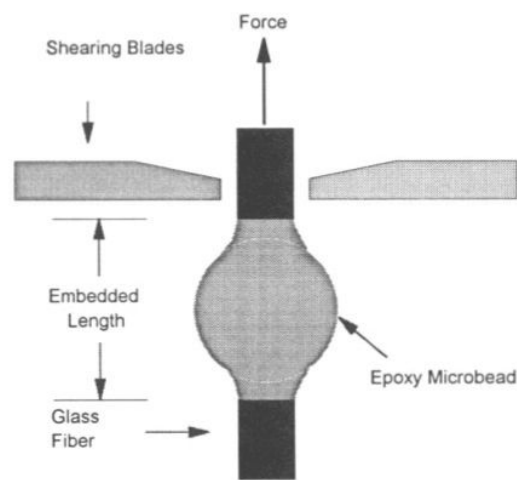


**Figure III.16 - Experimental setup for pull out test (Qian, 1994)**

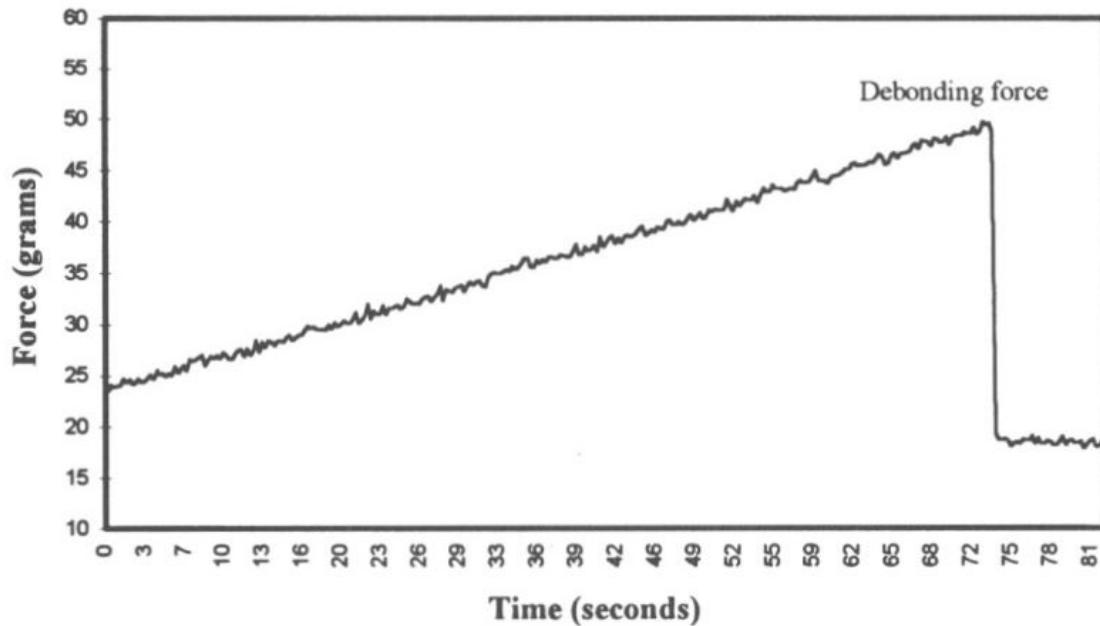
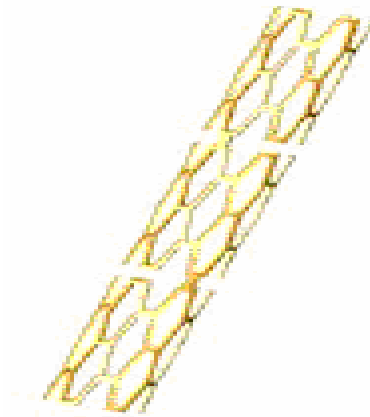


Figure III.17 - Force vs Time plot (Qian, 1994)

## III.2 Stent manufacture

### III.2.1 Investment casting

Investment casting can be used to make complex 3 dimensional shapes and structures. Figure III.18 shows a stent which was prepared using investment casting method. The investment casting process involves creating a wax pattern, this pattern was invested into a ceramic slurry which was dried and dewaxed in a steam autoclave. The mold was then fired. Followed by this the mold was preheated to an elevated temperature and then the alloy was poured into the investment. After solidification of the alloy the cast was removed with a high pressure water jet (Bohman, 1995).



**Figure III.18 - Palmaz stent (Bohman, 1995)**

### III.2.2 Laser processing

The laser source used for this process was an Nd-YAG laser. The use of laser in combination with rapid prototyping provides a convenient way to make complex 3 dimensional shapes. Figure III.19 illustrates how a laser was used for manufacturing stents. The laser beam provides the required energy to cut the metal in the desired shape (Manufacturelink, 2007).



**Figure III.19 - Laser machining (Manufacturelink, 2007)**

Alternative technique was laser sintering to form a desired 3 dimensional shape. The powders were binded upon, compacted and laser heated. Figure III.20 shows a stent which was manufactured by laser sintering (Kathuria, 1998).

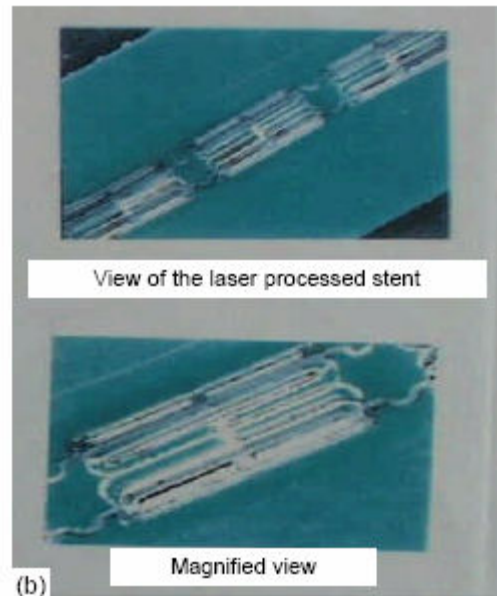


**Figure III.20 - The view of a laser micro processed stent using sintering (Kathuria, 1998)**

### III.2.3 Biodegradable stents

Biodegradable stents were first made not only to reduce platelet adhesion but also combat restenosis. The first biodegradable polymer used to make stents was polylactic acid. Stack et al (2004) at Duke University developed the first biodegradable stent and implanted it in animals. Figure III.21 (a) shows the helical geometry of the stent and III.21 (b) shows the porous structure of the stent. A polymer of poly-l-lactide was used for this prototype stent, which could withstand up to 1000 mm Hg of crush pressure and keep its radial strength for 1 month. The stent was almost completely degraded by 9 months. Subsequent clinical research with this device remained limited, despite the presence of minimal thrombosis, moderate neointimal growth and a limited inflammatory response in these early animal implants (Vogt, 2004).

Despite the early promise shown by biodegradable stents, interest in early biodegradable stents faded after experimentation with other polymers which demonstrated significant inflammatory response and neointimal growth. More recently the possibility of using biodegradable stents as a vehicle for local drug delivery has prompted the research in biodegradable polymer stents. In addition to problems like

initial inflammatory response there have also been problems associated with loss of radial strength.

The problems associated with the biodegradable stents and the metallic stents (discussed in the introduction) have led to the concept of hybrid cardio vascular stent using metal and biodegradable polymer.

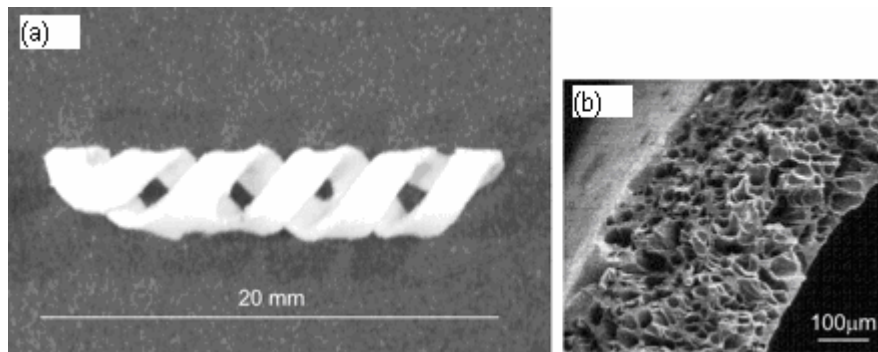


**Figure III.21 – (a) Helical geometry of stent (b) cross section of the stent (Vogt, 2004)**

### **III.3 Insert molding**

Insert molding is a process in which plastic is injected into a mold that contains a pre -placed insert. The result of insert molding is a single molded plastic piece with an insert surrounded by the plastic. Inserts can be made of metals or different types of plastic. Insert molding has been used in many industries. Applications of insert molding include insert-molded couplings, threaded fasteners, filters, and electrical components. Figure III.22 demonstrates how insert molding can be used to mold plastics over metallic inserts (Tuthill, 2007).



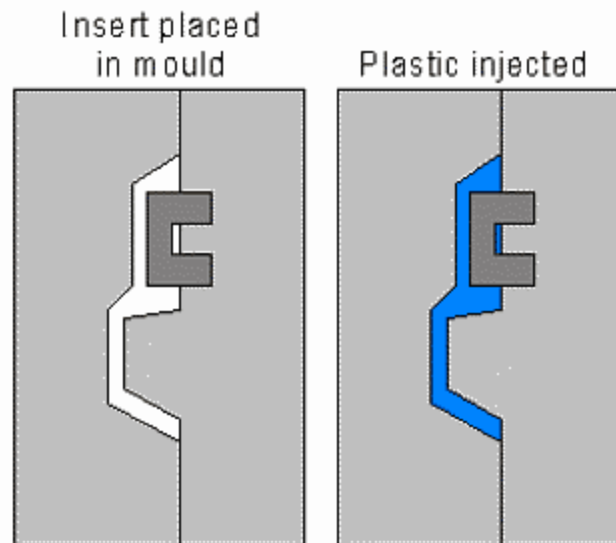


Figure III.22 - Insert molding to mold polymer around a metallic insert (Designinsite, 2007)

### III.4 Electrochemical etching

Electrochemical etching is a method by which surface modification of metals is achieved by dipping into an electrolyte and passing voltage through the metal on which surface modification is to be performed. The surface modification is a function of the voltage, the concentration of the electrolyte and the time for which the metal is exposed to the electrochemical reaction. In an electrochemical etching process the rate of removal of the material  $m$  is given by the equation III.1, for alloys the material removal rate  $m_a$  is given by equation III.2 (McGeough, 1974).

$$m = \frac{AI}{zF} \quad (\text{III.1})$$

Where,

A = Atomic weight

z = Valency

I = Current

F = Faraday's constant

$$m_{\text{alloy}} = \left(\frac{A}{z}\right)_{\text{alloy}} \frac{I}{F} \quad (\text{III.2})$$

Where,

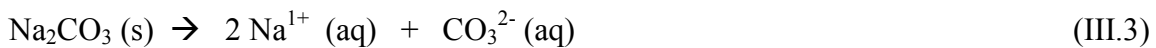
$$\left(\frac{A}{z}\right)_{\text{alloy}} = \frac{1}{100} \left[ X_a \left(\frac{A_a}{z_a}\right) + X_b \left(\frac{A_b}{z_b}\right) + X_c \left(\frac{A_c}{z_c}\right) + \dots \right]$$

$X_i$  = Weight percentage of alloy component i

$A_i$  = Atomic weight of each element i

$z_i$  = Valency of element i

Pitting of stainless steel happens due to corrosion on the chromium depleted zones. When the carbide is near the surface, protective passive film cannot be formed on Cr-depleted zone and pitting preferentially occurs at the zone, Figure III.23 (a). With the early dissolution of Cr-depleted zone, the corrosion product forms and covers the carbide, Figure III.23 (b). Under this condition, the mass transfer of ions between outer and inner of the pit becomes difficult. The presence of current accelerates the dissociation of sodium carbonate into sodium ions and carbonate ions (Equation III.3). At the same time water also dissociates to form hydrogen and hydroxide ions (Equation III.4). The presence of carbonate ions and hydrogen ions in the depleted zones decreases the pH and leads to acceleration in corrosion of the pit walls and the carbide (Figure III.23 (c)) (Zhang, 2005).



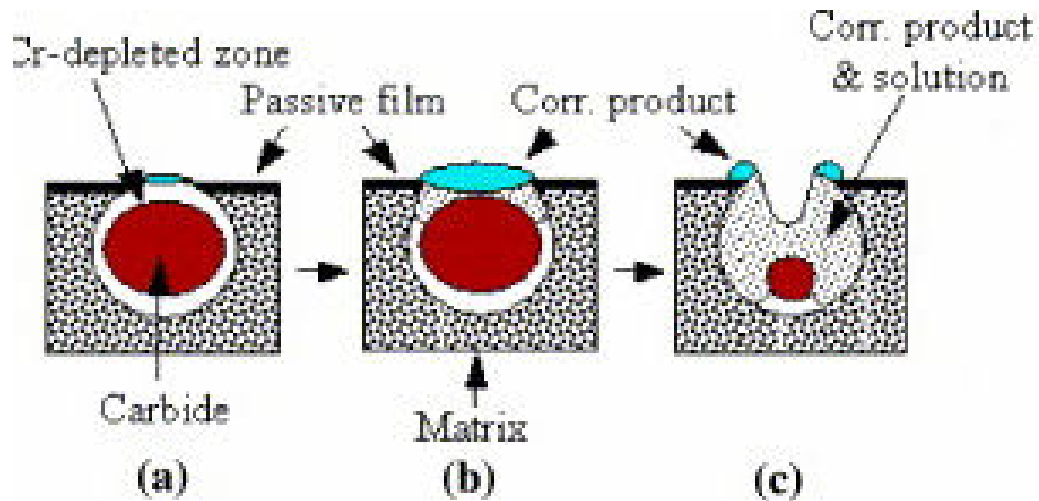
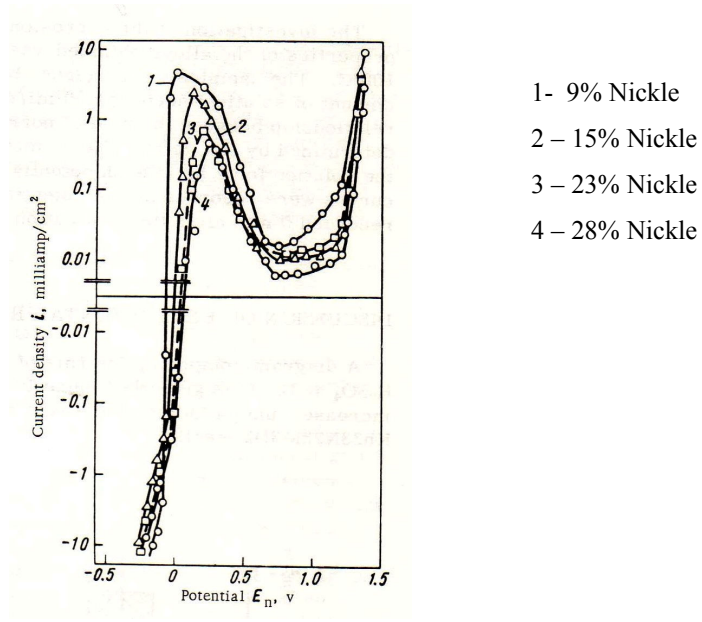


Figure III.23 - Pitting of stainless steel (Zhang, 2005)

#### III.4.1 Passivity

When an alloy like stainless steel is immersed in a concentrated solution, it is seen to immediately react with the solution, but after a while the reaction stops and the alloy enters a passive zone. This passive zone occurs due to the formation of a thin non porous oxide film, since the thickness of the film is below the wavelength of visible light and hence the film is transparent. At higher potentials this passive film is broken down and the alloy enters the transpassive zone where the depletion of the alloy starts again. Figure III.24 gives a graphical representation of this phenomenon on four stainless steels with varying nickel contents (Tomashov, 1965).



**Figure III.24 - Variation of current density with potential of four stainless steels with different nickel contents in 35% H<sub>2</sub>SO<sub>4</sub> at 40 oC (Tomashov, 1965)**

### III.4.2 Effect of pH

The acidic level or pH has a significant effect on corrosion rate. Figure III.25 shows the typical behavior of iron, mild steels and low alloy steels in aqueous electrolytic solutions. It can be seen from the graph that the rate of corrosion increases as the pH decreases (Kaesche, 2003). The pH level affects etching rate, therefore, will be useful for subsequent experiments.

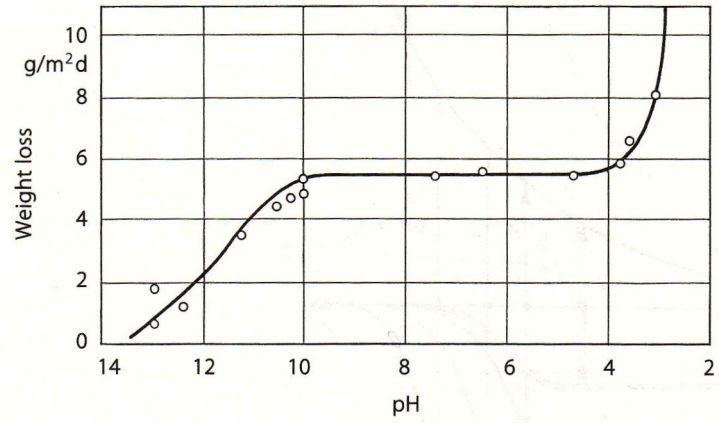


Figure III.25 - Variation of corrosion rate in solutions of different pH (Kaesche, 2003)

## **IV. EXPERIMENTS**

The objective of this study is to enhance metal polymer adhesion. This would find applications in manufacturing a hybrid cardiovascular stent. High density polyethylene (HDPE) was used instead of the biodegradable polymer for initial investigation. This section documents the experiment and the test procedure. The results will be presented and discussed in the next section.

### **IV.1 Surface preparation**

The use of adhesives is usually required to join two surfaces of different surface energies such as metal and polymer. Since the use of adhesives in sensitive areas is not desirable, the adhesive strength of the two surfaces can be increased by increasing surface roughness of either one of the surfaces. This would lead to enhanced micromechanical interlocking between stainless steel and polymer. To achieve this, various techniques to treat the surface of the metal will be discussed. The diameter of the wire selected was 0.254 mm. The composition of the 304 stainless steel used was Ni 9.25%, Cr 19.00%, Fe 68.595%, Si 1.00%, Mn 2.00%, C 0.080%, P 0.045%, S 0.030% (ESPI, 2007).

#### **IV.1.1 Mechanical abrasion**

The stainless steel wire was mechanically abraded. This was done using 240 grit size sandpaper. Sanding was done in order to increase the roughness of the material. The effect of sanding was seen when the wire was viewed under an optical microscope. The effect of unidirectional etching was seen on the wire, a ridge type structure was observed. This was good to provide interlocking in one direction but did not assure the same in the other direction. Cross sanding was conducted with the sandpaper of the same grade.

### IV.1.2 Chemical etching

Chemical etching involves the use of concentrated acids to make the required surface modification. To perform the experiment, 20 ml of 35% concentrated HCl was taken and placed under the hood. Different wires were dipped in the acid solution first for 15 minutes then for 3 hours. The wires were cleaned with distilled water and treated with 70% isopropyl alcohol in an ultrasonic bath.

## **IV.2 Electrochemical Etching**

### IV.2.1 Setup

Figures IV.1 and IV.2 show the experimental setup for electrochemical etching. It consisted of a DC supply voltage, a glass beaker, electrolyte, a specially shaped cathode and a non conductive disc to place the cathode. The positive side was connected to the wire which was to be etched, this forms the anode. The negative side was connected to the cathode. Figure IV.3 shows the design for the cathode. The cathode has two styrofoam discs to secure the wire in the center. Figure IV.4 shows the complete drawing with required dimensions.

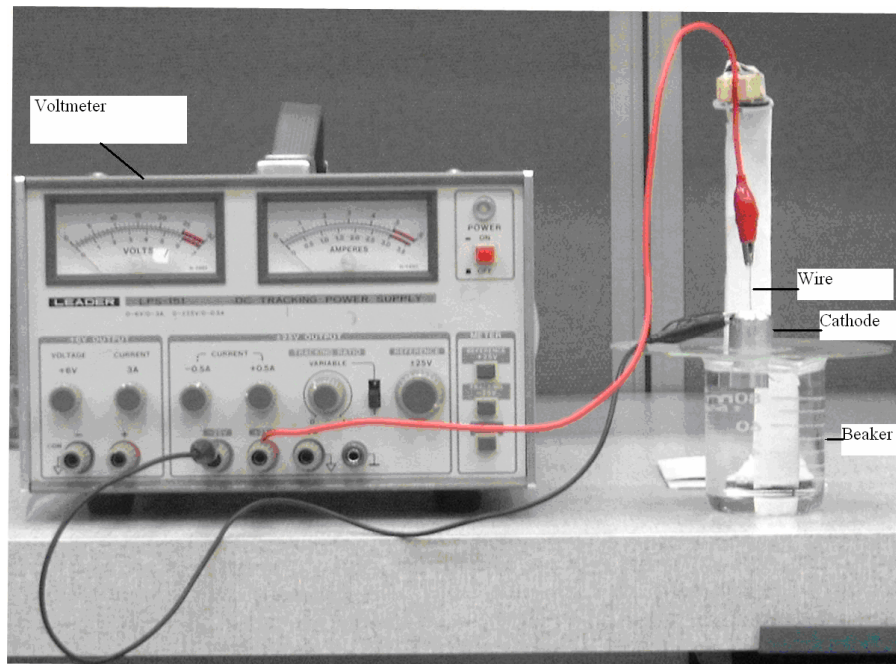


Figure IV.1 - Experimental setup for electrochemical etching

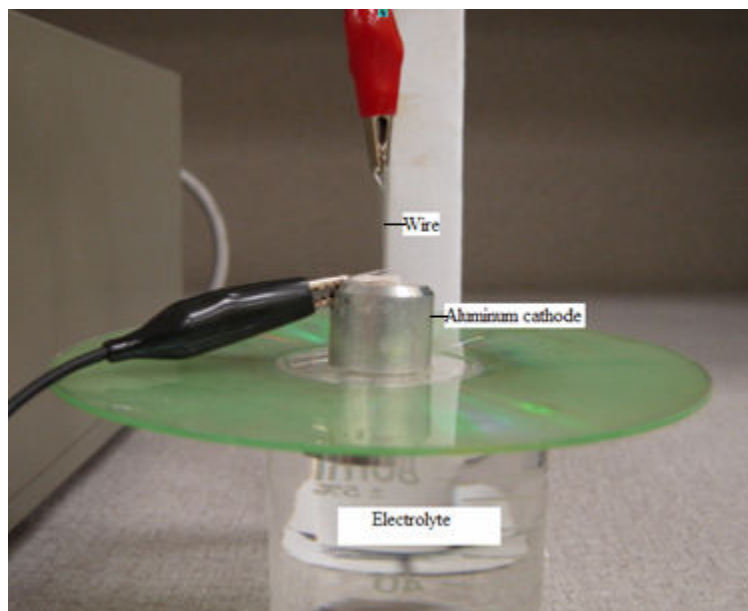


Figure IV.2 - Details of electrolytic cell to etch a stainless steel wire



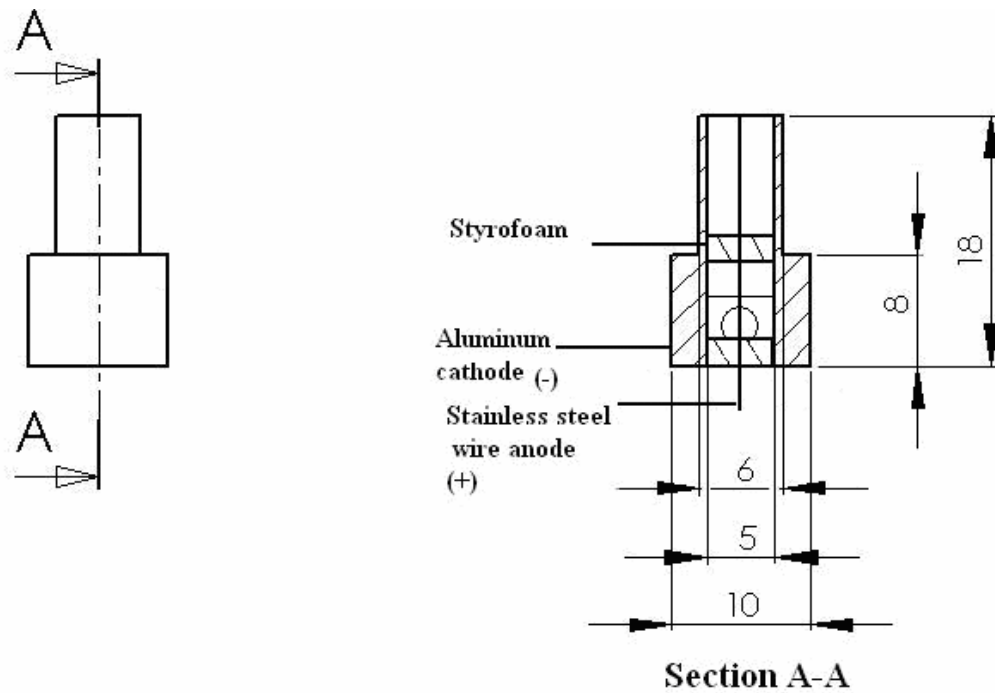


Figure IV.3 - Design for cathode (Material: Aluminum)

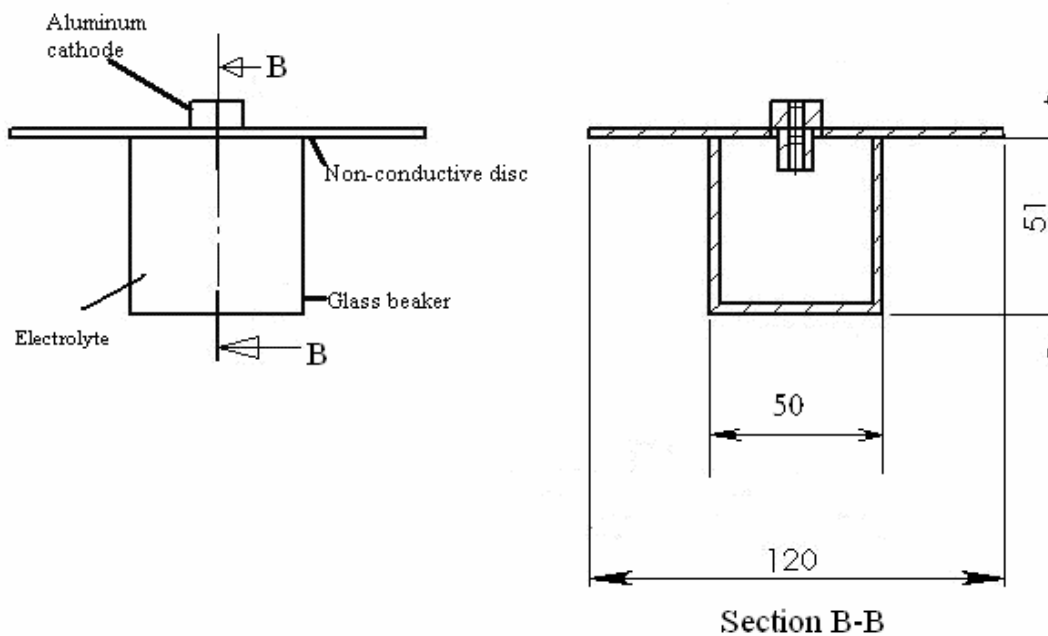


Figure IV.4 -Design of the electrolytic cell (All dimensions: mm)

An electrolyte containing a mixture of water and soap (sodium carbonate, anionic surfactants, sodium silicate, optical brighteners, antired deposition agents and processing acids, brand name “CLASSIC Xtra”) was used. Soap was used because of the presence of sodium carbonate. A pure sodium carbonate electrolyte was also used, the details this experiment are provided in section IV.2.2. The reason for using soap will be discussed in section V.6.2. Voltage was applied for varying time periods in solutions having different concentrations. The experiment was conducted at room temperature and repeated. Table IV.1 gives a range of voltages, times and concentration for which the electrochemical etching was done on the wire. Time of etch was recorded using a stop watch, applied voltage was measured with a voltmeter and the concentration of the electrolyte was varied with a weighing scale (Denver Instrument, Model A-250).

**Table IV.1 - Different conditions of electrochemical etching**

Voltage	Concentration of electrolyte (Soap solution)	Time
3v	5%	10s
3v	5%	20s
3v	5%	30s
3v	2.50%	10s
3v	2.50%	20s
3v	2.50%	30s
6v	5%	10s
6v	5%	20s
6v	5%	30s
6v	2.50%	10s
6v	2.50%	20s
6v	2.50%	30s
12v	5%	10s
12v	5%	20s
12v	5%	30s
12v	2.50%	10s
12v	2.50%	20s
12v	2.50%	30s

#### IV.2.2 Etching with sodium carbonate electrolyte

Etching with sodium carbonate was done to find out which ingredient in the soap causes pitting. A setup similar to Figure IV.1 was used to conduct electrochemical etching on stainless steel using sodium carbonate electrolyte. 2.5% by weight of the electrolyte was used and a voltage of 7 volts was applied for 120 seconds.

### IV.2.3 Measurement of pH

Soap solution and sodium carbonate solution, with 2.5 weight% concentrations were prepared and their pH levels were measured with the Symphony VHR (S870P) pH meter. It was calibrated with a buffer solution of known pH. Figure IV.5 shows the pH meter used for the experiment. The pH meter had a probe attached to it which can be immersed into the solution. The probe was rinsed in distilled water after measuring the pH of each solution to avoid errors.

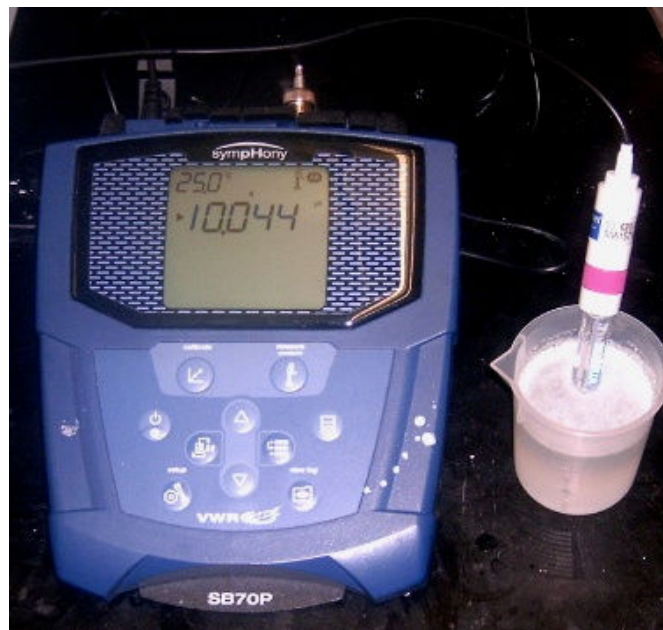


Figure IV.5 - pH measurement

### IV.2.4 Design of experiment

After the initial investigation using Table IV.1, a more structured experiment was done to characterize the effect of parameters. Design of Experiment involves designing a set of experiments, in which all relevant factors are varied systematically. When the results of these experiments are analyzed, they help to identify optimal conditions, rank the factors and establish possible interaction amongst factors.

Design of Experiment was used to find the relation between input parameters (voltage, concentration and time) and out put parameters (pit depth and pit density). The Design Expert software (Version 7.1) was used for conducting the analysis. During the analysis factors like voltage, time and concentration are coded. Because of this two ranges of each input parameter were used and the response variables were entered based on the average of the output parameters over selected areas on the stainless steel wire. Table IV.2 shows the input parameters like time, voltage and concentration which are on and the response or the output parameters like pit depth and pit density.

For performing the analysis the most significant terms were selected out of a half normal plot, this plotted the standardized effects as a function of the half normal percent probability. Once the terms were selected, the software performed an analysis of variation and gave the diagnostics for the function. This included the variation of the predicted value and the actual value and included suggested transformations which could be applied to the input data to get a more accurate model. For pit depth, there was no transformation required but for pit density a log transformation was applied. Details of the analysis can be found in the appendix A.

**Table IV.2 - Input and output data for Design Expert software**

Number	Input factors			Output responses			
	Voltage (volts)	Time (seconds)	Concentration (wt%)	Pit depth ( $\mu\text{m}$ )	Standard deviation for pit depth ( $\mu\text{m}$ )	Pit density (pits/ $\text{mm}^2$ )	Standard deviation for pit density (pits/ $\text{mm}^2$ )
1	6	20	5	13.87	3.33	224.35	45.32
2	12	20	2.5	8.12	1.66	673.07	45.32
3	12	30	2.5	20.62	5.11	96.15	45.32
4	6	20	2.5	16.87	4.78	416.66	45.32
5	12	20	5	7.25	2.06	1410.25	181.30
6	6	30	5	6.5	1.42	673.07	135.98
7	12	30	5	21.12	3.33	160.25	45.32
8	6	30	2.5	12.62	3.16	256.41	90.65

### IV.3 Molding

After etching the wires, the wire was molded with HDPE to test for adhesion strength. The drawing in Figure IV.6 shows the design and dimensions of the first mold used for insert molding. For the second mold (Figure IV.7) a hole of 300  $\mu\text{m}$  was drilled and it was aligned in such a way that when the wire would pass through this mold, the other end would go into the 300  $\mu\text{m}$  slot provided for the wire on mold 1. This arrangement made sure that the wire would remain straight while the polymer was being molded over the metallic wire.

A wire sample was cleaned in an ultrasonic bath using 70% isopropyl alcohol and placed inside the mold. Figure IV.8 shows the cross section of the assembly with the wire inside the mold. The polymer filled the mold through the  $\Phi 3.5$  mm and filled the chamber measuring 9.5 mm to mold around the inserted wire.

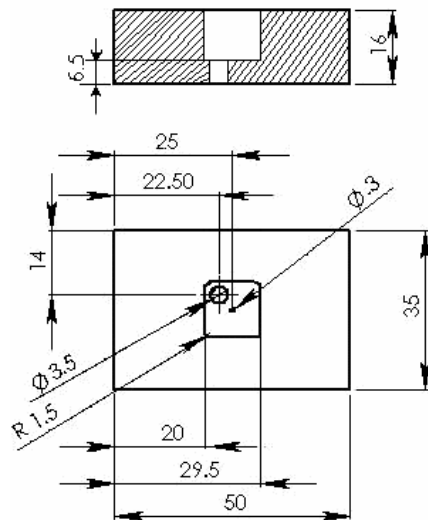


Figure IV.6 - Drawing for mold 1 (Material: aluminum, dimensions: mm);

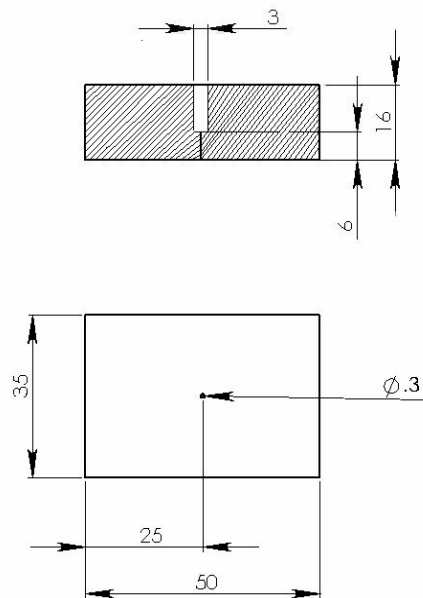
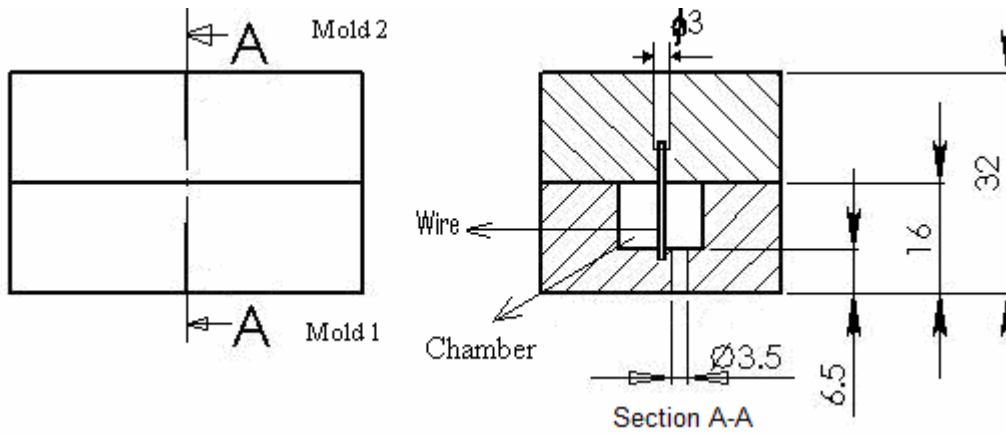


Figure IV.7 - Drawing for mold 2 (Material: aluminum, dimensions: mm)



**Figure IV.8 - Cross-section of the assembly (Material: Aluminum, dimensions: mm)**

#### IV.3.1. Molding machine specifications

The molding was accomplished using the Babyplast 6/10 molding machine (Figure IV.7) manufactured by Ferromatik Milacron. Figure IV.9 shows the molding machine and Figure IV.10 shows the mold inside the machine. The heating elements (Watlow FIREROD) can be seen inside the mold to control the temperature. The Figure IV.11 shows the front view and the side view, with all the parts labeled.





Figure IV.9 - Injection molding machine manufactured by Ferromatik Milacron, Model Babyplast

6/10

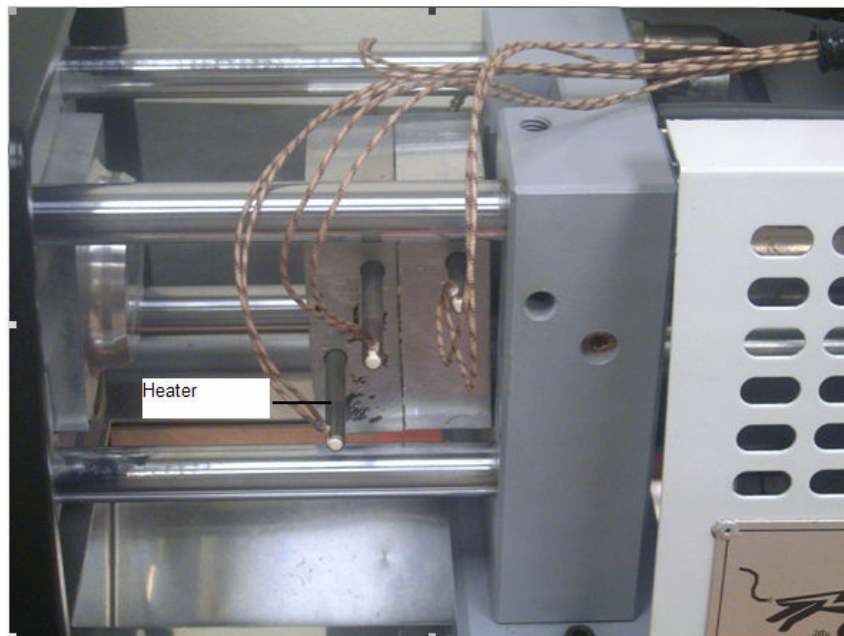
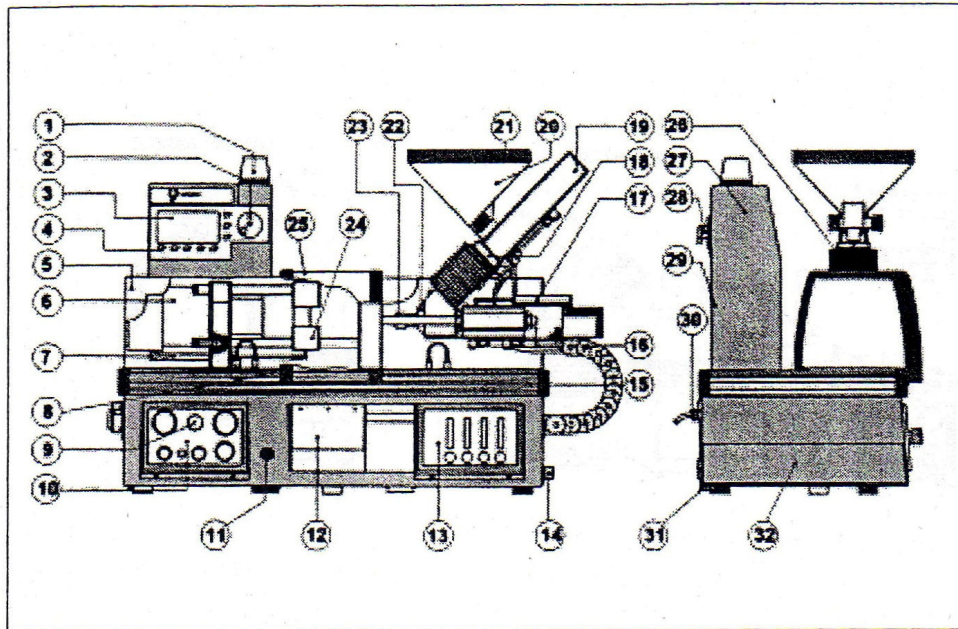


Figure IV.10 - Mold housing in the machine with the heaters for the mold



- |                                    |                                   |
|------------------------------------|-----------------------------------|
| 1-Alarm warning light.             | 17-Transducer - injection piston  |
| 2-Dial for changing data           | 18-Plastification chamber.        |
| 3-Display                          | 19-Injection piston               |
| 4-Function keys.                   | 20-Hopper                         |
| 5-Guard - Clamping piston          | 21-Hopper cover                   |
| 6-Clamping piston                  | 22-Injection chamber              |
| 7-Transducer- clamp.               | 23-Nozzle.                        |
| 8-Hydraulic safety device          | 24-Moving platten                 |
| 9-Emergency stop button            | 25-Transparent gate               |
| 10-Hydraulic control panel.        | 26-Guard - Plastification chamber |
| 11-Ejection speed regulator        | 27-Electronics housing            |
| 12-Exit chute for parts            | 28-Main switch                    |
| 13-Cooling system manifold         | 29-Inspection panel - fuses       |
| 14-Water inlet-outlet              | 30-Mains power supply cable       |
| 15-Aluminium slide rail for guards | 31-Drain.                         |
| 16-Injection carriage assembly     | 32-Chassis.                       |

Figure IV.11 - Injection molding machine with all parts (BABYPLAST 6/10, 2000)

### IV.3.2 Procedure

The water flow was regulated in the system and was kept at 10 LPM with the help of the cooling system manifold (13). The wire was inserted inside the mold and the mold was fixed inside the mold housing. This housing was mounted on the heaters with the help of four bolts. The heater for the mold was switched on and set at a temperature of 160<sup>0</sup> C. There were three heaters inside the machine, one of them was located inside the plastification chamber (18), one in the injection chamber (22) and one nozzle heater (23) the temperature is set to 204<sup>0</sup> C for two heaters and 213<sup>0</sup> C for the third heater, this was done with the help of the dial for changing the data (2). Once the temperature of the heaters reaches the set values the polymer was injected into the molds. The molds were allowed to cool for 25 minutes after which they were removed from the mold in the desired shape.

To verify if the etched pits on the stainless steel wire were filled with the polymer the following experiment was conducted. The molded samples were immersed in a solution containing 15 parts by volume epoxy (reaction product, bisphenol A epichlorohydrine, epoxy resin, number molecular weight < 700, brand name “Epofix embedding resin”) and 2 parts by volume hardener (triethylene tertramine, brand name “Epofix hardener”), the epoxy mixture hardened overnight. The samples were hand ground on a sandpaper with grit size 240 followed by 320, 400, then finally with 600. Once the sample was ground, it was polished with 1 micron alumina powder on the Buehler polishing table model 48-3072-116. The sample was taken and cleaned ultrasonically (using Struers, Metason 200) in 70% isopropyl alcohol for 10 minutes.

#### IV.4 Preparation of samples for pull out test

After molding the samples, it was required to cut the samples to required length for the pull out test. The samples were cut using a low speed saw (Buehler Isomet Low Speed saw). Figure IV.12 shows the saw. For cutting specimen, a precision diamond blade was fixed on the machine. There was a provision for a micrometer which makes sure that all readings are accurate. The chuck was attached to a support arm, which had a provision for weights and counter balance weights to be attached on to it. Once the sample was loaded on to the chuck, the weights were added onto the weight shaft and the counter balanced weight was set, the samples which had been molded were cut at a distance of 5.08 mm from the top. A mass of 150 grams was added on to the weight shaft. The speed of the cutting was maintained at 200 RPM.



**Figure IV.12 - Buehler Isomet low speed saw**

#### **IV.5 SEM pictures**

The SEM pictures were taken using the JEOL JSM-6400. The samples which were to be analyzed were treated in an ultrasonic bath using 70% isopropyl alcohol. These samples were fixed on the stage using a conductive tape and SEM pictures were obtained at various magnification levels.

#### **IV.6 Statistical study**

Once the optimum conditions for the etching were achieved, a model of the pits on the wire was created. For the statistical study, the pictures of samples at different conditions were taken and analyzed.

The wires to be analyzed for the statistical model were ultrasonically cleaned in a bath containing isopropyl alcohol. After cleaning the wires they were placed under an optical microscope (Olympus STM6, resolution = .0001mm, DP70 digital camera with 12.7 Mpixel) and 3 pictures of each wire were taken at different spots. Figure IV.13 shows one of the pictures which was taken for analysis. For the analysis of the images, an area of 140 mm X 30 mm on an enlarged sheet was chosen and the numbers of pits in each picture were counted. The pits with diameter less than 10 microns were not counted to simplify the analysis. Once the number of pits was calculated on the given area, the diameter of each pit in the area was calculated assuming that the pits were perfectly hemispherical, followed by which a calculation was made to determine the center to center distance between two successive pits. Once all the calculations were done, the average and the standard deviation of the number of pits, the pit diameter and the distance between pits was calculated. Pit depth of the wire was taken as half of the pit diameter, this was checked using the data from the optical microscope in which the depth of pits on different wires was measured. A plot of the pit diameter vs pit depth was constructed to check for the deviation from the initial assumption.

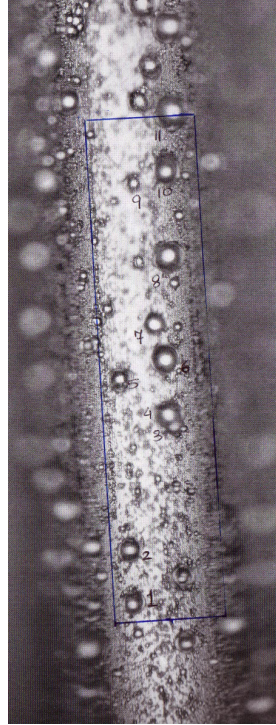


**Figure IV.13 - Sample picture taken for analysis**

#### IV.6.1 Analysis with image tool

The results of this statistical analysis were compared with the results obtained by UTHSCSA Image tool (Version 3.0), which is an imaging software downloadable from <http://ddsdx.uthscsa.edu/dig/itdesc.html>. Figure V.14 shows a sample which was analyzed using image tool, the image was uploaded on to the software and the points to be measured were marked with pointers. The software automatically calculates the distance between these pointers and gives it in a spread sheet format.

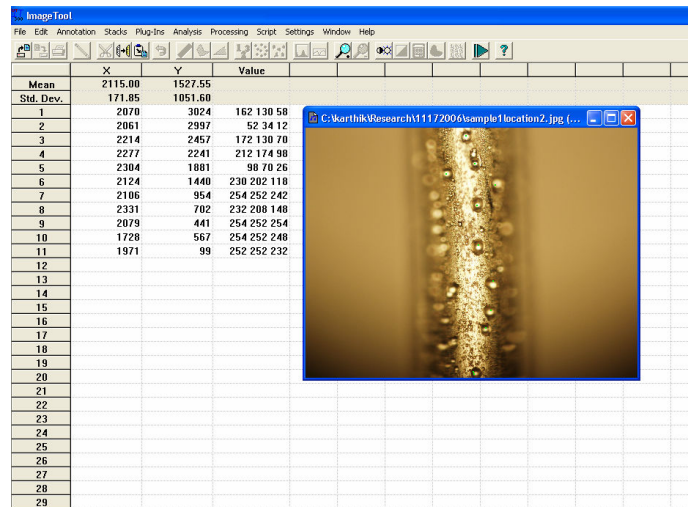


Figure IV.14 - Image analysis with Image Tool (Version 3.00)

#### IV.7 Pull out test

To measure the shearing force required to overcome the adhesive strength between metal and polymer, a pull out test was conducted on the Instron Universal testing machine M10-24411, with a load cell capacity of 5 KN and accuracy of +/- .5%. The advanced features of the machine facilitate automatic calibration of the machine. Figure IV.15 shows the machine used for the test. The wire was pulled out at .51 mm /minute, this corresponds to the lowest speed of the machine, this was done since a very small sample was being tested.



**Figure IV.15 - Instron Universal testing machine M10-24411**

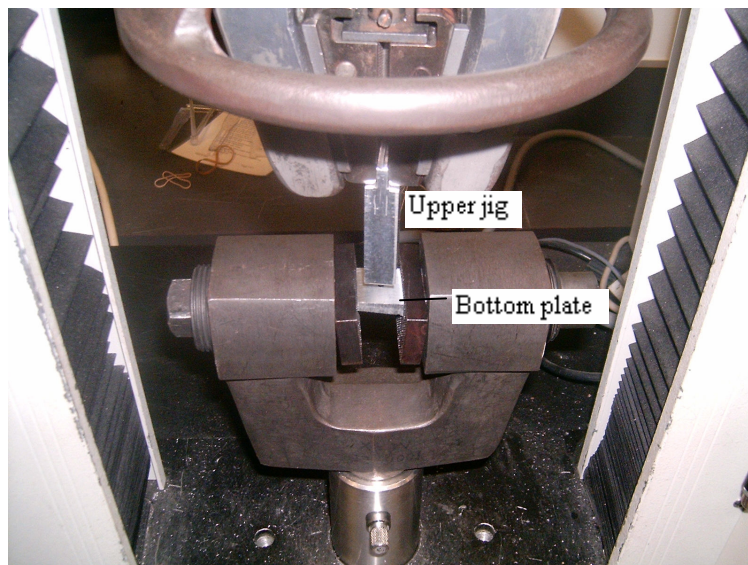


**Figure IV.16 - Pull out test**



Figure IV.16 shows the experimental setup of the test. When the machine was switched on, the upper jig pulled on the wire. The bottom plate ensured that the force was applied in such a way that the wire gets pulled out of the polymer. Figure IV.17 shows a drawing for the jig which is used to clamp the wire. Figure IV.18 shows the drawing for the bottom plate and Figure IV.19 shows the assembly with required dimensions.

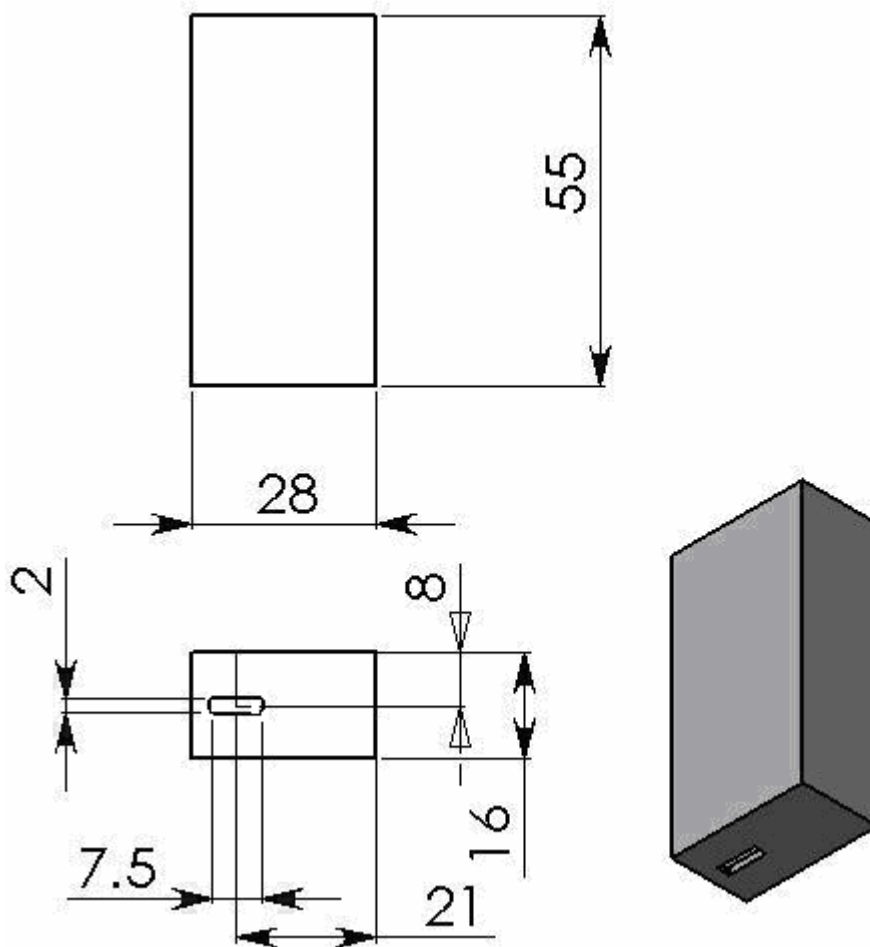


**Figure IV.17 - Drawing for upper jig (dimensions: mm, material: aluminum)**

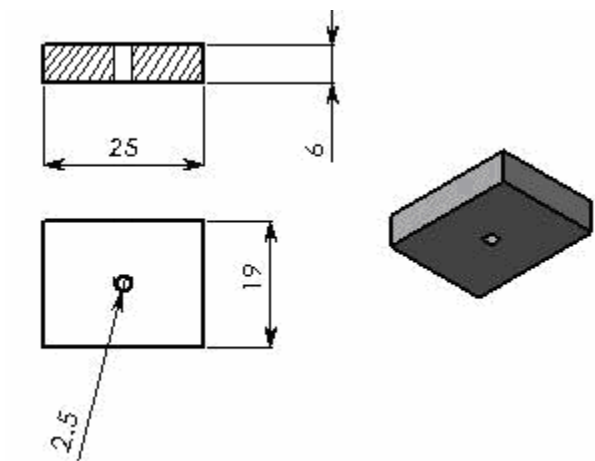


Figure IV.18 - Drawing for the bottom plate (All dimensions: mm, material: aluminum)

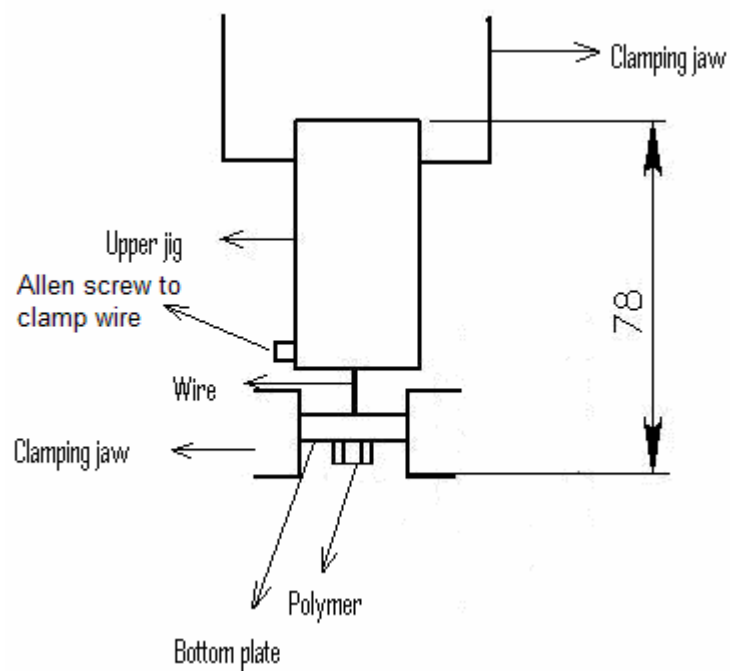


Figure IV.19 - Assembly for the pull out test

## V. RESULTS AND DISCUSSION

### V.1 Mechanical abrasion

The results of unidirectional mechanical abrasion can be seen on Figure V.1. The ridges form in one direction. From Figure V.2 the effect of cross sanding can be seen. The ridges form in both directions.

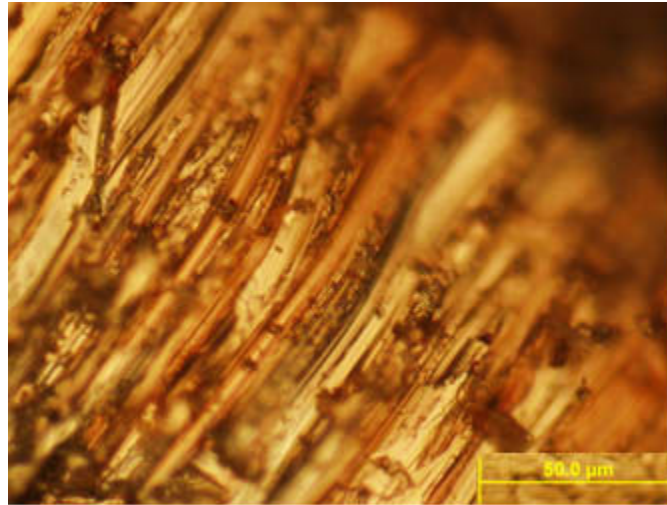


Figure V.1 - Surface of 304 stainless steel after unidirectional sanding with 240 grit size sand paper

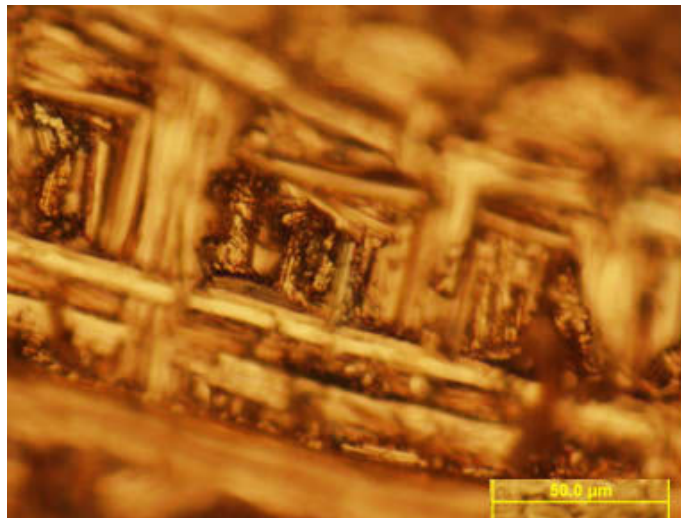
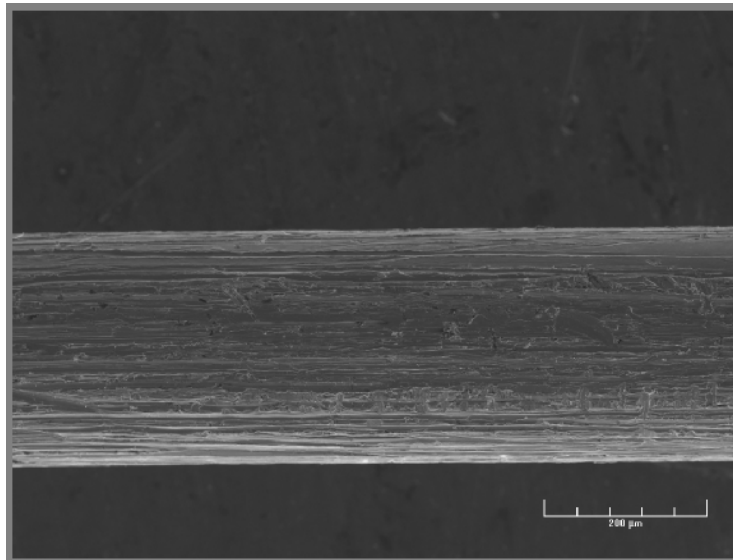
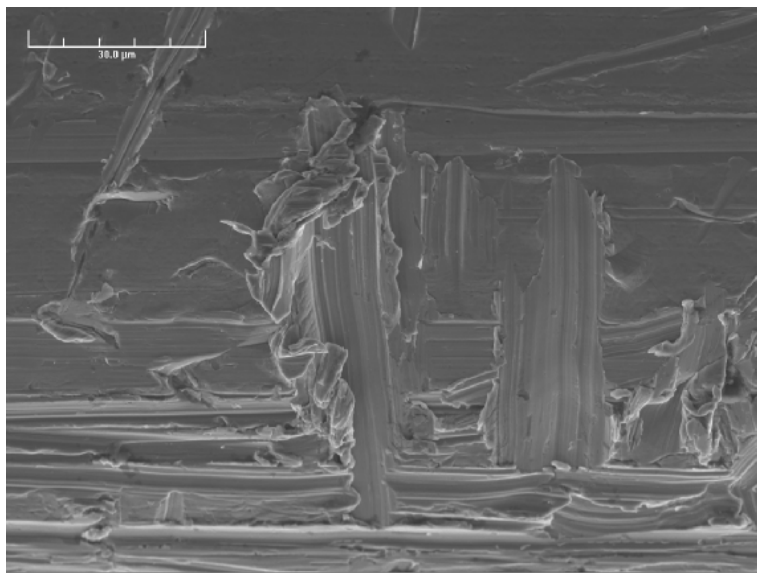


Figure V.2 - Surface of 304 stainless steel after cross sanding with 240 grit size paper

Figure V.3 and Figure V.4 show some pictures which have been taken with SEM. Figure V.4 shows the image taken at a higher magnification, at this magnification it was possible to see the burrs which were created due to mechanical abrasion. The presence of these burrs was not desirable because they can hurt sensitive tissues and cause undesired complications.



**Figure V.3 - SEM image of mechanically abraded wire**



**Figure V.4 - SEM of mechanically abraded wire**

## V.2 Chemical etching

Figures V.5-V.6 shows the wires that have been etched with HCl for varying time periods.

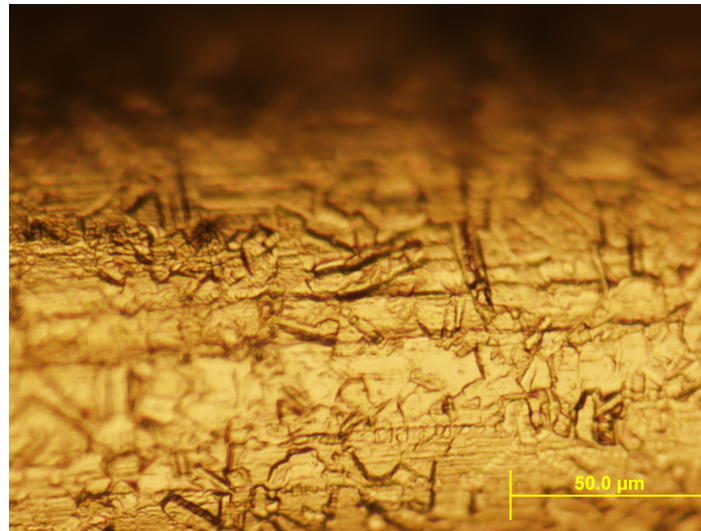


**Figure V.5 - Optical image of stainless steel wire dipped in 35% concentrated hydrochloric acid for 15 minutes**

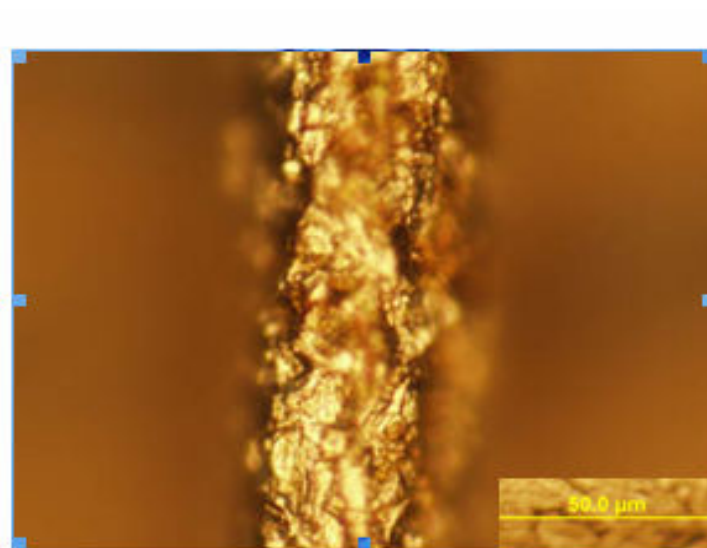


**Figure V.6 - Optical image of stainless steel wire dipped in 35% concentrated hydrochloric acid for 3 hours**

From Figure V.5 it can be seen that though the surface has been modified but there were no pits on the surface of the wire. From Figure V.6 it was seen that there was greater unevenness in the surface but there was drastic loss in the cross-sectional area of the wire as seen with the SEM pictures (Figure V.7 and Figure V.8). The reduction of the wire size would decrease the strength in the wire, which would be required during expansion of the stent.

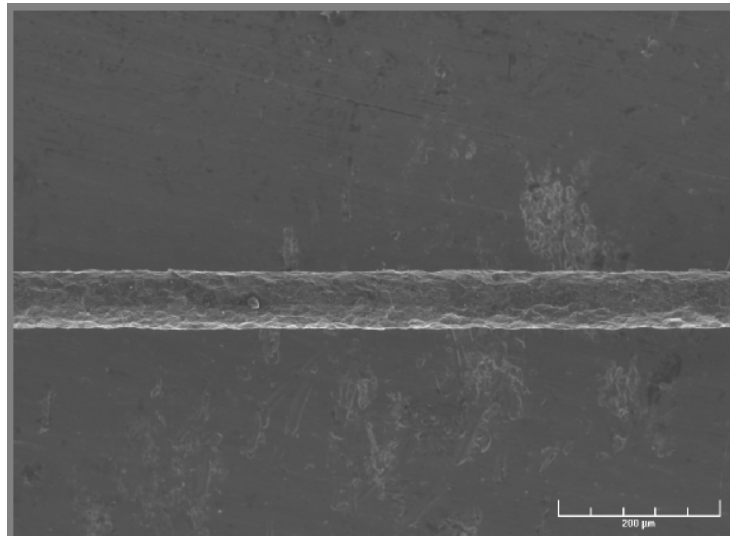


**Figure V.7 - SEM image of stainless steel wire dipped in 35% concentrated hydrochloric acid for 3 hours**

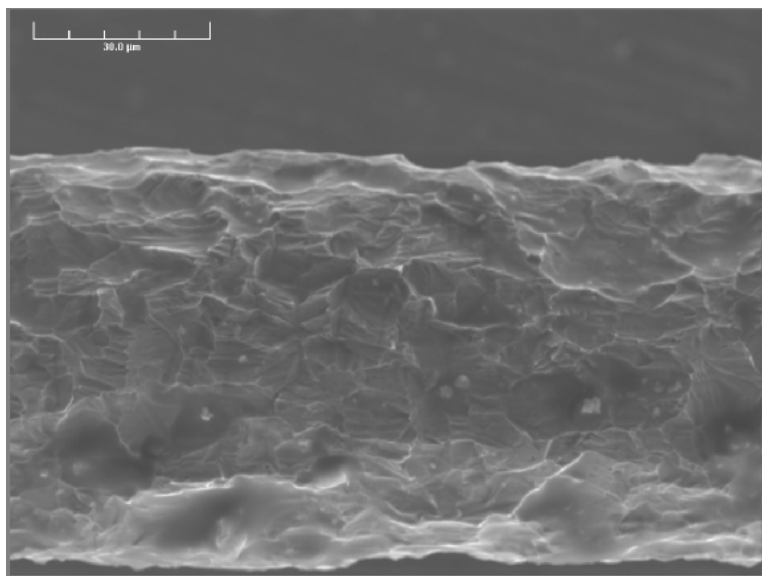


**Figure V.8 - SEM image of stainless steel wire dipped in 35% HCl for 3 hours**

### V.3 Electrochemical Etching

Figure V.9 shows the effect of pitting. A comprehensive list of photographs for different etching conditions can be viewed in appendix B. It was observed that at low voltages there was hardly any pitting. With the increase in the voltage and time of etching, pitting was observed on the wire.

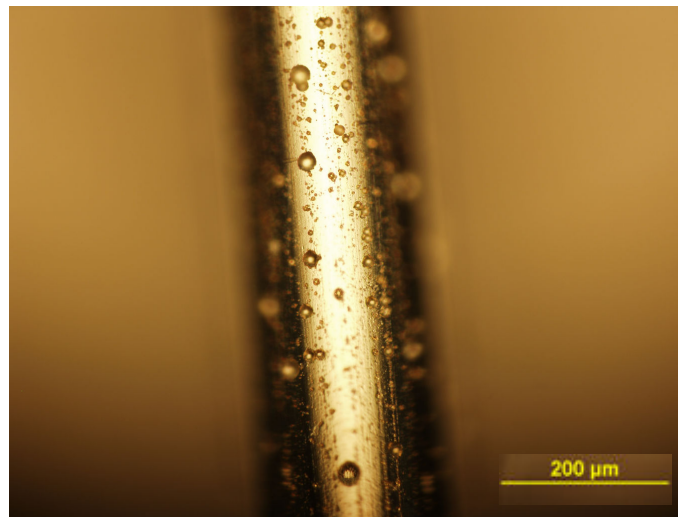


**Figure V.9 - Stainless steel wire after electrochemical etching in 5% soap solution at a voltage of 6 volts for 10 seconds**

#### V.3.1 Design of experiment

Figure V.10 shows the effect of voltage and time on the pit depth ( $\mu\text{m}$ ). It can be seen that maximum pit depth can be obtained by applying a higher voltage for a longer time period, the curves on the time – voltage plane represent isobars or conditions at which the same pit depth can be obtained. Figure V.11 shows the effect of voltage on pit density, it can be seen that the maximum pit density can be achieved by applying a higher voltage for a short duration of time, the isobars can be seen on the time - voltage plane which represent conditions where similar pit density can be obtained. For finding the

optimum conditions, which in this case would be the condition with maximum pit depth and pit density, it is important to define a function called desirability.

Desirability is an objective function that ranges from zero outside the limits to one at the goal. The numerical optimization finds a point that maximizes the desirability function. For this analysis, a condition which would be able to maximize pit depth and pit density would have desirability of one and the condition which would have minimum pit depth and pit density will have a desirability of zero. Since in this case it is not possible to obtain a desirability of one due to given constraints between input and output factors. The software optimizes the conditions within the specified range of input parameters and generates the maximum possible desirability. From Figure V.12 it can be seen that the maximum desirability occurs at an applied voltage of 6.18 volts for 20 seconds at a concentration of 2.56 wt%. It was also observed that concentration does not have significant effect on desirability; this result is discussed in more detail in section V.6.2.

An equation for pit depth and pit density was generated based on the statistical analysis. Equation V.1 gives the pit depth as a statistical function of applied voltage and time. As discussed earlier, a logarithmic transformation was applied between the input parameters and the pit density which made the model more accurate. Equation V.2 shows the transformation and equation V.3 shows how the value of pit density can be calculated based on the applied voltage and time. It can be seen that both pit depth and pit density are independent of concentration. The reason for this will be discussed in section V.6.2.

$$P_d = 57.16 - 6.32 V - 1.7055 t + 0.25 V t \quad (V.1)$$

$$\ln(P_p) = 0.0188 + 0.9155 V + 0.2271 t - 0.0361 V t \quad (V.2)$$

$$P_p = e^{(0.0188 + .9155 V + .2271 t - .0361 Vt)} \quad (V.3)$$

Where,

$P_d$  = Pit depth in  $\mu\text{m}$

$P_p$  = Pit density in Pits/ $\text{mm}^2$

$V$  = Applied voltage in Volts (Range 6-12)



t = time in seconds (Range 20-30)

Design-Expert® Software

Pit Depth

21.12

7.25

X1 = A: Voltage

X2 = B: Time

Actual Factor

C: Concentration = 2.56

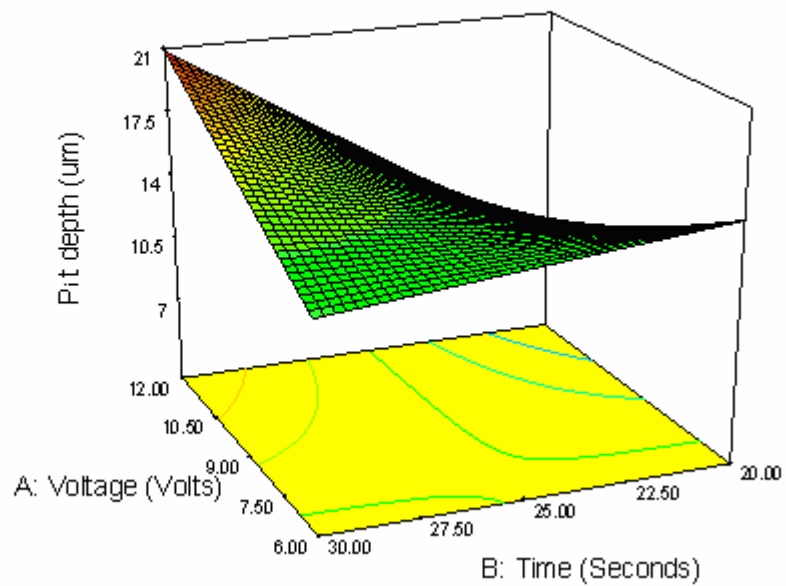


Figure V.10 - Pit depth as a function of time and voltage (equation V.1)

Design-Expert® Software  
Original Scale  
Pit Density  
1410  
96  
X1 = A: Voltage  
X2 = B: Time  
Actual Factor  
C: Concentration = 2.56

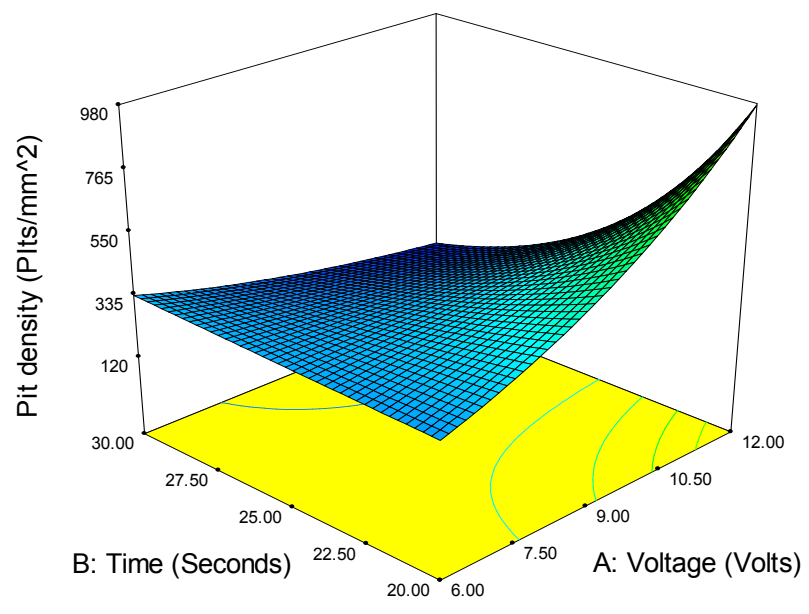


Figure V.11 - Pit density as a function of time and voltage (equation V.3)

Design-Expert® Software  
Desirability  
1  
0  
X1 = A: Voltage  
X2 = B: Time  
Actual Factor  
C: Concentration = 2.56

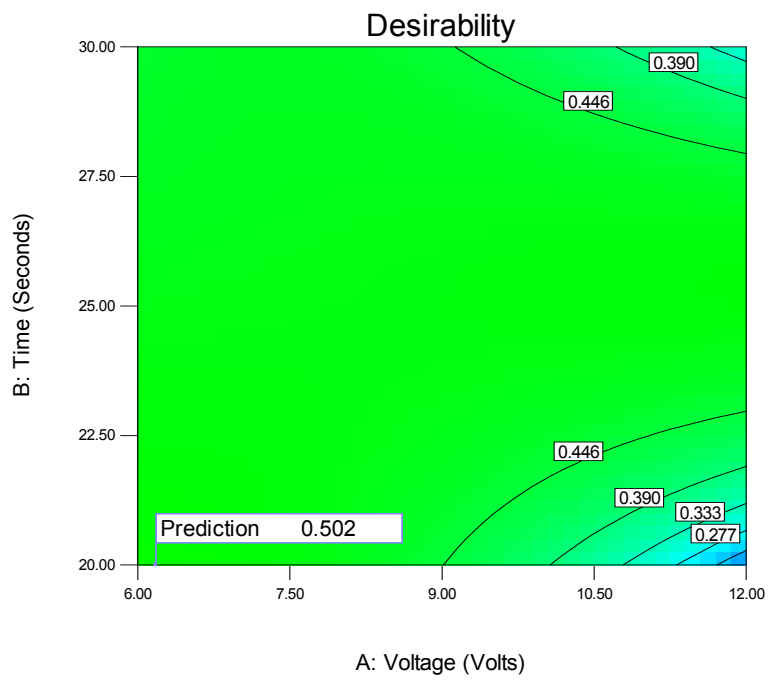


Figure V.12 - Desirability as a function of time and voltage

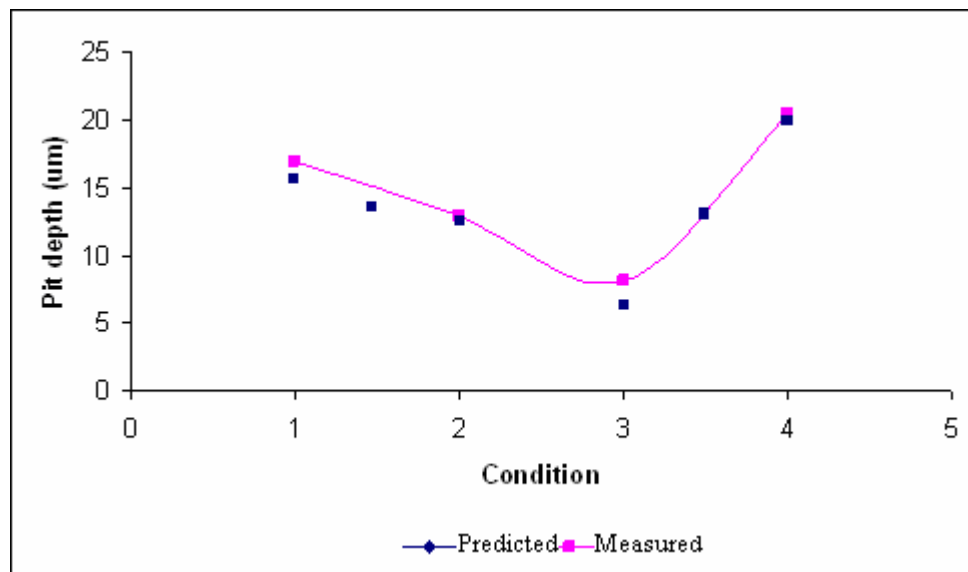
The results of the model were compared with measured data. Table V.1-V.2 show the deviation of the model from the actual result. Figure V.13 and V.14 compare the values of pit depth and pit density for the model and the experiment. Figure V.13 plots conditions which corresponds to the conditions in Table V.1 against the measured pit depth and predicted pit depth. Similarly Figure V.14 plots conditions corresponding to the conditions in Table V.2 against measured pit density and predicted pit density.

**Table V.1 - Deviation of model values of pit depth from actual values**

Condition	Voltage (Volts)	Time (seconds)	Pit depth ( $\mu\text{m}$ )			Difference	Percentage error (%)
			Predicted	Measured Average	Standard deviation for measured value		
1	6	20	15.37	16.87	4.78	1.49	8.89
2	6	25	14.1	-	-	-	-
3	6	30	13.4	13	1.42	0.43	3.34
4	12	20	7.68	8.12	2.06	0.43	5.35
5	12	25	13.68	-	-	-	-
6	12	30	20.87	20.5	3.33	0.37	1.8
				Average	2.89	0.68	4.84

**Table V.2 - Deviation of model values of pit density from actual values**

Condition	Voltage (Volts)	Time (Seconds)	Pit density (Pits/mm <sup>2</sup> )			Difference	Percentage error
			Predicted	Measured	Standard deviation for measured value		
1	6	20	305.12	325	45.32	19.87	6.11
2	6	25	381.26	-	-	-	-
3	6	30	338.69	315	90	23.69	7.52
4	12	20	973.28	1042.5	45	69.21	6.63
5	12	25	412	-	-	-	-
6	12	30	123.77	160	45.32	36.22	22.64
				Average	56.41	37.25	10.72

**Figure V.13 - Comparison of pit depth predicted by the model with actual data**

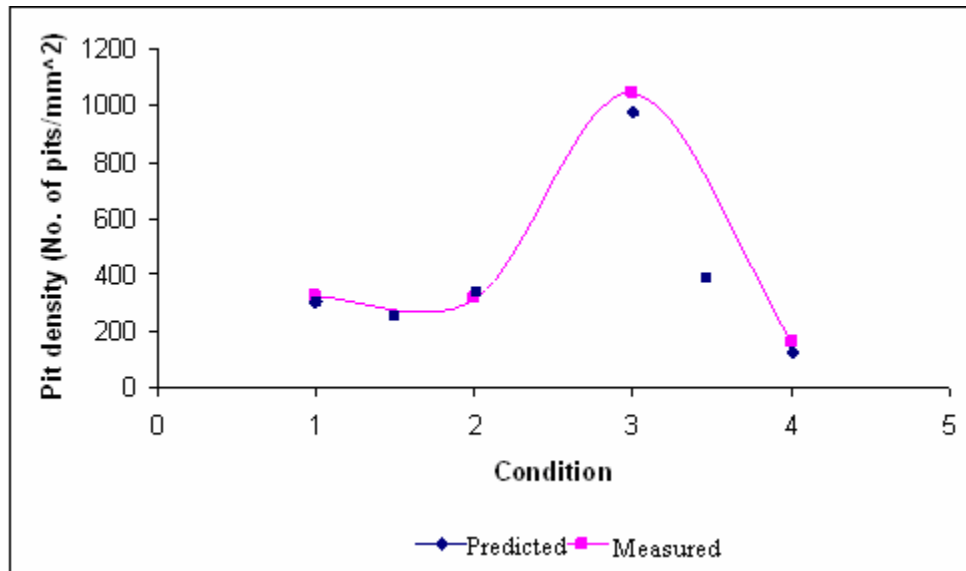


**Figure V.14 - Comparison of pit density predicted by the model with actual data**

Based on the results of the above analysis, the most optimum conditions for electrochemical etching was found to be 6.18 volts applied for 20 seconds. Since the model does not take into account the concentration of the electrolyte if the concentration is between 2.5% and 5%, the wire etched at 6 volts for 20 seconds and at an electrolytic concentration of 2.5% by weight was selected. The effect of electrochemical etching of this wire can be seen in Figure V.15.

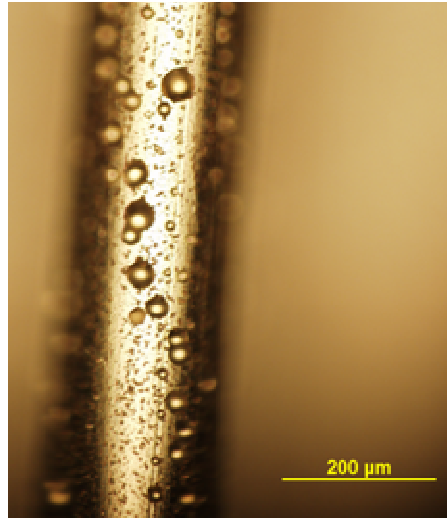


**Figure V.15 - Wire etched at optimum conditions**

SEM images demonstrated the absence of burrs. Figures V.16 and V.17 show the SEM pictures which have been taken at different magnification levels to demonstrate the absence of burrs and the shape of the pit.

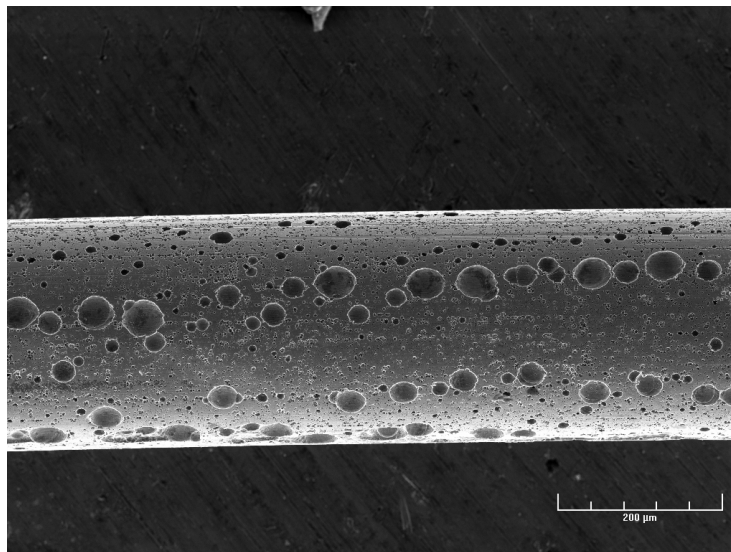


**Figure V.16 - SEM image of electrochemically etched wire at 6 volts for 20 seconds in an electrolyte having concentration 2.5%**

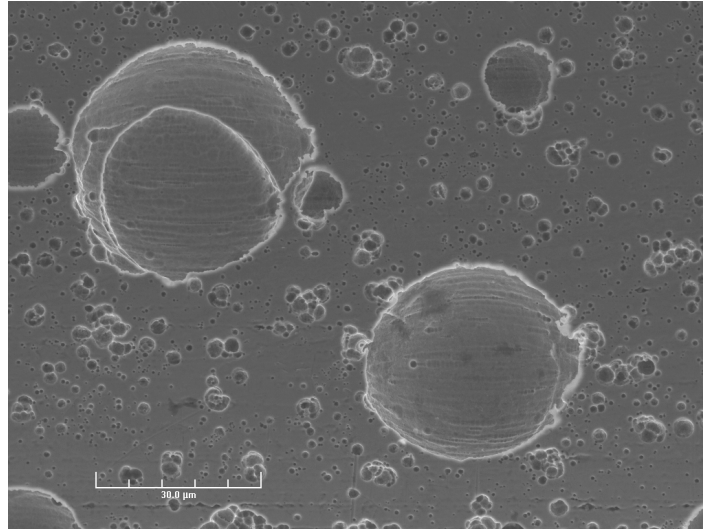


**Figure V.17 - SEM image of electrochemically etched wire at a higher magnification**

### V.3.2 Electrochemical etching using sodium carbonate

From the experiment section, it can be recalled that the etching using sodium carbonate was done to detect the ingredient in soap which causes pitting. Figure V.18 shows the effect of electrochemical etching with sodium carbonate on stainless steel. The SEM picture (Figure V.18) show the presence of pits on the surface of the stainless steel wire. Figure V.19 shows the magnified view of the picture where the pits can be clearly seen on the surface of the stainless steel wire. The results using sodium carbonate as the electrolyte indicate that pitting occurs due to the presence of sodium carbonate in soap.

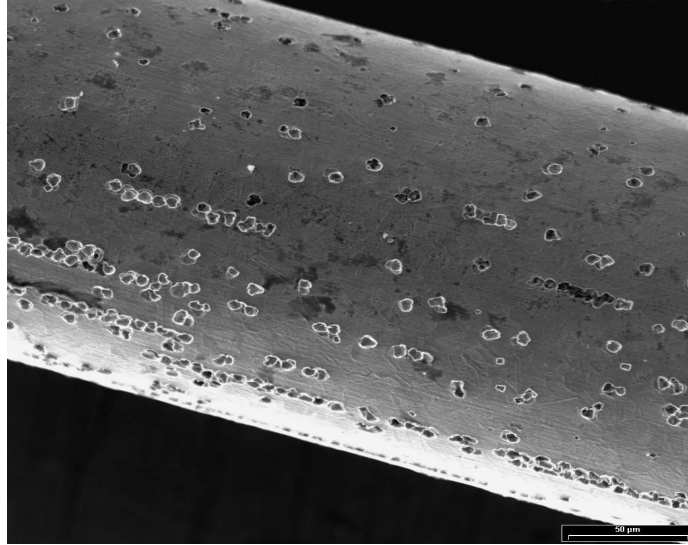


**Figure V.18 - Stainless steel wire etched in 2.5% sodium carbonate solution at 7 volts for 120 seconds**

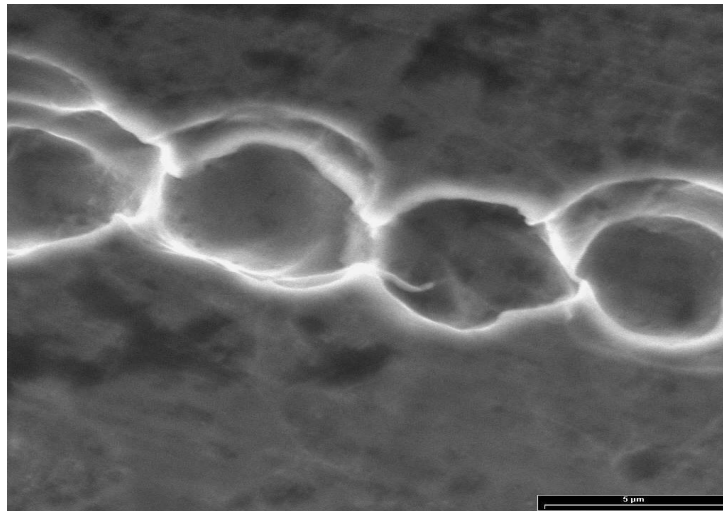


**Figure V.19 - Magnified view of the pits on the surface of stainless steel etched with sodium carbonate electrolyte 2.5% sodium carbonate solution at 7 volts for 120 seconds**

### V.3.3 Measurement of pH

Table V.3 gives the pH of 2.5% by weight sodium carbonate solution and soap solution. It can be seen that the pH of the soap solution is less than that of the sodium carbonate solution.



**Table V.3 - pH of sodium carbonate and soap solution**

	pH		
	Sodium carbonate solution (2.5 wt %)	11.22	11.24
Soap Solution (2.5 wt %)	10.02	10.04	10.03

#### V.4 Statistical study

Figure V.20 shows the correlation between the predicted value and the measured value, a microscopic measured reading of pit depth was made corresponding to each predicted reading. It was seen that the predicted and the measured values were closely related. Hence it was assumed that the pit depth was half of the pit diameter.

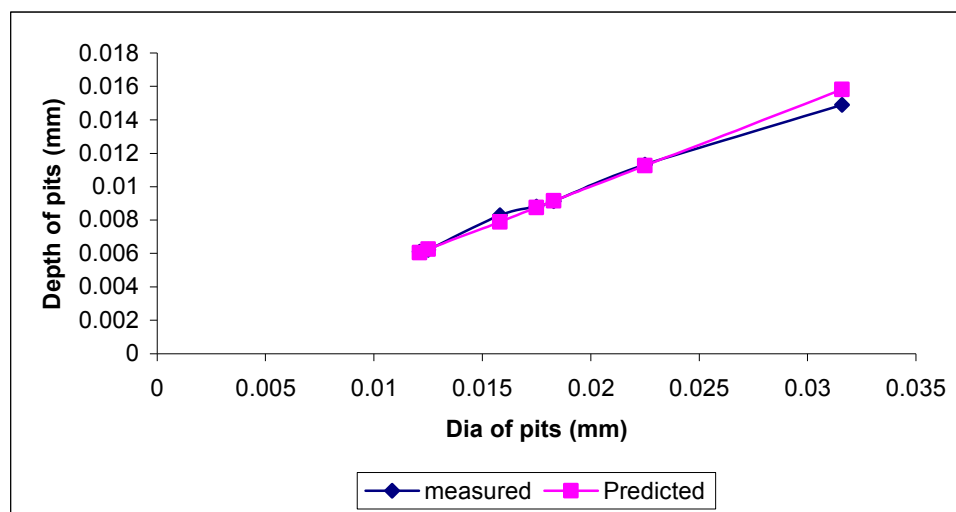


**Figure V.20 - Diameter of pits vs depth of pits**

#### V.4.1 Calculations

Equation V.4 shows how the standard deviation ( $\sigma$ ) for pit diameter was calculated

$$\sigma = \sqrt{\frac{1}{N} \sum_{i=1}^N (x_i - \bar{x})^2} \quad (\text{V.4})$$

$\sigma$  = Standard deviation

N = Number of pits in chosen area.

$x_i$  = Diameter of chosen pit

$\bar{x}$  = Average diameter

Similarly other calculations were made for distance between 2 pits and density of pits. A comprehensive list of results is available in appendix C. The parameters measured were diameter of the pit, distance between pits, and number of pits in a given area. Table V.6 shows the results of the complete analysis. Table V.5 shows the analysis for the same sample which was done using the image tool software. Figure V.21 and V.22 compare the results of the two methods. The results show very good correlation.

**Table V.4 - Statistical analysis (sample number 1, etched at 6 volts for 20 seconds using soap concentration of 2.5%)**

Pit Number	Diameter of pit ( $\mu\text{m}$ )	Distance between 2 pits in ( $\mu\text{m}$ )	Cumulative distance from first pit ( $\mu\text{m}$ )	Depth of pit ( $\mu\text{m}$ )
1	25.84	51.68	51.68	12.92
2	32.3	74.29	125.97	16.15
3	29.07	74.29	200.26	14.53
4	25.84	74.29	274.55	12.92
5	32.3	74.29	348.84	16.15
6	9.69	80.75	429.59	4.84
7	27.45	87.21	516.8	13.72
8	6.46	32.3	549.1	3.23
9	38.76	80.75	629.85	19.38
10	29.07	87.21	717.06	14.535
11	35.53	83.98	801.04	17.765
12	35.53	41.99	843.03	17.765
13	32.3	64.6	907.63	16.15
Average	27.70	69.81		13.85
St Dev	9.55	17.47		9.55

**Table V.5 - Comparison with image tool (Sample number 1, etched at 6 volts for 20 seconds using soap concentration of 2.5%)**

Pit No.	Microscopic measurement ( $\mu\text{m}$ )		Image tool readings ( $\mu\text{m}$ )	
	Pit diameter ( $\mu\text{m}$ )	Distance between 2 pits ( $\mu\text{m}$ )	Pit diameter ( $\mu\text{m}$ )	Distance between 2 pits ( $\mu\text{m}$ )
1	25.84	51.68	25.84	48.15
2	32.3	74.29	28.05	69.86
3	29.07	74.29	24.95	69.28
4	25.84	74.29	20.34	66.38
5	32.3	74.29	27.75	84.08
6	9.69	80.75	11.68	86.25
7	27.455	87.21	19.04	84.25
8	6.46	32.3	7.86	30.93
9	38.76	80.75	32.03	78.54
10	29.07	87.21	21.9	79.18
11	35.53	83.98	27.16	83.64
12	35.53	41.99	29.57	40.53
13	32.3	64.6	28.2	63.71
Average	27.7	69.81	23.41	61.92
St Dev	9.55	17.47	7.11	23.38

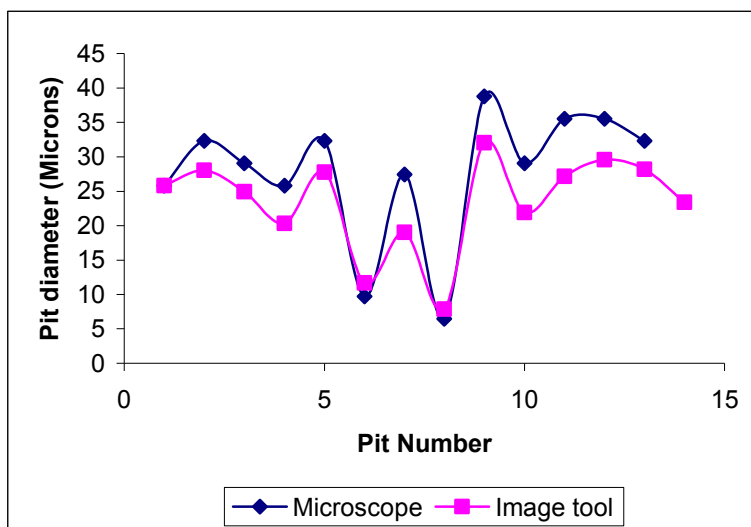


Figure V.21 - Pit number vs pit diameter (sample number 1, etched at 6 volts for 20 seconds using soap concentration of 2.5%)

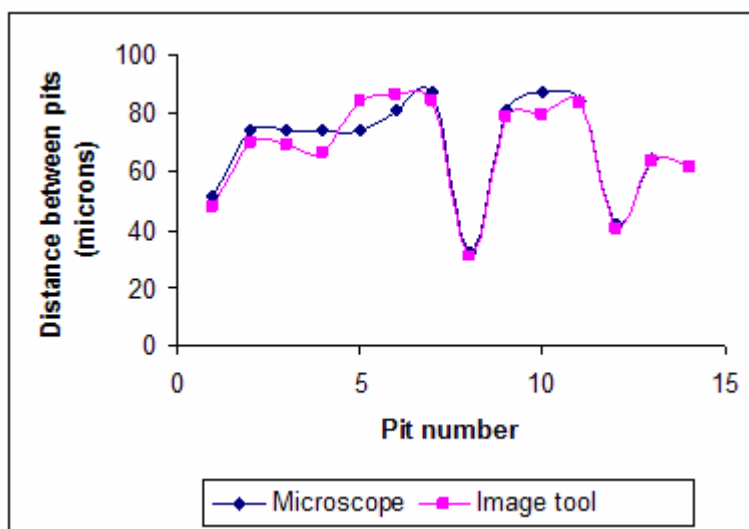


Figure V.22 - Pit number vs distance between pits (sample number 1, etched at 6 volts for 20 seconds using soap concentration of 2.5%)

Seven pictures of four samples were studied, the average diameter, average distance between pits, pit density and number of pits were calculated. Table V.6 shows the results of the entire analysis.

**Table V.6 - Final analysis for etched wire**

Sample No.	Average pit diameter ( $\mu\text{m}$ )	Average distance between 2 pits ( $\mu\text{m}$ )	Pit Density (number of pits / $\text{mm}^2$ )	No of pits
1	27.70	69.81	297	13
2	20.32	50.33	251	11
3	25.96	38.51	274	13
4	24.62	46.83	342	15
5	27.13	74.45	205	9
6	18.6	44.88	411	18
7	17.87	53.72	320	14
Average	23.176	54.07	300	13.28
Standard Deviation	4.14	13.26	66	2.87

Based on the results of Table V.6, the following graphs were plotted to get the variation of the various parameters like pit diameter and distance between two pits to form an over all average for the model of the etched wire.

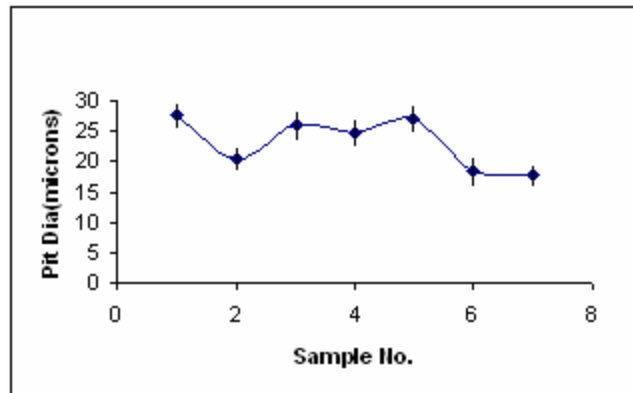


Figure V.23 - Sample number vs pit diameter

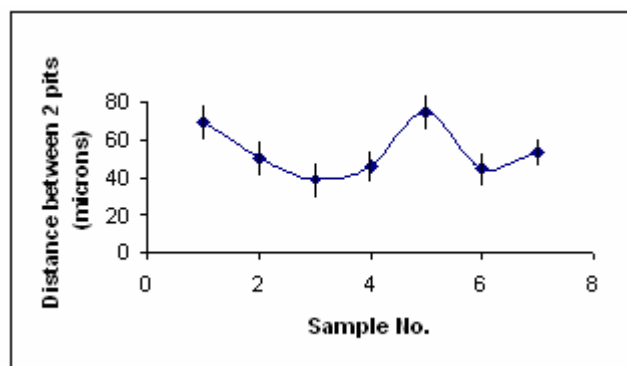


Figure V.24 - Sample number vs distance between 2 pits

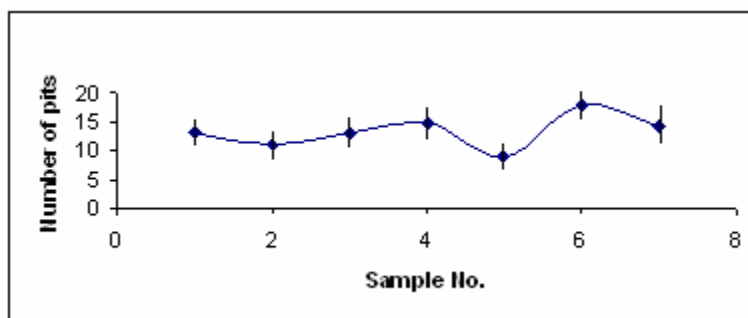
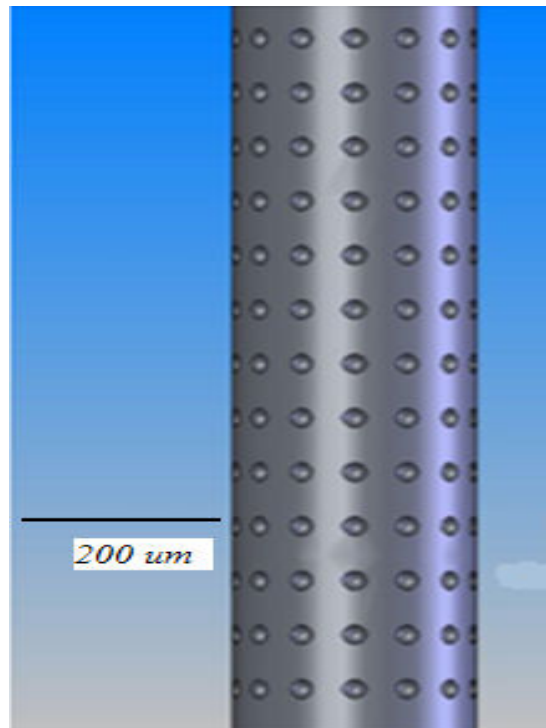


Figure V.25 - Sample number vs number of pits

Figure V.26 shows a statistical model for the wire which has been “electrochemically etched,” it can be seen that the pits are of equal dimensions and the pits are equally spaced through out the wire. The objective of creating this model was to calculate the force required to pull the wire out of the polymer matrix.



**Figure V.26 - Model of the etched wire**

## **V.5 Force calculation**

### V.5.1 Theoretical values

To estimate the force required a statistical model was created and followed by which the number of pits and the pit size was estimated, this provided the data regarding the size of the hemispherical pits.

To calculate the force required to shear off these hemispheres, the shear force required for shearing one hemisphere was calculated. This was followed by multiplying the total number of pits in the area occupied by the pits. Based on the known shear



strength of polyethylene the force required to shear off the polymer flown into the pits was calculated.

Figure V.27 shows the cross section of the polymer molded over the etched wire. The “random” pit size and distribution are modeled as arrays of pits with fixed size and distance. The pit size and pit distance in the model are the averaged values obtained from statistical analysis. Pullout force calculated in this model will be compared with experimental force, and the adhesive strength is calculated as guideline for designers.

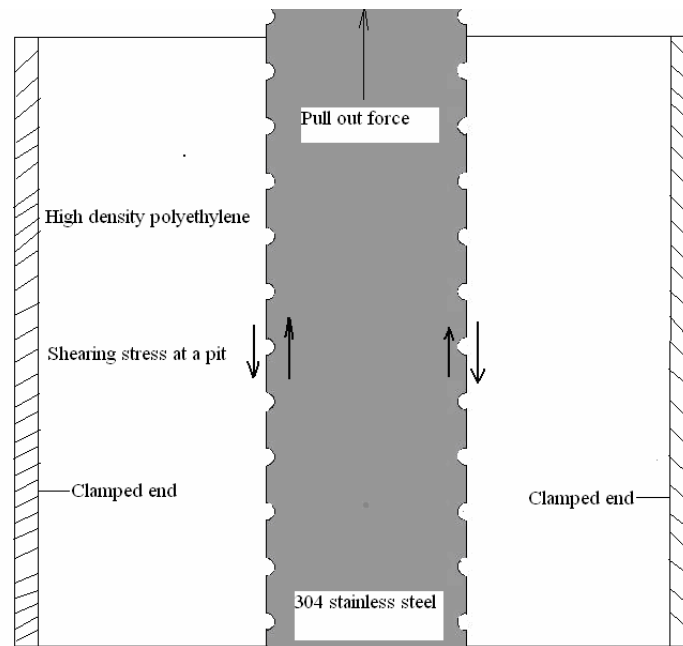


**Figure V.27 - Shearing of hemispherical pits**

Definition:

$A_p$  = Shearing area of one pit

$A_s$  = Total surface area of the wire covered with HDPE

$A_{sa}$  = Area chosen for statistical study

$A_t$  = Total area occupied by the pits

$d_a$  = Average diameter of one pit

$d_w$  = Diameter of the wire

$f_1$  = Force required to shear off the pits

$f_2$  = Force required to shear off the unetched wire out of the molded HDPE (measured experimentally)

$f_3$  = Total force required to shear off the etched wire out of the molded HDPE

$l_1$  = Length of the wire surrounded by HDPE

$n_a$  = Average number of pits in the statistical area

$n_p$  = Total number of pits in the area surrounded by HDPE

$\sigma_{\text{HDPE}}$  = Tensile strength of HDPE

$\tau_{\text{HDPE}}$  = Shear strength of HDPE

We would assume that when the wire is being pulled out of the polymer, it would try to shear off the polymer which has flown into the pits. The area of a pit,  $A_p$ , can be calculated by knowing  $d_a$ .

$d_a = 2.31 \times 10^{-5}$  m (from Table V.6)

$$A_p = \frac{\pi}{4} d_a^2 = \frac{\pi}{4} (2.31 \times 10^{-5})^2 = 4.191 \times 10^{-10} \text{ m}^2 \quad (\text{V.5})$$

$d_w = 2.54 \times 10^{-4}$  m (measured using calipers)

$l_1 = 4.19 \times 10^{-3}$  m (measured using calipers)

$$A_s = \pi d_w l_1 = \pi \times 2.54 \times 10^{-4} \times 4.19 \times 10^{-3} = 3.341 \times 10^{-6} \text{ m}^2 \quad (\text{V.6})$$

The area,  $A_{sa}$ , chosen for the statistical study was 140mmX30mm which was equal to  $4.38 \times 10^{-8} \text{ m}^2$  are on the wire when the appropriate scaling is done. To determine  $n_p$ , the number of pits in the area chosen for statistical study was known so it was possible to find the number of pits through the length of the wire by substituting  $A_{sa}$  and  $A_s$  in equation V.7.

$n_a = 13.2$  (from table V.6)

$$n_p = \frac{A_s}{A_{sa}} n_a = \frac{3.341 \times 10^{-6}}{4.38 \times 10^{-8}} \times 13.2 = 1007.5 \quad (\text{V.7})$$

Once the area of one pit and the total number of pits is known, the total area occupied by the pits,  $A_t$ , can be determined by equation V.8.

$$A_t = n_p A_p = 1007.5 \times 4.191 \times 10^{-10} = 4.22 \times 10^{-7} \text{ m}^2 \quad (\text{V.8})$$

Force required,  $f_1$ , to shear off the polymer which has flown into the pits due to etching can be calculated using equation V.9, if the shear strength of high density polyethylene is known.

$$\sigma_{HDPE} = 2.33 \times 10^7 \text{ Pascal (Exxonmobil, 2007)}$$

$$\tau_{HDPE} = .577 \sigma_{HDPE} = .577 \times 2.33 \times 10^7 = 1.34 \times 10^7 \text{ Pa (Shigley, 1989)}$$

$$f_1 = \tau_{HDPE} A_t = 1.34 \times 10^7 \times 4.22 \times 10^{-7} = 5.64 \text{ N} \quad (\text{V.9})$$

The force,  $f_1$  is the force required to shear off the pits, in addition there exists some friction between the unetched wires and the polymer. This force was experimentally measured. If this force is added to force required to shear off the pits, the total amount of force required to pull the wire out of the polymer can be calculated.

$$f_2 = 4.6 \text{ N (Experimentally measured forces for unetched wires, from Figure V.31)}$$

$$f_3 = f_1 + f_2 = 5.64 + 4.6 = 10.24 \text{ N} \quad (\text{V.10})$$

Adhesive strength of the sample can be calculated using equation V.11. This calculated adhesive strength will then be compared with the strength derived by pullout forces.

$$S_1 = \frac{f_3}{\pi d_w l_1} = \frac{10.24}{3.14 \times 2.54 \times 10^{-4} \times 4.19 \times 10^{-3}} = 3.06 \times 10^6 \text{ Pa} \quad (\text{V.11})$$

## V.5.2 Experimental values

This section discusses the results of the pull out test. Figure V.28 shows the displacement vs force plot for all the unetched samples. Figure V.29 shows the force vs displacement diagrams for the etched samples, from the data it can be seen that the amount of force required to shear the etched samples is higher.

Figure V.30 shows the results which were normalized and superimposed. It shows the graph between the adhesive strength ( $S_1$ ) calculated using the equation V.11 and change

in length per unit original length. Figure V.31 compares the average force required to shear off the etched and the unetched wires.

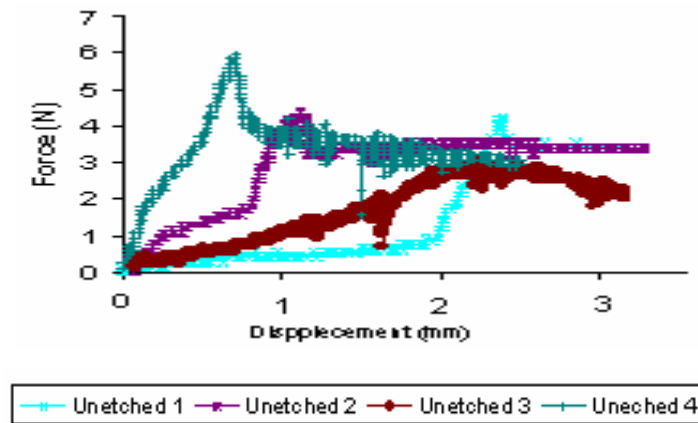


Figure V.28 - Displacement vs pullout force for unetched wires

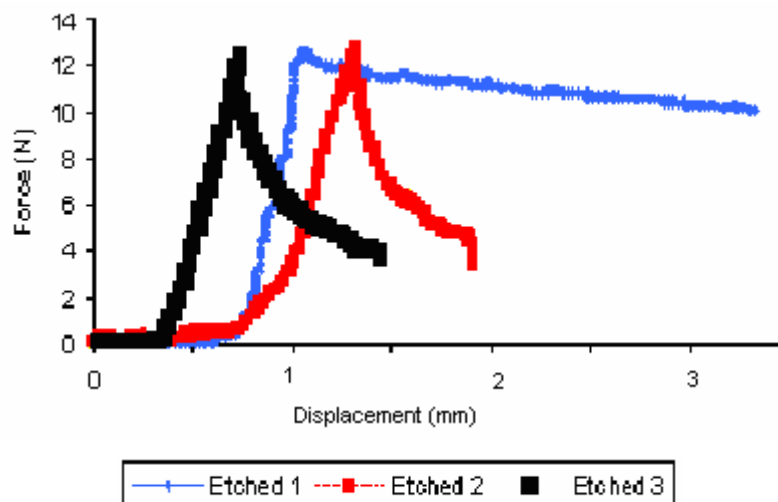


Figure V.29 - Displacement vs pull out force for etched wires (Etched at 6 volts for 20 seconds at soap concentration of 2.5%)

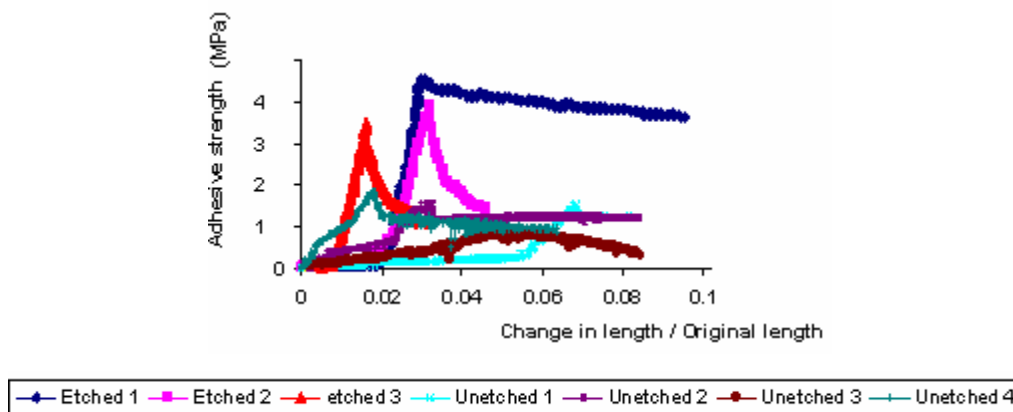


Figure V.30 - Change in length/original length vs adhesive strength

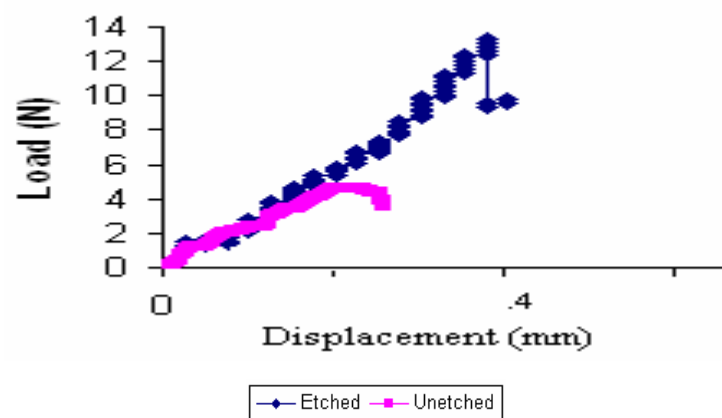
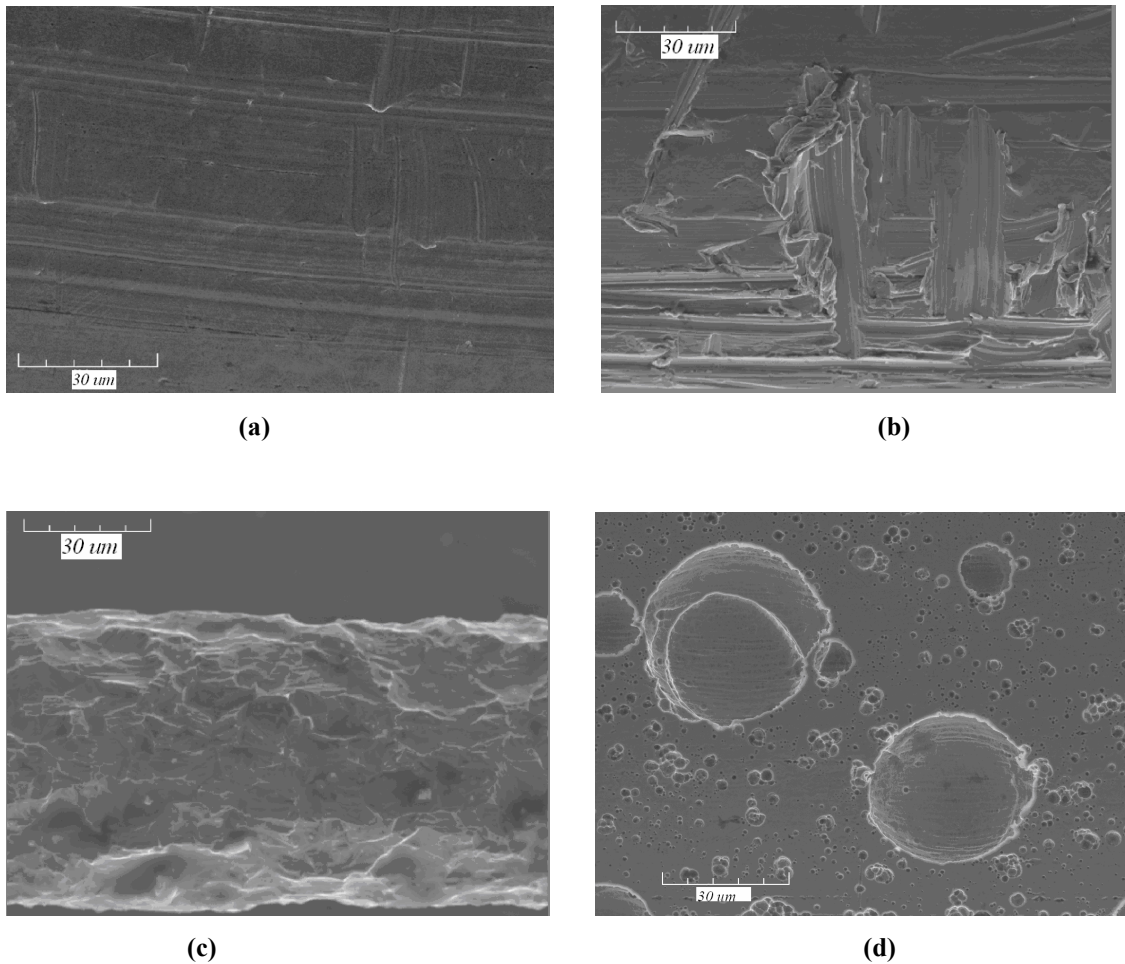


Figure V.31 - Average displacement Vs Average Force

## V.6 Discussion

### V.6.1 Surface of stainless steel

Many surface modification techniques were tried on the 304 stainless steel wire, Figure V.32 compares the surface of each technique.



**Figure V.32 - Comparison of different surfaces (a) unetched surface (b) mechanical abrasion (c) chemical etching (d) electrochemical etching**

Figure V.32 compares the surface of the stainless steel. There are some marks on the surface of unetched stainless steel after extrusion. These lines could be the reason for interlocking between metal and polymer in the unetched wire. From V.32 (b) it can be seen that there are a lot of burrs on the surface which was why the mechanical abrasion process was not used. Figure V.32 (c) shows the wire which was chemically treated, it can be seen that there is drastic loss in cross section of the wire. Figure V.32 (d) shows the surface of the wire which was electrochemically etched, the presence of pits would lead to interlocking.

## V.6.2 Electrochemical etching

The pits on the sample etched with sodium carbonate suggested that, the pitting occurs due to the presence of sodium carbonate in the soap, but it was observed that the pitting was more prominent when the soap solution was used. This can be explained based on the pH of the soap and the pH of sodium carbonate. Sodium carbonate solution had a pH of 11.22 and soap solution has a pH of 10.04. This means the soap solution is more acidic when compared to the sodium carbonate solution. The effect of material removal rate on pH of the electrolyte has already been discussed in the review and this explained the higher pitting in the case of soap solution.

The material used for manufacturing the cathode for electrochemical etching was aluminum. Initially a steel cathode was tried and rejected due to severe oxide formation on the surface which prevented repeated use of the cathode. Aluminum solved this problem. It formed an aluminum oxide which prevented it from further corrosion.

The model generated by the software demonstrated that if the concentration was between 2.5% and 5% by weight, it does not have any effect on the pit depth or the pit density. This suggested that the soap solution just provides a path to carry the ions in the electrochemical process and the concentration does not play an important part in determining the pit depth or pit density. Figure V.33 shows desirability as a function of time voltage and concentration, it can be seen that concentration does not have any effect on the desirability.

Design-Expert® Software

Desirability  
 X1 = A: Voltage  
 X2 = B: Time  
 X3 = C: Concentration

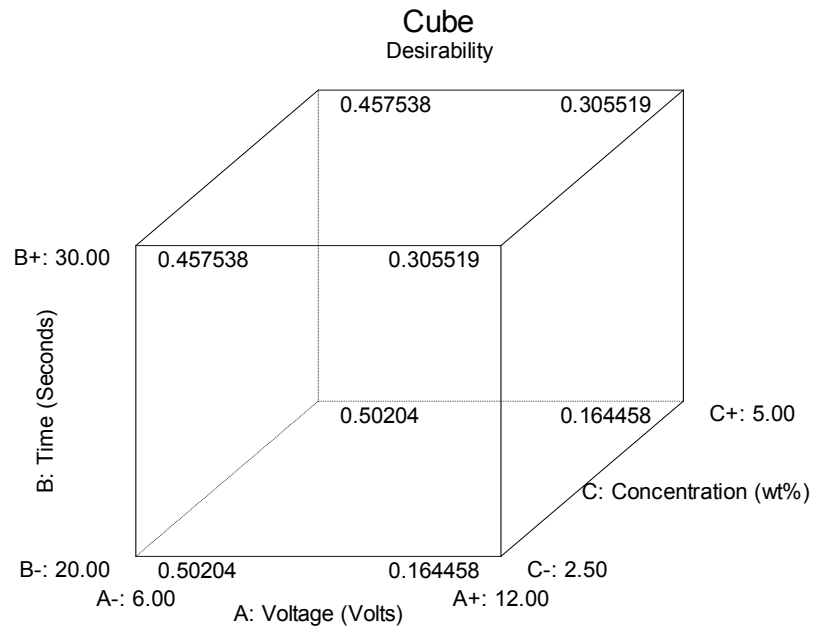


**Figure V.33 - Desirability as a function of time, voltage and concentration**

### V.6.3 Molding

According to the proposed interlocking theory, when the polymer was molded over the etched wire, it would flow into the pits created by electrochemical etching. It can be seen from Figure V.34 and Figure V.35 that the pits have been filled up with the polymer. These pits which have been filled up would provide the required interlocking.



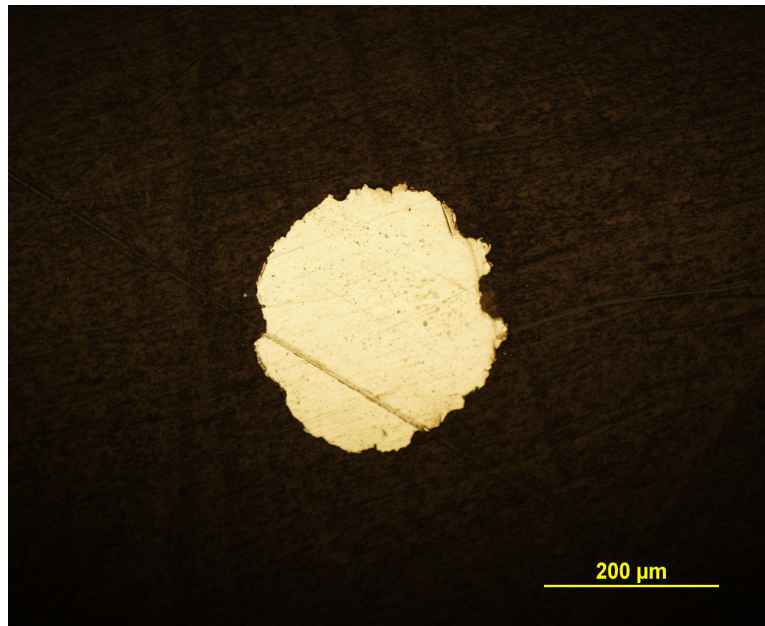


**Figure V.34 - Cross-section of the molded polymer over etched stainless steel wire**

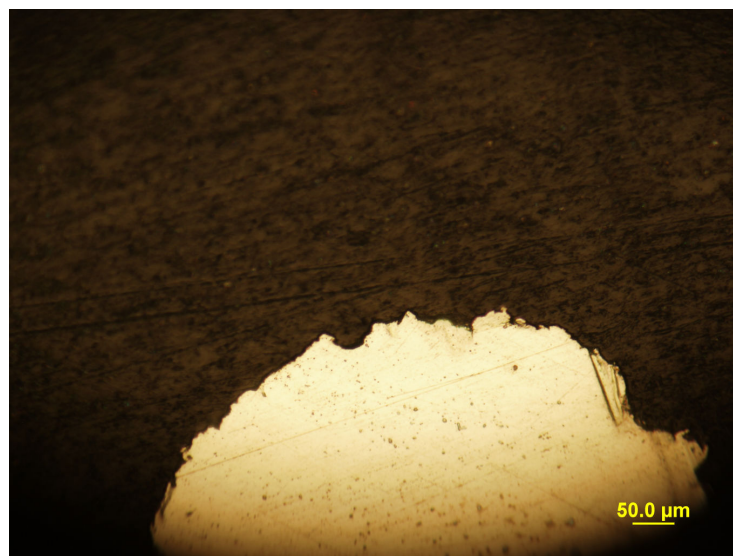


**Figure V.35 - Magnified view of cross section of molded polymer over etched stainless steel wire**

#### V.6.4 Adhesive strength

The average adhesive strength of the unetched and the etched samples was calculated based on the results shown in Figure V.30. Table V.6 compares the adhesive strengths between an unetched and an etched sample, it can be seen that there is a significant difference between the adhesive strength of the unetched and the etched samples, which proves that pitting will improve adhesive strength.

**Table V.7 – Comparison of average adhesion strength between etched and unetched wire**

Average adhesive strength of unetched wire (MPa)	Average adhesive strength of etched wire (MPa)	Percentage improvement (%)
1.47	4.06	276

The theoretically calculated value of pull out force in section V.5.1 was compared with the experimental values of the same using Figure V.31. Table V.7 compares the experimental values of force with the theoretical values. It can be seen that there is good correlation between the results of the experimental and the theoretical analysis. The small deviation could be due to neglecting the smaller pits during the analysis.

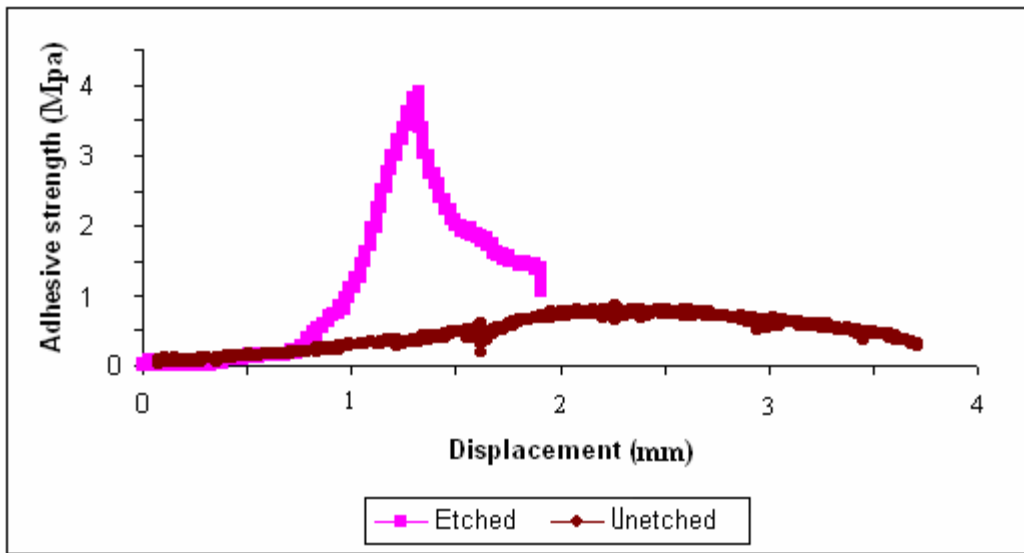
**Table V.8 - Comparison of theoretical and experimental value of pull out force**

Averaged experimental force (N)	Calculated force (N)	Percentage difference (%)
13.25	10.24	22.7

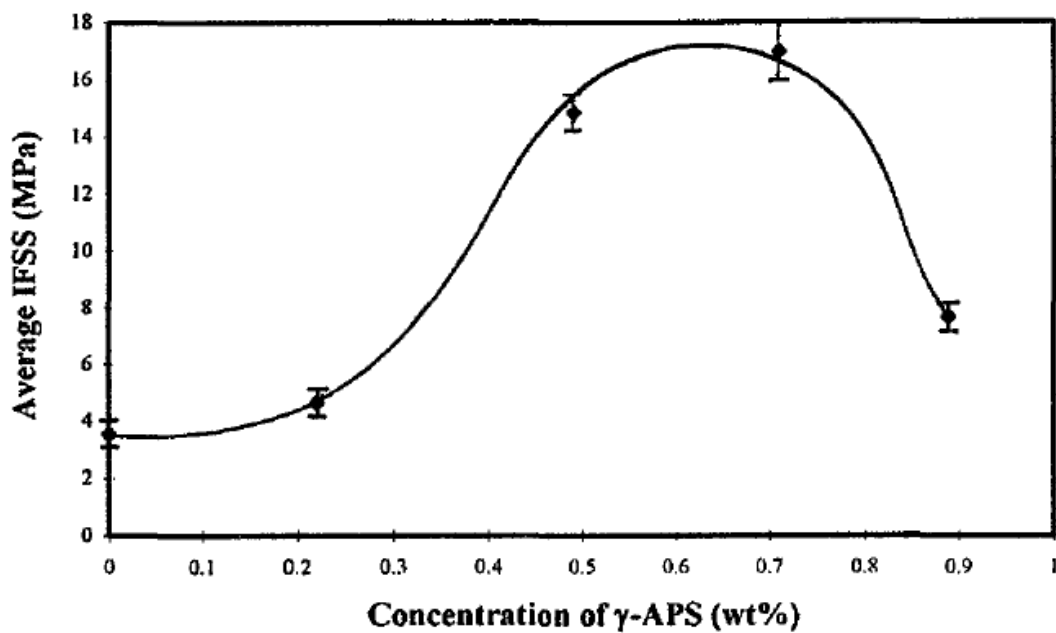
Most of the work in the field of metal polymer adhesion has been done on flat surfaces, thus it is not very common to see pull out tests, the more common tests in the metal polymer field are the peel off test to measure the adhesive strength of thin films on metal substrates, there is little work on finding interfacial shear strength of metal polymer systems. Interfacial shear strength is a parameter which is often calculated when polymer

composites are involved. Due to the geometry of the metal, a pull off test was considered rather than conventional tests to check for adhesive strength between metal and polymer.

A similar pull out test was conducted by Qian et al to test the adhesion of epoxy on a glass fiber. The details of the test can be found in the literature review section. From Figure V.36 (b) it can be seen that as the concentration of 3-aminopropyltriethoxysilane ( $\gamma$ -APS) was increased, there was an increase in adhesive strength. The  $\gamma$  – APS modified the surface of the glass fiber and enhanced interlocking between epoxy and glass fiber. This result is comparable to Figure V.36 (a) where the presence of pits in the electrochemically etched samples significantly increased the adhesive strength when compared with the unetched samples.



(a)



(b)

Figure V.36 - Comparison of pull off tests (a) Comparison of adhesive strengths between an electrochemically etched sample and an unetched sample (b) Comparison of interfacial shear strength (IFSS) of glass fibers treated with varying concentration of  $\gamma$ -APS (3-aminopropyltriethoxysilane) (Qian, 1995)

## VI. CONCLUSIONS AND RECOMMENDATIONS

Adhesion of molded polymer on stainless steel wire was the objective of this study. Different techniques were explored to improve surface adhesion of high density polyethylene on 304 stainless steel wire that leads to manufacture of hybrid stents.

It was shown that:

1. Mechanical abrasion, chemical etching and electrochemical etching were studied. Using electrochemical etching, it is possible to control pit size and pit density using a statistical model which makes electrochemical etching ideal for surface treatment of the stainless steel wire.

2. Burrs were formed by mechanical abrasion but were absent after electrochemical etching. Absence of burrs is critical as it finds applications in medical implantation.

3. The calculated pull out force and measured values were off by 22.7%. The lower value of calculated force could be due to neglecting some of the smaller pits while performing the analysis. The average adhesive strength of the etched samples was 276% higher than the adhesive strength of the unetched samples. It can be concluded that the adhesive strength between metal and polymer depends on the pit size and pit distribution in the etched wire.

4. The pitting on the stainless steel wire occurs due to sodium carbonate in soap. A statistical model has been proposed to predict pit density and pit size based on input parameters such as concentration, voltage and time. Based on experimental conditions, it was observed that while voltage and time of etching significantly affect the pit depth and pit density, concentration does not have any significant effect on pit size and pit density.

To successfully manufacture the hybrid stent, more investigations are recommended:

1. The integrity of the metal/polymer joint in a hybrid stent should be studied due to expansion of the stent during implantation and operating conditions.

2. The pit size and pit distribution of the electrochemically etched wire has to be optimized to maximize the adhesive strength.

3. The etching should be repeated with sodium carbonate rather than soap to eliminate effect of other additives in soap.
4. The similar experiment should be repeated for the actual stent metal and the biodegradable polymer to verify the adhesive strength.
5. Future work is also proposed to study the biological effect of pits on the surface of actual stent metal once biodegradable polymer has degraded.

## REFERENCES

- Abbot Vascular. Angioplasty. [www.abbotvascular.com/global/url/content](http://www.abbotvascular.com/global/url/content) (Accessed, Nov 2005).
- American Psychological Association. *Wikipedia, the free encyclopedia*.  
[www.reference.com/browse/wiki/Thrombogenicity](http://www.reference.com/browse/wiki/Thrombogenicity) (Accessed, June 2007).
- American Psychological Association. *Wikipedia, the free encyclopedia*.  
[www.reference.com/browse/wiki/Atheroma](http://www.reference.com/browse/wiki/Atheroma) (Accessed, June 2007).
- American Psychological Association. *Wikipedia, the free encyclopedia*.  
[www.reference.com/browse/wiki/Cytotoxicity](http://www.reference.com/browse/wiki/Cytotoxicity) (Accessed, June 2007).
- American Psychological Association. *Wikipedia, the free encyclopedia*.  
[www.reference.com/browse/wiki/Haemocompatibility](http://www.reference.com/browse/wiki/Haemocompatibility) (Accessed, June 2007).
- American Psychological Association. *On-line Medical Dictionary*.  
[www.dictionary.reference.com/browse/hyperproliferation](http://www.dictionary.reference.com/browse/hyperproliferation) (Accessed, June 2007).
- American Psychological Association. *Wikipedia, the free encyclopedia*.  
[www.reference.com/browse/wiki/Endothelium](http://www.reference.com/browse/wiki/Endothelium) (Accessed, June 2007).
- American Psychological Association. *Wikipedia, the free encyclopedia*.  
[www.reference.com/browse/wiki/Intimal\\_hyperplasia](http://www.reference.com/browse/wiki/Intimal_hyperplasia) (Accessed, June 2007).
- American Psychological Association. *Wikipedia, the free encyclopedia*.  
[www.reference.com/browse/wiki/Restenosis](http://www.reference.com/browse/wiki/Restenosis) (Accessed, June 2007).
- Bolz, A., Michael, A., Ozbek, C., Heublien, B., Schaldash, M. (1996). Stents with semiconductor to improve their Haemocompatibility. *Tex. Hrt. Inst. Journal*. 23:162-166.
- Bhuyan, A., Gregory, B., Lei, H., Seow, Y.Y., Gianchandani, Y.B. (2005). Pulse and Dc electro polishing of stainless steel stents and other devices. *IEEE*. 314:317.
- Bohman, J. M. (1995). Coronary artery stent design using rapid prototyping.  
<http://www.msoe.edu/reu/jackiefinalpaper.doc>.
- Buser, D., Neydegger, T., Oxland, T., Chochran, D. L., Schenk, R. K., Hirt, H. P., Snetivy, D., Nolte, L. P. (1998). Interfaced shear strength of titanium implants

- with sand blasted and acid etched surface: A biomechanical study in the maxilla of miniature pigs. *J. Biomed. Mater. Res.* 45(2):75-83.
- Colombo, A., Karvouni, E. (2000). Biodegradable Stents. *Amr. Hrt. Assn. J.* 102:1-4.
- Dklee, J. L., Thelen. H., Blenert, H., Vorwerk, D., Hocker, H. (1999). Improvement of Haemocompatibilty of metallic stents by polymer coating. *J. Mater. Sc.: Mater. Med.* 10:443-448.
- DSM Engineering Plastics. Adhesive bonding. [www.dsm.com](http://www.dsm.com) (Accessed June 2007).
- Electronic Space Products International. Stainless steel 304 alloy composition. [www.espimetals.com/tech/.html](http://www.espimetals.com/tech/.html) (Accessed March 2007).
- Exxon Mobil Chemical. High density injection molding resin. *Polyethylene* [www.exxonmobilchemical.com](http://www.exxonmobilchemical.com) (Accessed May 2007).
- Greenwood, J. A., Williamson, J. B. P. (1966), "Contact of nominally flat surfaces", *Proc.Roy. Soc. A* 295: 300-319.
- Kaeshe, H. Uniform electrolytic corrosion. In *Corrosion of metals*. Springer: Berlin, 2003, 136pp.
- Karpenko, A. Y., Adnan, A (2001). A numerical model of friction between rough surfaces. *Tribology International.* 34(8):531-545.
- Kathuria, Y. P. (1998). Laser microprocessing of stent for medical therapy. *IEEE.* 111-114.
- Kharas, G. B., Sanchez, R. F., Severson, D. K. (1994). Polymers of lactic acid. In *Plastics from microbes, microbial synthesis*. Mobley. D. P., Ed Hanser publishers Munich. pp 93-137.
- Kragelsky. I. V. (1965). *Friction and wear*, Butterworth, Washington (1965).
- Lee, H. Y., Qu, J. (2003). Micro structure adhesion strength and failure path at a polymer/roughened metal interface. *J Adh Sc Tech.* 17:119-215.
- Manufacturelink. Laser cutting of a surgical stent. *Micro laser cutting and welding.* [www.industrysearch.com.au/Products/Micro\\_Laser\\_Cutting\\_and\\_Welding-15185](http://www.industrysearch.com.au/Products/Micro_Laser_Cutting_and_Welding-15185) (Accessed Feb 2007).



- Mayo Clinic. Procedures to restore and improve blood flow. *Coronary artery disease*.  
[www.health.yahoo.com/media/mayoclinic/images/image.jpg](http://www.health.yahoo.com/media/mayoclinic/images/image.jpg). (Accessed Nov 2005).
- McGeough, J.A. Metals and electrolytes in ECM. In *Principles of electrochemical machining*. Chapman and Hall: London, 1974; pp 85-88.
- Nakayama, Y., Nishi, S., Hatsue I. U., Matsuda, T. (2002). Fabrication of micropored elastomeric film covered stents and acute phase performances. *J. Biomed. Mater Res.* 54:52-61.
- Patient-uk. Atherosclerosis. *Atheroma*. [www.patient-uk.com](http://www.patient-uk.com) (Accessed Nov 2005).
- Piskin, E. (1994). Biodegradable polymers as bio materials. *J. Bio. S. Poly.* 6:775-795.
- Pizzi, A., Mittal, K.L., (2003). Theories and mechanisms of adhesion. In *Handbook of adhesive technology*, 2<sup>nd</sup> edition. Marcel Dekker publication: New York, 2003, pp 54-64.
- Plasmachem. Disadvantages of conventional stents. *Biodiamond stents*.  
[www.plasmachem.com](http://www.plasmachem.com) (Accessed Feb 2006).
- Qian, L. L., Bruce, A. F., Kellar, J. J., Winter, R. M. (1995). An instrument for testing interfacial shear strength in polymer matrix composites. *J. Meas. Sci. Tech.* 6:1009-1015.
- Ruygrok, P. N., Jaegere, P. T., Domburg, R. T., Vandenbrand, M. J., Serruys, P. W., De Feyter, P. J. (1996). Clinical outcome 10 years after attempted percutaneous transluminal coronary angioplasty in 856 patients. *J. Coll. Card.* 27:1669-1677.
- Shigley, E. J., Mischke, R. C (1989). Failure prevention. In *Mechanical engineering design*, 5<sup>th</sup> edition. McGraw Hill publication: New York, 1989, pp 250.
- Specialchem. Adhesion theory.  
[www.specialchem4adhesives.com/resources/adhesionguide](http://www.specialchem4adhesives.com/resources/adhesionguide) (Accessed June 2007).
- Thomas, N. Insert molding (mass conserving process). *Design insite*.  
[www.designinsite.dk/htmsider/pb2004.htm](http://www.designinsite.dk/htmsider/pb2004.htm) (Accessed Feb 2007).

- Tomashov, N.D., Mirolyubov, E.N. The influence of additions of silver and palladium on the corrosion and electrochemical behavior of stainless steels. In *Corrosion of metals and alloys*, Collection No.2. Israel program for scientific translation Ltd: Jerusalem, 1966, 10pp.
- Turner, T. L., Lach, L. C., Cano, J. R. (2001). Fabrication and characterization of SMA hybrid composites. *SPIE 8<sup>th</sup> annual international symposium on smart structures and materials*. 4333:40-52.
- Tuthill Corporation. Stainless steel molding. *Insert molding and overmolding*. [www.plastics.tuthill.com](http://www.plastics.tuthill.com) (Accessed Feb 2007).
- Vogt, F., Stein, A., Rettemeier, G., Krott, N., Hoffmann, R., Vom, J. D., Bosserhoff, A., Michaeli, W., Hanrath, P., Weber, C., Blindt, R. (2004). Long-term assessment of a novel biodegradable paclitaxel-eluting coronary polylactide stent. *Eur. Hrt. J.* 25:1330-1340.
- Zhang, Q., Wang, R., Kato, M., Keijiro, N. (2005). Observation by atomic force microscope of corrosion product during pitting corrosion on SUS304 stainless steel. *Script. Mater.* 52(3):227-230.

**APPENDIX A – DESIGN OF EXPERIMENT**

## Analysis of pit depth

Design-Expert® Software  
Pit Depth

Shapiro-Wilk test  
W-value = 0.937  
p-value = 0.634  
A: Voltage  
B: Time  
C: Concentration  
■ Positive Effects  
■ Negative Effects

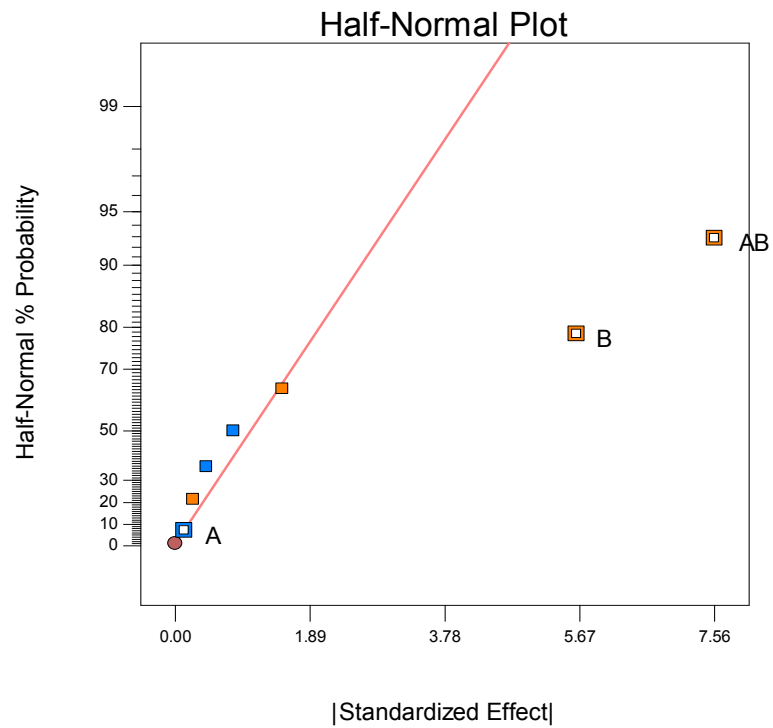
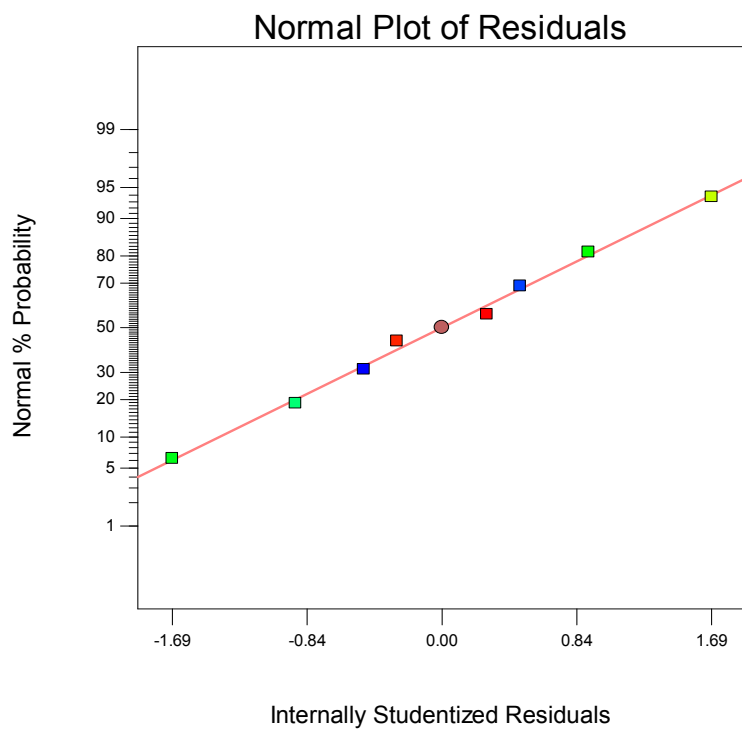
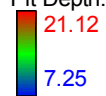


Figure A.1 - Standardized effect vs half normal % probability

Design-Expert® Software  
Pit Depth

Color points by value of  
Pit Depth:



**Figure A.2 - Internally standardized results vs normal % probability**

Design-Expert® Software  
Pit Depth

Color points by value of  
Pit Depth:

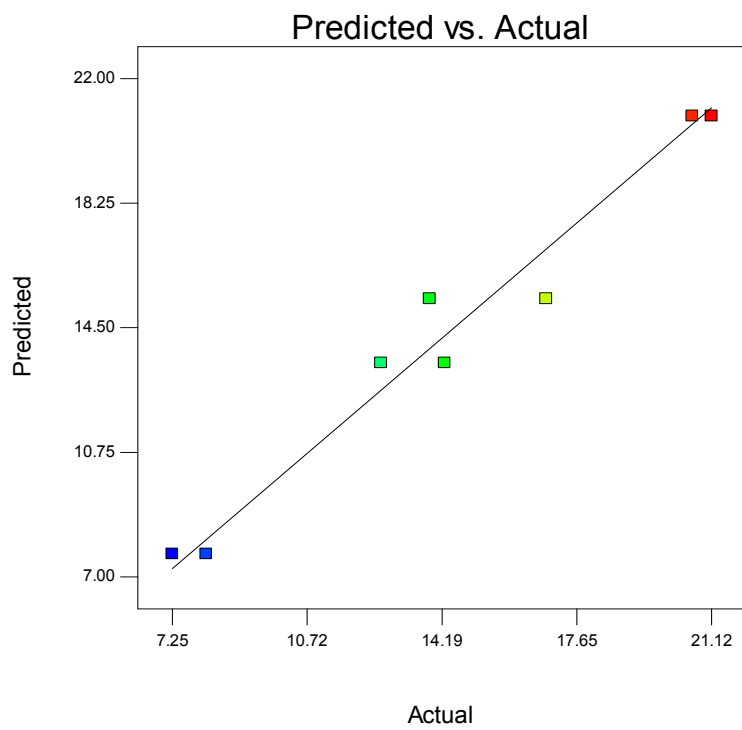
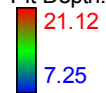


**Figure A.3 - Actual vs predicted**

Design-Expert® Software  
Pit Depth

Lambda  
Current = 1  
Best = 0.25  
Low C.I. = -2.08  
High C.I. = 4.49

Recommend transform:  
None  
(Lambda = 1)

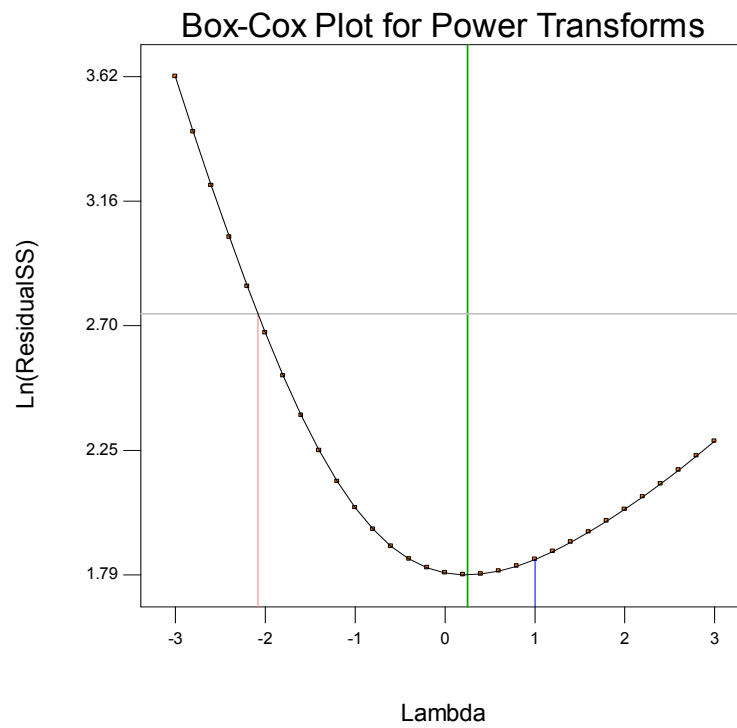


Figure A.4 - Lambda vs ln (residuals)

## Analysis of pit density

Design-Expert® Software  
Ln(Pit Density)

Shapiro-Wilk test  
W-value = 0.733  
p-value = 0.026  
A: Voltage  
B: Time  
C: Concentration  
■ Positive Effects  
■ Negative Effects

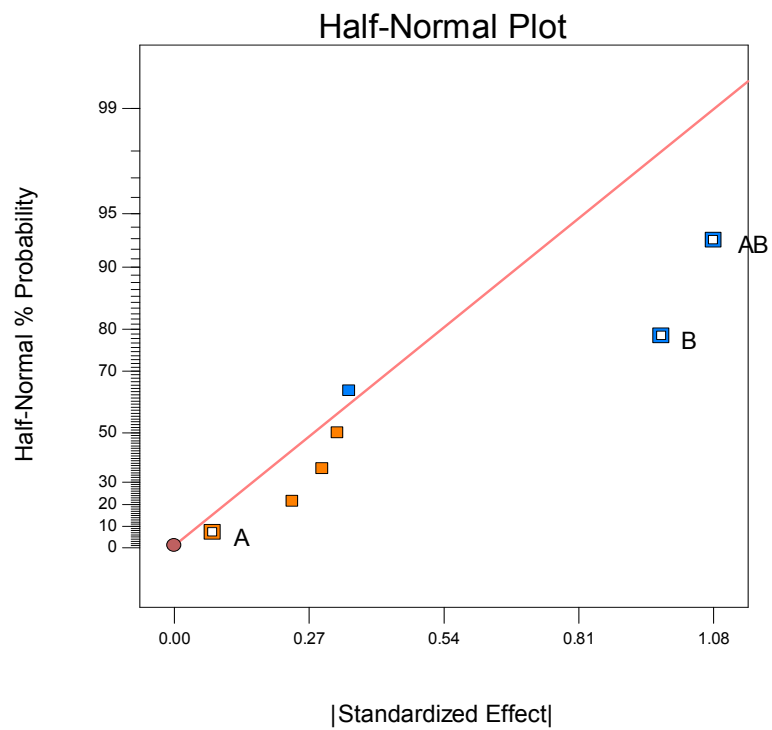
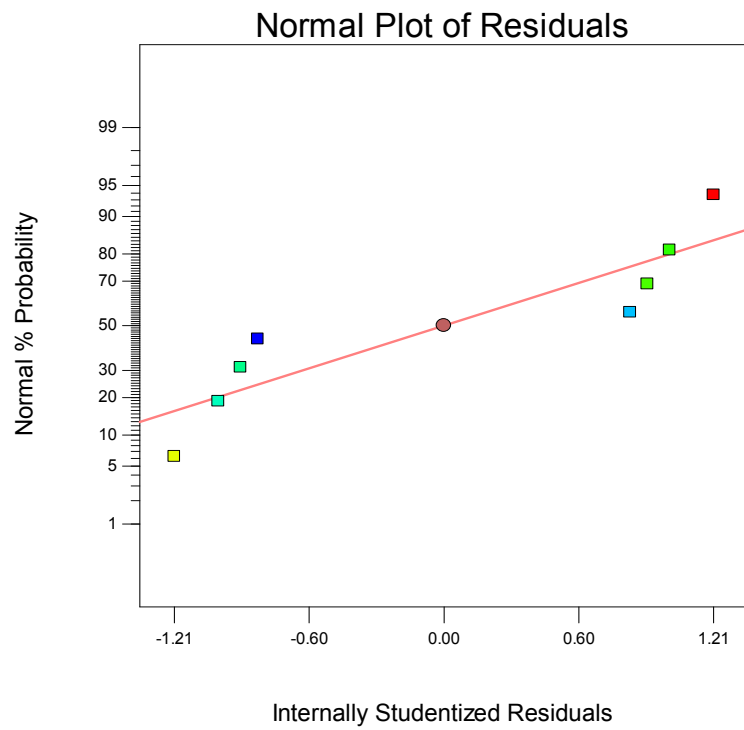
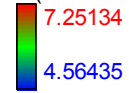


Figure A.5 - Standardized effect vs half normal % probability

Design-Expert® Software  
Ln(Pit Density)

Color points by value of  
Ln(Pit Density):



**Figure A.6 - Internally standardized results vs normal % probability**



Design-Expert® Software  
Ln(Pit Density)

Color points by value of  
Ln(Pit Density):

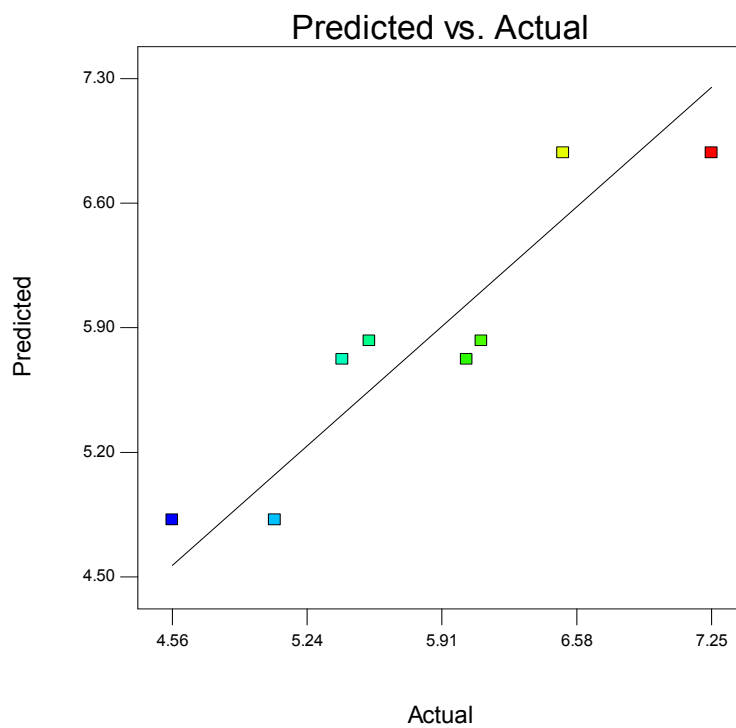
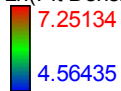


**Figure A.7 - Actual vs predicted**

Design-Expert® Software  
Ln(Pit Density)

Lambda  
Current = 0  
Best = -0.17  
Low C.I. = -1.2  
High C.I. = 0.79

Recommend transform:  
Log  
(Lambda = 0)

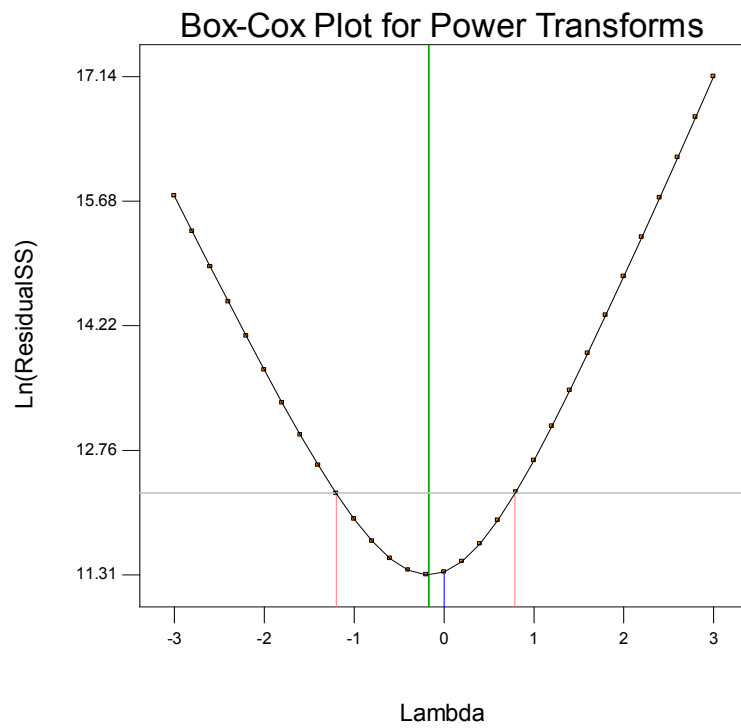
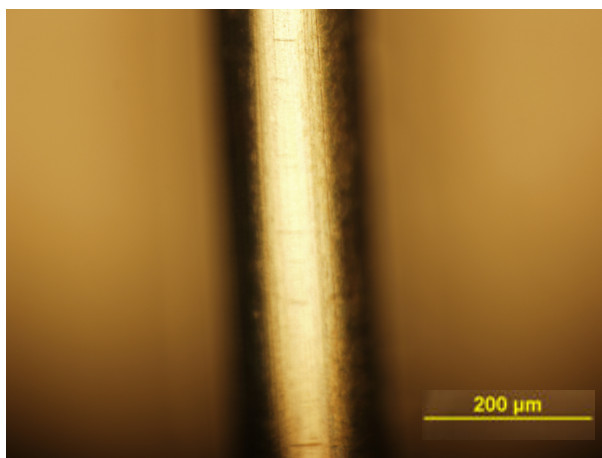
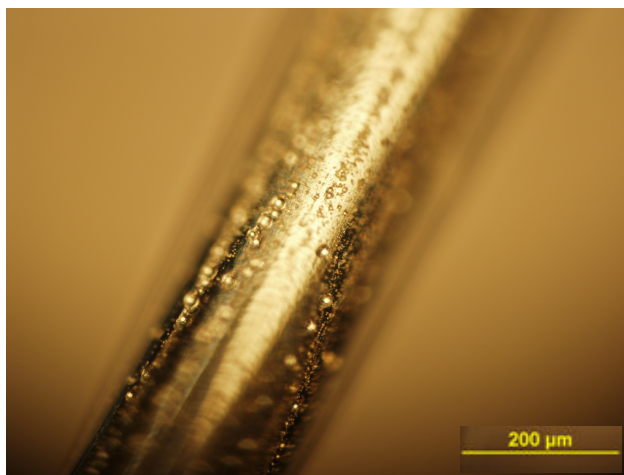


Figure A.8 - Lambda vs ln (residuals)

**APPENDIX B - ELECTROCHEMICAL ETCHING PICTURES**

**Figure B.1 - Wire etched for 20s at an applied voltage of 3v in soap solution of concentration 2.5% by weight**



**Figure B.2 - Wire etched for 10s at an applied voltage of 6v in soap solution of concentration 2.5% by weight**

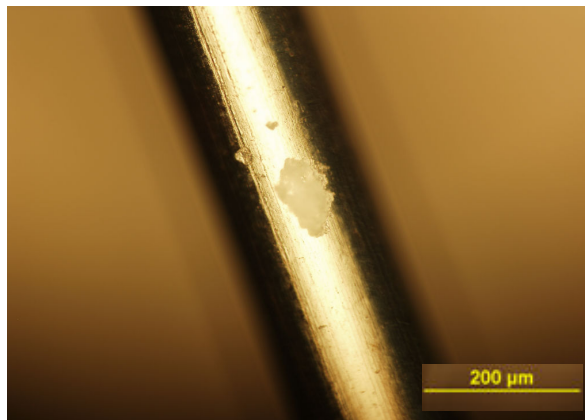


**Figure B.3 - Wire etched for 30s at an applied voltage of 3v in soap solution of concentration 2.5% by weight**

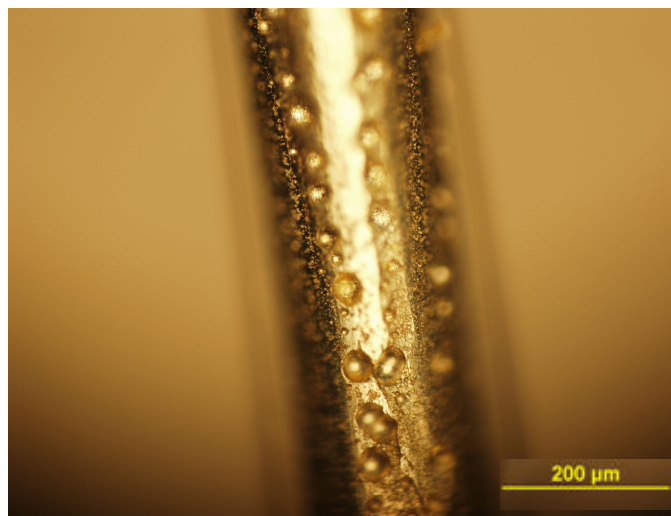


**Figure B.4 - Wire etched for 30s at an applied voltage of 6v in soap solution of concentration 2.5% by weight**

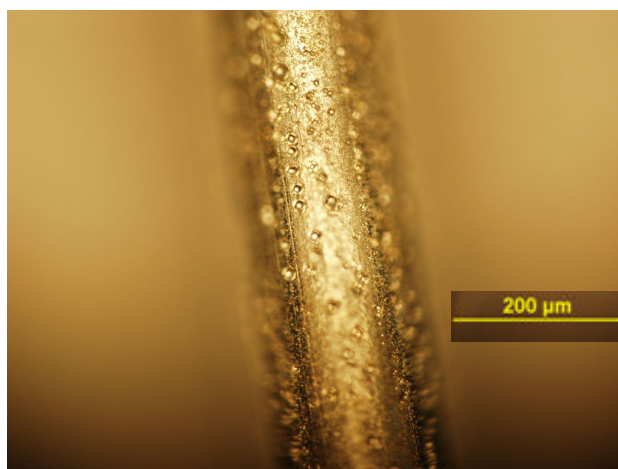


**Figure B.5- Wire etched for 10s at an applied voltage of 12v in soap solution of concentration 2.5% by weight**

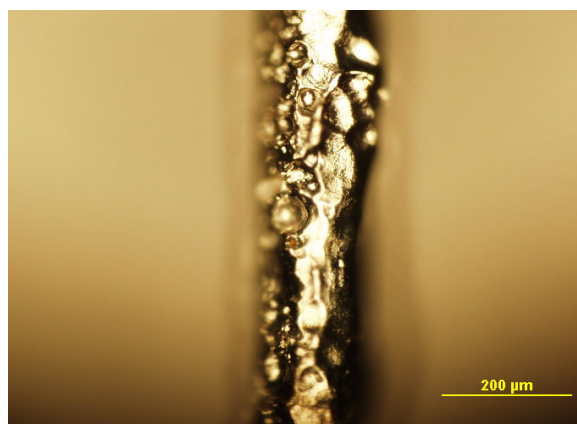


**Figure B.6 - Wire etched for 30s at an applied voltage of 12v in soap solution of concentration 2.5% by weight**

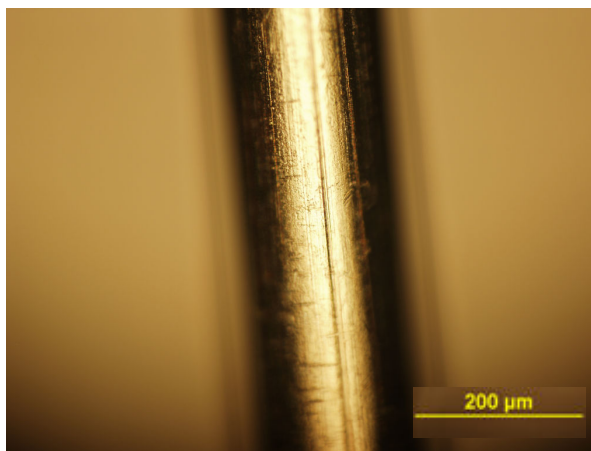


**Figure B.7 - Wire etched for 10s at an applied voltage of 3v in soap solution of concentration 5% by weight**

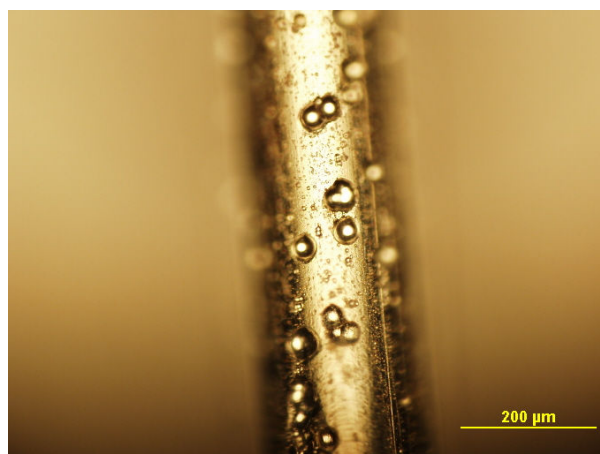


**Figure B.8 - Wire etched for 20 s at an applied voltage of 6v in soap solution of concentration 5% by weight**

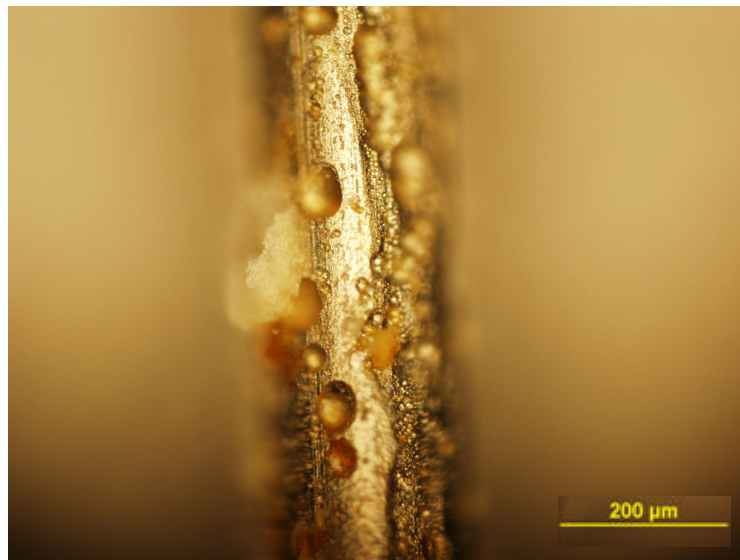


**Figure B.9 - Wire etched for 30s at an applied voltage of 12v in soap solution of concentration 5% by weight**

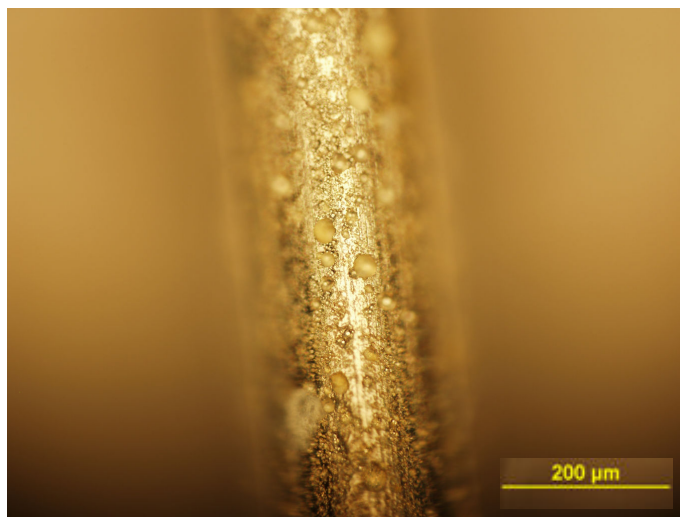


**Figure B.10 - Wire etched for 20s for an applied voltage of 12v in soap solution concentration 5% by weight**

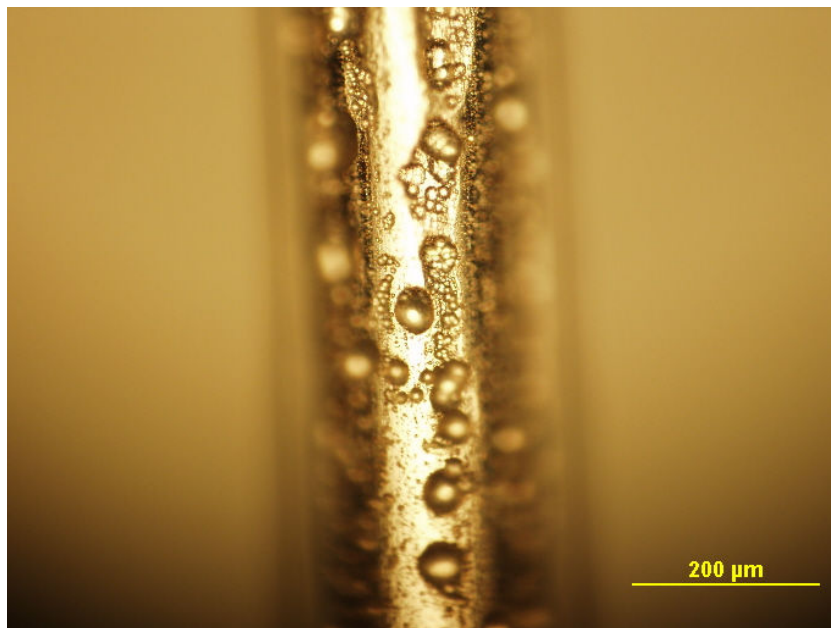


**Figure B.11 - Wire etched for 30s at an applied voltage of 6v in soap solution of concentration 5% by weight**



## APPENDIX C – STATISTICAL ANALYSIS

**Table C.1 - Statistical Analysis (sample 2)**

Pit Number	Diameter of pit (µm)	Distance between 2 pits (µm)	Cumulative distance (µm)	Depth of pit (µm)
1	22.61	54.91	54.91	11.305
2	17.76	148.58	203.49	8.8825
3	16.15	12.92	216.41	8.075
4	22.61	51.68	268.09	11.305
5	16.15	48.45	316.54	8.075
6	24.22	35.53	352.07	12.1125
7	19.38	64.6	416.67	9.69
8	29.07	74.29	490.96	14.535
9	12.92	32.3	523.26	6.46
10	27.45	48.45	571.71	13.7275
11	35.53	32.3	604.01	17.765

**Table C.2 - Statistical analysis (Sample 3)**

Pit Number	Diameter of pit ( $\mu\text{m}$ )	Distance between 2 pits ( $\mu\text{m}$ )	Cumulative distance ( $\mu\text{m}$ )	Depth of pit ( $\mu\text{m}$ )
1	25.84	61.37	61.37	12.92
2	22.61	22.61	83.98	11.305
3	25.84	67.83	151.81	12.92
4	41.99	51.68	203.49	20.995
5	16.15	32.3	235.79	8.075
6	16.15	12.92	248.71	8.075
7	19.38	35.53	284.24	9.69
8	41.99	48.45	332.69	20.995
9	22.61	19.38	352.07	11.305
10	29.07	48.45	400.52	14.535
11	38.76	35.53	436.05	19.38
12	37.145	64.6	500.65	18.57

**Table C.3 - Statistical analysis (Sample 4)**

Pit Number	Diameter of pit ( $\mu\text{m}$ )	Distance between 2 pits ( $\mu\text{m}$ )	Cumulative distance ( $\mu\text{m}$ )	Depth of pit ( $\mu\text{m}$ )
1	29.07	58.14	58.14	14.535
2	22.61	25.84	83.98	11.305
3	19.38	22.61	106.59	9.69
4	19.38	54.91	161.5	9.69
5	29.07	64.6	226.1	14.53
6	30.68	64.6	290.7	15.34
7	19.38	54.91	345.61	9.69
8	29.07	32.3	377.91	14.53
9	29.07	38.76	416.67	14.53
10	29.07	41.99	458.66	14.53
11	32.3	74.29	532.95	16.15
12	30.685	45.22	578.17	15.34
13	22.61	35.53	613.7	11.30
14	25.84	80.75	694.45	12.92
15	25.84	54.91	749.36	12.92

**Table C.4 - Statistical analysis (Sample 5)**

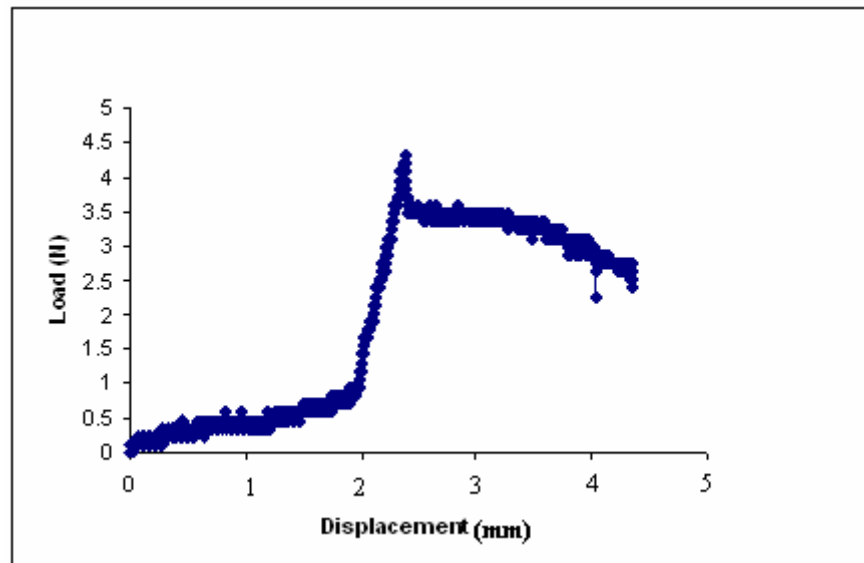
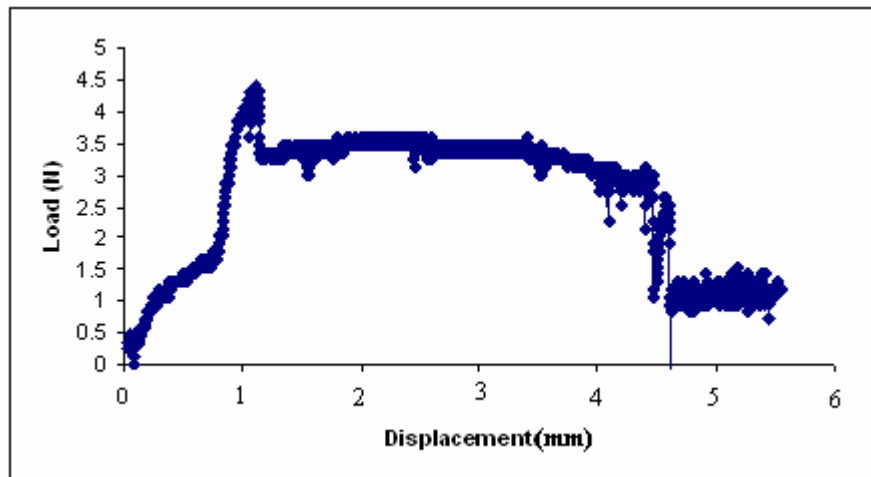
Pit Number	Diameter of pit ( $\mu\text{m}$ )	Distance between 2 pits ( $\mu\text{m}$ )	Cumulative distance ( $\mu\text{m}$ )	Depth of pit ( $\mu\text{m}$ )
1	32.3	74.29	74.29	16.15
2	25.84	113.05	187.34	12.92
3	38.76	74.29	261.63	19.38
4	12.92	59.755	321.385	6.46
5	9.69	45.22	366.605	4.845
6	41.99	129.2	495.805	20.995
7	41.99	113.05	608.855	20.995
8	32.3	48.45	657.305	16.15
9	35.53	87.21	744.515	17.765

**Table C.5 - Statistical analysis (Sample 6)**

Pit Number	Diameter of pit ( $\mu\text{m}$ )	Distance between 2 pits ( $\mu\text{m}$ )	Cumulative distance ( $\mu\text{m}$ )	Depth of pit ( $\mu\text{m}$ )
1	20.995	100.13	100.13	10.4975
2	25.84	58.14	158.27	12.92
3	22.61	83.98	242.25	11.305
4	29.07	51.68	293.93	14.535
5	12.92	16.15	310.08	6.46
6	16.15	29.07	339.15	8.075
7	20.995	58.14	397.29	10.4975
8	22.61	41.99	439.28	11.305
9	12.92	32.3	471.58	6.46
10	9.69	64.6	536.18	4.845
11	29.07	51.68	587.86	14.535
12	25.84	51.68	639.54	12.92
13	25.84	48.45	687.99	12.92
14	25.84	48.45	736.44	12.92
15	16.15	16.15	752.59	8.075
16	11.305	25.84	778.43	5.6525
17	12.92	64.6	843.03	6.46
18	12.92	9.69	852.72	6.46

**Table C.6 - Statistical analysis (Sample 7)**

Pit Number	Diameter of pit (µm)	Distance between 2 pits (µm)	Cumulative distance (µm)	Depth of pit (µm)
1	22.61	74.29	74.29	11.305
2	16.15	38.76	113.05	8.075
3	9.69	17.765	130.815	4.845
4	12.92	35.53	166.345	6.46
5	19.38	96.9	263.245	9.69
6	19.38	93.67	356.915	9.69
7	25.84	77.52	434.435	12.92
8	22.61	80.75	515.185	11.305
9	25.84	35.53	550.715	12.92
10	12.92	12.92	563.635	6.46
11	16.15	48.45	612.085	8.075
12	29.07	48.45	660.535	14.535
13	19.38	71.06	731.595	9.69
14	16.15	74.29	805.885	8.075

**APPENDIX D - PULL OUT TEST****Figure D.1 - Displacement Vs Force (Unetched Sample 1)****Figure D.2 - Displacement Vs Force (Unetched Sample 2)**

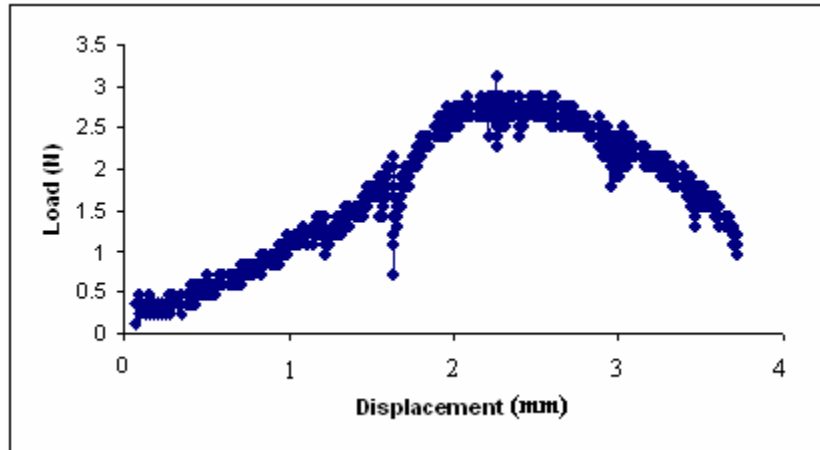


Figure D.3 - Displacement Vs Force (Unetched Sample 3)

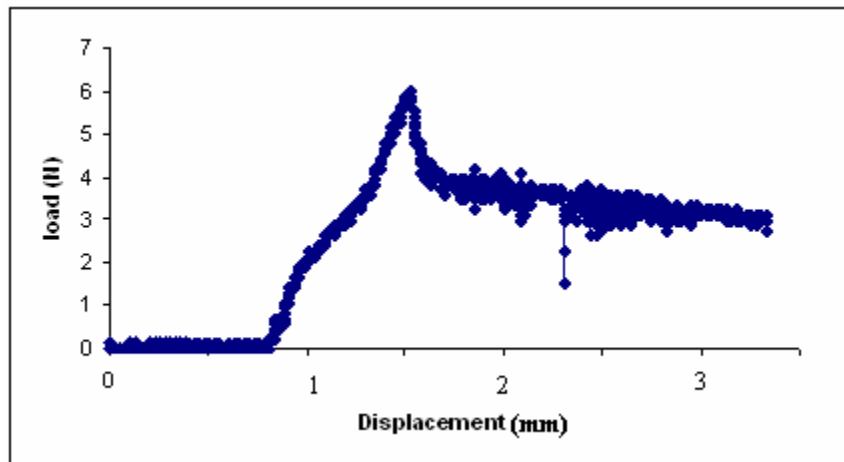


Figure D.4 - Displacement Vs Force (unetched Sample 4)



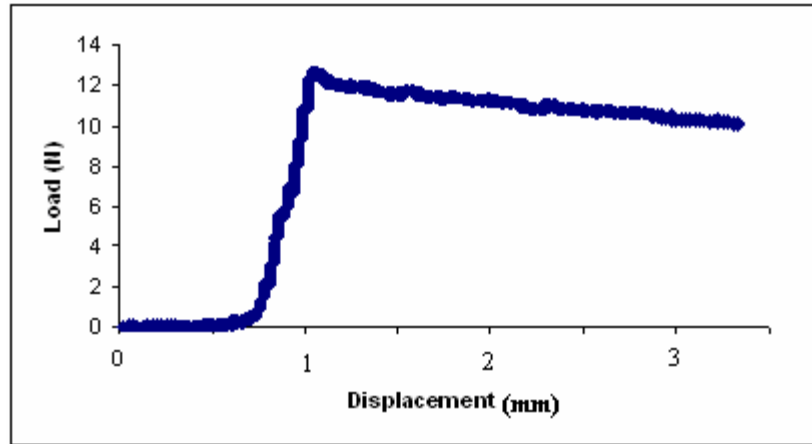


Figure D.5 - Displacement Vs Force (etched Sample 1)

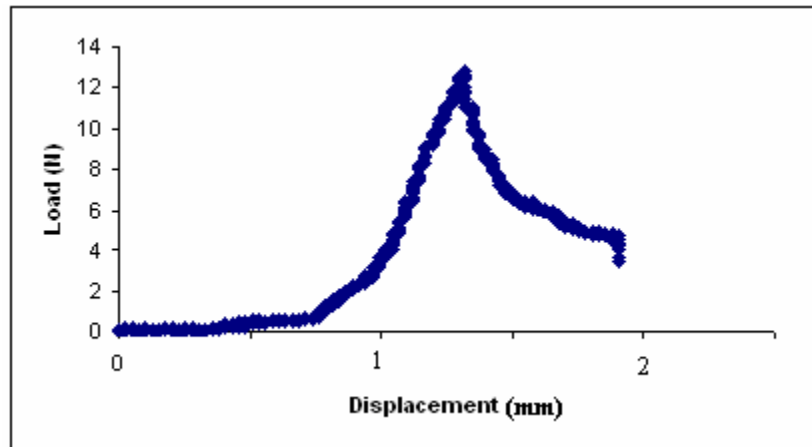


Figure D.6 - Displacement Vs Force (etched Sample 2)

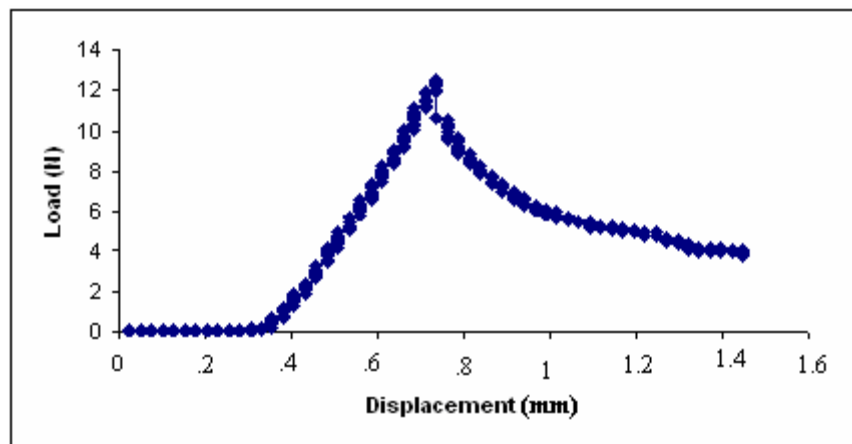


Figure D.7 - Displacement Vs Force (etched Sample 3)

## VITA

Karthik Mohan was born in Delhi, India. He studied at the Delhi Public School, one of the city's best institutions where right from an early age the emphasis was on personal development. He did his undergraduate studies at Hindustan College of Engineering, affiliated with Anna University, one of the nation's largest open universities. He pursued a degree in Mechanical Engineering and received his Bachelor of Engineering degree with distinction in 2005. He did his final year project from the Indian Institute of Technology on wave propagation studies. It was here that he was inspired to pursue further studies. He developed a strong inclination towards mechanics and materials. He moved to the United States in 2005 to pursue his master's in Mechanical Engineering at the Texas A&M University, a pioneer in imparting quality education. He finished his master's studies at Texas A&M University in August 2007. He worked in the Micro and Nano Manufacturing Laboratory under the guidance of Dr. Wayne Hung. His focus area of interest is in enhancing adhesion between biocompatible stainless steel and biodegradable polymers.

Karthik's permanent home address is:

A 206 MOD CGHS,

Vasundhra Enclave,

Delhi – 110096

India